Universität Potsdam

Defining moisture sources and (palaeo)environmental conditions using isotope geochemistry in the NW Himalaya

Kumulative Dissertation

zur Erlangung des akademischen Grades
"doctor rerum naturalium" (Dr. rer. nat.)
in der Wissenschaftsdisziplin Geologie

Eingereicht an der
Mathematisch-Naturwissenschaftlichen Fakultät
der Universität Potsdam

Von
Iris van der Veen

Potsdam, den 4. Februar 2021

“Each molecule recovered from an ancient sediment carries information about the organism that produced it. Through chemotaxonomic associations, the structure can indicate the identity of the producer. The isotopic composition of the molecule can indicate the isotopic composition of the parent organism and that, in turn, can reveal the carbon source utilized by the producer and thus its position within the ancient ecosystem. (Hayes, 1993).

Published online on the
Publication Server of the University of Potsdam:
https://doi.org/10.25932/publishup-51439
https://nbn-resolving.org/urn:nbn:de:kobv:517-opus4-514397

I hereby declare that this work has not been submitted to any other institute of higher education. This dissertation was prepared independently and exclusively with the funding sources that are listed in each individual chapter.

Iris van der Veen

Abstract

Anthropogenic climate change alters the hydrological cycle. While certain areas experience more intense precipitation events, others will experience droughts and increased evaporation, affecting water storage in long-term reservoirs, groundwater, snow, and glaciers. High elevation environments are especially vulnerable to climate change, which will impact the water supply for people living downstream. The Himalaya has been identified as a particularly vulnerable system, with nearly one billion people depending on the runoff in this system as their main water resource. As such, a more refined understanding of spatial and temporal changes in the water cycle in high altitude systems is essential to assess variations in water budgets under different climate change scenarios.

However, not only anthropogenic influences have an impact on the hydrological cycle, but changes to the hydrological cycle can occur over geological timescales, which are connected to the interplay between orogenic uplift and climate change. However, their temporal evolution and causes are often difficult to constrain. Using proxies that reflect hydrological changes with an increase in elevation, we can unravel the history of orogenic uplift in mountain ranges and its effect on the climate.

In this thesis, stable isotope ratios (expressed as $\delta^{2}H$ and $\delta^{18}O$ values) of meteoric waters and organic material are combined as tracers of atmospheric and hydrologic processes with remote sensing products to better understand water sources in the Himalayas. In addition, the record of modern climatological conditions based on the compound specific stable isotopes of leaf waxes ($\delta^{2}Hwax$) and brGDGTs (branched Glycerol dialkyl glycerol tetraethers) in modern soils in four Himalayan river catchments was assessed as proxies of the paleoclimate and (paleo-) elevation. Ultimately, hydrological variations over geological timescales were examined using $\delta^{13}C$ and $\delta^{18}O$ values of soil carbonates and bulk organic matter originating from sedimentological sections from the pre-Siwalik and Siwalik groups to track the response of vegetation and monsoon intensity and seasonality on a timescale of 20 Myr.

I find that Rayleigh distillation, with an ISM moisture source, mainly controls the isotopic composition of surface waters in the studied Himalayan catchments. An increase in *d*-excess in the spring, verified by remote sensing data products, shows the significant impact of runoff from snow-covered and glaciated areas on the surface water isotopic values in the timeseries.

In addition, I show that biomarker records such as brGDGTs and δ2Hwax have the potential to record (paleo-) elevation by yielding a significant correlation with the temperature and surface water δ^2H values, respectively, as well as with elevation. Comparing the elevation inferred from both brGDGT and δ^2Hwax, large differences were found in arid sections of the elevation transects due to an additional effect of evapotranspiration on δ2Hwax. A combined study of these proxies can improve paleoelevation estimates and provide recommendations based on the results found in this study.

Ultimately, I infer that the expansion of C4 vegetation between 20 and 1 Myr was not solely dependent on atmospheric pCO_2, but also on regional changes in aridity and seasonality from to the stable isotopic signature of the two sedimentary sections in the Himalaya (east and west).

This thesis shows that the stable isotope chemistry of surface waters can be applied as a tool to monitor the changing Himalayan water budget under projected increasing temperatures. Minimizing the uncertainties associated with the paleo-elevation reconstructions were assessed by the combination of organic proxies (δ^2Hwax and brGDGTs) in Himalayan soil. Stable isotope ratios in bulk soil and soil carbonates showed the evolution of vegetation influenced by the monsoon during the late Miocene, proving that these proxies can be used to record monsoon intensity, seasonality, and the response of vegetation. In conclusion, the use of organic proxies and stable isotope chemistry in the Himalayas has proven to successfully record changes in climate with increasing elevation. The combination of δ^2Hwax and brGDGTs as a new proxy provides a more refined understanding of (paleo-)elevation and the influence of climate.

Zusammenfassung

Die Auswirkungen des menschgemachten Klimawandels wirken sich auch auf den Wasserkreislauf aus. Während manche Regionen höhere Niederschlagsmengen zu erwarten haben, werden andere mit stärkeren und häufigeren Trockenperioden zu konfrontiert sein. Diese Veränderungen haben einen unmittelbaren Einfluss auf Evaporation, Langzeit-Wasserreservoire, Grundwasserbildung, Schneefall und Gletscher. Da Gebirge und Hochplateaus überdurchschnittlich von den Auswirkungen des Klimawandels betroffen sind, ist die Wasserversorgung der Menschen entlang der dort entspringenden Flüsse gefährdet. Insbesondere der Himalaya gilt als instabile Region, dessen Abflüsse die Wasserversorgung von annähernd einer Milliarde Menschen gewährleisten. Um zu erwartende Veränderungen des Wasserbudgets in Abhängigkeit von verschiedenen möglichen Klimawandelszenarien abschätzen zu können, ist ein detaillierteres Verständnis des Wasserkreislaufs in Hochgebirgen und -plateaus erforderlich.

Neben dem globalen Klimawandel gibt es weitere Faktoren, die sich auf den Wasserkreislauf auswirken. Das Wechselspiel zwischen Gebirgsbildung und klimatischen Bedingungen beeinflusst den Wasserkreislauf auf geologischen Zeitskalen. Entsprechende Veränderungen und ihre Auswirkungen lassen sich jedoch nur eingeschränkt bestimmen. Mittels geeigneter Proxies für höhenbedingte Änderungen der Hydrologie lassen sich der Orogeneseverlauf sowie dessen klimatische Auswirkungen allerdings genauer rekonstruieren.

In der vorliegenden Arbeit werden die Verhältnisse stabiler Isotope (als δ^2H und $\delta^{18}O$ ausgedrückt) von meteorischen Wassern sowie von organischem Material mit Methoden der Satellitenfernerkundung als Indikator für atmosphärische und hydrologische Prozesse kombiniert, um ein besseres Verständnis der verschiedenen Wasserquellen des Himalaya zu erlangen. Darüber hinaus wurde der Link zwischen modernen klimatischen Bedingungen und verbindungsspezifischen stabilen Isotopen von Blattwachsen (δ^2H_{wax}) sowie von brGDGTs (branched Glycerol dialkyl glycerol tetraethers) rezenter Bodenproben aus den Einzugsgebieten vierer Flüsse

des Himalaya hergestellt, um sie als Paläo-Klima- und Paläo-Höhenproxy verwenden zu können. Zu guter Letzt wurden hydrologische Veränderungen auf einer Zeitskala von 20 Mio. Jahren anhand von $\delta^{13}C$- and $\delta^{18}O$-Werten von Bodencarbonat und organischem Material aus Sedimentschnitten der pre-Siwalik und Siwalik-Einheiten nachvollzogen. Die Erkenntnisse dieser tragen zu einer deutlich genaueren Rekonstruktion von Vegetationsänderungen und der Entwicklung der Monsun-Intensität sowie -Saisonalität bei.

Die Isotopenzusammensetzung der Oberflächenwasser der untersuchten Flüsse wird hauptsächlich durch Rayleigh-Destillation der im Wesentlichen vom Indischen Sommer Monsun eingetragenen Feuchtigkeit bestimmt. Der durch Satellitenfernerkundungsdaten bestätigte Anstieg des Deuterium-Exzesses (*d*-excess) im Frühjahr verdeutlicht den signifikanten Einfluss von Schnee- und Gletscherschmelze, der auch in Zeitreihen von Oberflächenwasserproben erkennbar ist.

Sowohl brGDGT als auch δ^2H_{wax} können potentiell die absolute Höhe zum Zeitpunkt ihrer Synthese abbilden, da sie stark mit der Lufttemperatur, bzw. mit Oberflächenwasser δ^2H und somit indirekt auch mit der Höhe korreliert sind. Im direkten Vergleich der mittels brGDGT und δ^2H_{wax} rekonstruierten Höhen ergaben sich insbesondere in ariden Teilen der Höhenprofile große Unterschiede. Diese sind hauptsächlich auf verstärkte Evapotranspiration und deren Auswirkung auf Pflanzenwasser und -wachse zurückzuführen. Basierend auf den Erkenntnissen der vorliegenden Arbeit können weitere vergleichende Untersuchungen beider Proxies genauere Paläo-Höhenstudien ermöglichen.

Diese Arbeit zeigt, dass die Isotopie von Oberflächenwassern genutzt werden kann, um den sich ändernden Wasserhaushalt des Himalya im Kontext voraussichtlich weiter ansteigender Temperaturen zu beobachten. Unsicherheiten bei der Rekonstruktion von Paläo-Höhen konnten durch eine vergleichende Analyse zweier organischer Proxies (δ^2H_{wax} and brGDGTs) aus Paläo-Bodenproben des Himalayas minimiert werden. Verhältnisse stabiler Isotope von Blattwachsen aus diesen Bodenproben spiegeln die Entwicklung

der Vegetation unter dem Einfluss des Monsuns im späten Miozän wider. Zusammenfassend wurde erfolgreich gezeigt, dass organische Proxies und stabile Isotope höhenabhängige Änderungen des Klimas im Himalaya aufzeichnen können.

Die Kombination von δ^2H_{wax} and brGDGTs als neuer Proxy ermöglicht eine deutlich differenziertere Betrachtung von rekonstruierten Paläo-Höhen sowie Paläo-Klima.

Acknowledgements

First of all I would like to thank my supervisor Dirk Sachse for his continuous support during the years of my PhD. I appreciate all the encouragement during the experiments, conferences and paper-writing phases and all the time you have invested in this thesis and me. It was a great opportunity for me to learn all aspects of being a scientist, from learning to understand all laboratory equipment until the publication of scientific papers.

I am very grateful to Manfred Strecker and Bodo Bookhagen, who supported my project continuously. Thank you for always being there for me, reviewing my papers and providing me with advice on my academic career and publications.

A special thanks goes to Bernd Hoffmann, who acted as a big PhD brother throughout my whole career at the University of Potsdam. He taught me everything about the laboratory, attempted to teach me German, and was always there to support me during hard times, and cheer me on during the good times.

Work at the university of Potsdam and the GFZ were greatly improved by the presence of Silvio, Melanie, Stephanie, Nicole, Gamze, Nico, Niels, Alessia, Sebastian, Heiko, Christian, Viktoria, Nicolas, Henry, Franzi, Veronica, Yannick, Johanna, James, Steffi, Fabiana, Patricia, Görkem, Asma, Resvana, Magda and Alex.

The iTECC graduate school has been a great addition to my scientific development. The large variation in topics and scientific interests really broadened my horizon. For the scientific discussions to fieldtrips in the Himalaya, to work as a visitor in the CRPG in Nancy, I am very thankful. A big thanks to Natalie, Lorenzo, Mo, Ruben, Jesse, Svetlana, GZ, Madeleine, Zakaria, Mike, Alessandro, Eric, and in loving memory of Gwladys.
I want to thank Ansgar Kahmen, Jason West and Francien Peterse for allowing me to work in their lab and research group. This experience has taught me several different analytical techniques, and has greatly contributed to my scientific development.

For the friends I made along the way: Cristina, Remco, Anna & Cos, thanks for showing me your career paths and teaching me about your PhD projects. Also a great thanks to the Berlin Social Runners, Koen and Joey that listened to me speak about my PhD during many many kilometers of running and helped me keep my mind and body in balance during these years.

During the last 2,5 years of my PhD I worked in an environmental consultancy firm in the Netherlands, just having the weekends and some Fridays to work on the last parts of my PhD. I want to thank the management and colleagues from Tauw for their trust in me, and them taking over my projects during my “PhD days”.

Ultimately, I want to thank my family for motivating me during my bachelors and masters degree, and pursue a PhD & helping me move to Berlin. Heel erg bedankt voor jullie jarenlange steun en vertrouwen.

Table of Content

List of figures

Author Contributions

Chapter 2

Identifying seasonal snowmelt in the western Himalaya using stable isotopes of modern surface waters and remote sensing

Iris van der Veen, Hima J. Hassenruck – Gudipati, Taylor Smith, Eric Deal, Henry Wichura, Manfred R. Strecker, Bodo Bookhagen, Dirk Sachse
In Revision at Hydrological processes (HYP-20-1016) since October 30th 2020

Iris van der Veen, Manfred Strecker, Bodo Bookhagen and Dirk Sachse developed the project and determined sample and research strategy for the research project. Hima J. Hassenruck-Gudipati performed the calculations on the Rayleigh distillation model. Taylor Smith provided the remote sensing data and provided support with the statistical analysis. Bodo Bookhagen provided support in analyzing the remote sensing data products. Iris van der Veen, Bodo Bookhagen, Eric Deal, and Dirk Sachse performed fieldwork. Dirk Sachse, Bodo Bookhagen, Eric Deal, and Henry Wichura contributed to fieldwork organization and sampling in the Himalaya. Iris van der Veen wrote the manuscript with contributions from all co-authors. Iris van der Veen performed lab work in the laboratory of the University of Potsdam together with Dirk Sachse. Iris van der Veen wrote the paper with input from all co-authors.

Chapter 3

Validation and calibration of soil δ^2H and brGDGTs along (E-W) and strike (N-S) of the Himalayan climatic gradient

*Iris van der Veen, Francien Peterse, Jesse Davenport, Bernd Meese, Bodo Bookhagen, Christian France-Lanord, Ansgar Kahmen, Hima J. Hassenruck – Gudipa*ti, *Ananta Gajurel, Manfred R. Strecker, Dirk Sachse*
Published in Geochimica et Cosmochimica Acta 2020

Iris van der Veen, Manfred Strecker, Bodo Bookhagen and Dirk Sachse developed the project and determined sample and research strategy. Jesse Davenport sampled and processed the samples for the Khudi transect and Bernd Hoffmann sampled and processed the samples for the Arun transect. Iris van der Veen processed and measured the Sutlej and Alaknanda samples. Christian France-Lanord determined sampling strategy in the Khudi and took soil samples. Iris van der Veen, Eric Deal, Bodo Bookhagen, and Dirk Sachse sampled the soils in the Sutlej and Alaknanda catchment. Ansgar Kahmen provided the lab and support during xylem water measurements. Francien Peterse provided the lab and support during GDGT measurements (Alaknanda, Sutlej, Arun, Khudi), which were measured by Iris van der Veen. Iris van der Veen wrote the manuscript with contributions from all co-authors.

Chapter 4

Lateral variations in vegetation in the Himalaya since the Miocene and implications for climate evolution

Natalie Vögeli, Yani Najman, Peter van der Beek, Pascale Huyghe, Peter M. Wynn, Gwladys Govin, Iris van der Veen, Dirk Sachse

Published in EPSL, 2017

Natalie Vögeli, Gwladys Govin and Yani Najman carried out fieldwork. Natalie Vögeli, Peter van der Beek, Yani Najman and Pascale Huyge interpreted the Himalayan geology, sedimentary record, and the paleo-climatology in the Himalaya. Peter Wynn guided and supported the interpretation of the stable isotope measurements. Natalie Vögeli and Iris van der Veen did the analysis of biomarkers. Natalie Vögeli, Dirk Sachse, and Iris van der Veen interpreted the biomarker data. Natalie Vögeli wrote the manuscript with contributions from all co-authors.

1. Introduction

1.1. Motivation - Climate change and its impact on the landscape

Earth's climate is a complex and dynamic system that is controlled by interactions between the atmosphere, land, ocean, biosphere, and cryosphere. As a consequence, Earth's surface is shaped by interplay between tectonics and climate, creating high mountains where plates collide (e.g. Himalayan range and Tibetan Plateau), and deep valleys where plates diverge (e.g. East African Rift). The mountain ranges that are created can have an influence on regional and global climate by blocking moisture trajectories resulting in a humid climate (leeward side) on one side of the mountain rage, and desert conditions (windward side) on the other side of the mountain range. These natural processes result in the possibility to use the current landscape as an archive as a recorder for changes in tectonics and climate.

Climate plays an important role in mountain weathering and erosion processes, which are more effective under warm and wet conditions. Increasing anthropogenic carbon emissions are predicted to have a significant impact on Earth's current climate as continued greenhouse gas emissions will result in further warming and changes in all components of the climate system are expected (IPCC, 2014). The projected climate change and its associated increase in rain intensity in one place, and aridification in other places can cause significant changes in the landscape and the hydrological cycle.

An important part of assessing the future changes in climate is understanding the development of climate in the past, which shaped the current conditions and landscape. This requires reconstruction of precipitation patterns, (palaeo)-elevation and other climate conditions. By studying organic geochemical proxies and stable isotopes in modern soil and

water, and assessing their relationship with the current climate, a robust technique can be developed to infer climate conditions from the past.

1.2. The hydrological cycle in the Himalayas

The hydrological cycle plays a large role in understanding Earth's climate: the presence of water in a system is key for important processes to take place that define the climate: e.g. growth of vegetation, the degree of erosion, the formation of rivers and the development of weather patterns. The hydrological cycle can be described as all processes in which water continuously moves between different reservoirs, for example glaciers, rivers, precipitation and the oceans. In this cycle mountains play a large role, storing massive amounts of water in glaciers and snow at high elevation, and subsequently transport meltwater in mountain streams and rivers. In many cases, meltwater originating from high mountains functions as an essential resource for people downstream. One of the mountain ranges in which this water resource is particularly important is the Himalayan orogen.

Himalayan rivers such as the Indus, Ganges and Tsangpo-Brahmaputra are a water supply to nearly a billion people living in their catchments (Immerzeel *et al.*, 2009; Bookhagen and Burbank, 2010). The hydrological budget of these rivers is dominated by both monsoonal precipitation and snowmelt. Snow falls mainly in the high-elevation catchments of the Himalaya, being stored in winter, after which it melts and is transported to the rivers downstream (Bookhagen and Burbank, 2010). The Himalayan foreland and lower elevation Himalayas are dominated by Indian Summer Monsoon (ISM) precipitation originating from the Bay of Bengal or the Arabian Sea. The areas where the ISM collides with the Southern Himalayan Front (SHF), show a strong rainout gradient, with decreasing amounts of moisture from the wet foreland to the arid Tibetan Plateau (Winiger *et al* 2005; Immerzeel *et al.*, 2009; IPCC, 2014; Smith and Bookhagen, 2018).

The relative contribution of snowmelt and monsoon precipitation (and their part in the hydrological budget) to river catchments in the Himalaya is not well constrained due to the lack of meteorological stations across this mountain range. However, the spatial and temporal distribution of water in this area is important regarding the projected future climate change (IPCC, 2014) and the large populations that depend on the downstream water availability. Moreover, in the projected climate change there will be a different spatial division of water, where certain areas become dryer and others wetter. Early in the year (March – May) a relative high percentage of the surface water will originate from glacial and snowmelt, while during the monsoon season more water in the rivers will originate from precipitation. The projected increasing temperatures and an already clear decline in the size of glaciers in the Himalaya could be disastrous for the water availability for people downstream. This leads to the first research question in this thesis: Can we get a more refined understanding of spatial and temporal changes of water contributions from different sources (precipitation, glacial and snowmelt) in order to predict varying budgets under climate change scenarios?

1.3. Feedback between mountain range uplift and climate

One of the main drivers of the current monsoon system in the Himalayas is the temperature gradient between land and ocean, caused by the high orographic barrier. The insulation of warm moist air over the continent that originates from the dryer northern latitudes produces a strong monsoon, resulting in strong southeasterly winds from the Bay of Bengal, forming vortices along the SHF (Lang and Barros, 2004; Bookhagen and Burbank, 2006, 2010; Galewsky, 2009). The monsoonal winds collide with the mountain front in summer causing a two-peak rainfall belt (Bookhagen and Burbank 2010), with wet frontal regions in the leeward side of the mountain and dry interior parts on the Tibetan Plateau (Wulf, Bookhagen and

Scherler, 2010). In winter, this temperature effect reverses, creating northeastern wind systems changing the rainfall distribution, transporting more precipitation to the Himalayan syntaxes in contrast to the Himalayan central (Bookhagen and Burbank 2010). By understanding the regional precipitation patterns in the Himalaya and on the Tibetan Plateau, and its relationship with elevation, it allows us to use this relationship in order to estimate elevation.

The uplift of the Himalayan region begun approximately 55 - 45 Myr ago, resulting in a continent-continent collisional belt (Yin and Harrison, 2000; Zhisheng *et al.*, 2001; Clift *et al.*, 2008). However, the reconstruction of the formation of the Himalayas, influenced by the dynamic coupling of erosion, climate and mountain uplift proves to be a difficult task. Climate models and geological archives demonstrate that the uplift of the Himalayan orogen could have affected global temperatures, diversion of westerly winds and increased erosional and carbon fluxes (e.g. Ruddiman and Kutzback 1989, Zhisheng *et al.*, 2001; Clift *et al.*, 2008; Whipple, 2009)). Reconstructing the timing of mountain range uplift and the evolution of high-altitude plateaus is important when attempting to understand potential feedbacks between tectonics and climate at geological timescales.

The exact timing of the Tibetan/Himalayan uplift has been a debatable topic, while these parameters are important for general models linking large-scale orogenic events (uplift) with lithospheric-scale geodynamic processes (Quade *et al* 2007). The reconstruction from paleoelevation can only be deduced from information originating from geological archives. Paleoclimate research has focused on recovering information from a wide variety of archives; ice cores, (lake) sediments, corals, speleothems tree rings, and microfossils, studied with the goal to infer information about past climatic conditions (Ruddiman, 2007). As past climatic parameters cannot be measured directly, paleoclimatology relies on so-called proxies, i.e., chemical, biological or physical components preserved in geological archives, which contain information about paleoclimatic conditions at the time of deposition.

Attempts to get a handle on elevation history of mountain ranges has been studied using isotopes in authigenic and pedogenic carbonates (Garzione *et al.*, 2000; Quade, Garzione and Eiler, 2007), tooth enamel (Wang *et al.*, 2008; Xu *et al.*, 2010), leaf wax lipids (Sauer *et al.,* 2001; Huang *et al.,* 2004; Sachse *et al.,* 2004; Smith *et al.,* 2006; Hou *et al.,* 2008) and Glycerol Dialkyl Glycerol Tetraethers (GDGTs)(Sinninghe Damsté *et al.*, 2008; Peterse *et al.*, 2009; Ernst *et al.*, 2013; Nieto-Moreno *et al.*, 2016; Wang *et al.*, 2017)). In these studies a linear relationship between $\delta^2H/\delta^{18}O$ values and elevation is observed, with decreasing δ^2H values at higher elevations. This is caused by decreasing temperatures and progressive rainout processes with increasing elevation (Poage, 2001; Rowley *et al* 2001; Hren *et al.*, 2009; Bershaw *et al* 2012). The isotopic value in precipitation serves as a source for the leaf wax lipids, tooth enamel and pedogenic carbonates, allowing us to use the relationship between isotopic values and elevation in order to reconstruct paleoelevation,

Stable isotopes ($\delta^{18}O$) in fossil teeth were used to reconstruct paleoelevation on the Tibetan Plateau, and can be well used as a proxy due to its low susceptibility to diagenetic alteration Wang *et al.*, 2008; Xu *et al.*, 2010). The data from these studies are valuable as a source of information for paleoelevation, but can be influenced by the fact that oxygen isotopes of tooth enamel consists of a mixture of drinking water and diet. A tooth enamel dataset should therefore be paired with a modern river water stable isotope dataset, in order to correct for the mixture of source water in the tooth enamel.

The use of stable isotopes in pedogenic carbonates ($\delta^{18}O$) in order to reconstruct paleoelevation was demonstrated in the Himalayas (Garzione & Dettman, *et al.*, 2000) showing implications for the debate on the timing of Tibetan Plateau uplift. Moreover, a study based on lake and paleosols oxygen isotopic composition of carbonates showed that elevations >4.000 m were reached as early as 40 million years ago (Rowley and Currie, 2006). However, in a review of the method by Quade et al. (2007) several complications are mentioned, that can be summarized as that $\delta^{18}O$ is a

function of both temperature and $\delta^{18}O$ of rainfall (variably modified by evaporation). The incorporated evaporative effect could lead to significant underestimations of paleoelevation.

The compounds used in the aforementioned studies rely on the preservation of sedimentary terraces or well-characterized mineral assemblages, which are often not present in high elevation terrains. A solution for this can be the use of stable isotopes in soils to be used for paleoelevation reconstruction. Soils are ubiquitous in the environment allowing for a larger elevation range of elevation to be studied (Mulch *et al.*, 2004). In our current study, we studied stable isotopes in water and soils and brGDGTs in soils to test if these are suitable proxies to infer paleoelevation. A more detailed description on this methodology is described in paragraph 1.4.

1.4. The use of stable isotopes and organic proxies to infer paleoelevation

1.4.1. Meteoric waters

A tool that has been applied in order to trace processes in the hydrological cycle are the use of stable isotope ratios (expressed as $\delta^{2}H$ and $\delta^{18}O$ values) in meteoric water (Dansgaard, 1964; Gat, 1996; Fröhlich, 2001). Stable isotopes have been applied in surface water studies for hydrograph separation (Karim and Veizer, 2002; Maurya *et al.*, 2011), differentiation of moisture sources (Rohrmann *et al.*, 2014) or as an input for hydrological modeling and weather models, which requires a sound understanding of isotope fractionation processes (Bowen *et al.* 2003; Norris *et al.*, 2016).

Numerous studies which relied on stable isotopes obtained from stream waters have been carried out along altitudinal gradients in the Himalaya to constrain the moisture sources contributing to the rivers (Garzione *et al.*, 2000; Karim and Veizer 2002; Hren *et al.*, 2009; Maurya *et al.*, 2011; Bershaw *et al.* 2012). In these studies a linear relationship between $\delta^{2}H/\delta^{18}O$ values of meteoric waters and elevation is observed, with

decreasing δ^2H values at higher elevations. This is caused by decreasing temperatures and progressive rainout processes with increasing elevation (Poage, 2001; Rowley *et al* 2001; Hren *et al.*, 2009; Bershaw *et al* 2012).

The use of the aforementioned trends in isotopic values and the hydrological cycle can provide more insight into the different (seasonal) hydrological components contributing to the Himalayan river water.

1.4.2. Leaf wax δ^2H

Leaf epicuticular waxes are present in the protective outer layer on the surface of leaves, which supports the plants water balance. The amount of leaf waxes varies between species, and the composition consists of complex mixtures of long-chain alkanes, alcohols, ketones, aldehydes, acetals, esters and acids (Eglinton and Hamilton, 1967). *n*-Alkanes are straight chain-hydrocarbons that lack functional groups, making them into a suitable molecule that can function as a biomarker and can survive in the fossil records for millions of years (Eglinton and Logan, 1991; Peters *et al.,* 2005)

Stable isotopes in leaf wax *n*-alkanes (δ^2H_{wax}) derived from higher terrestrial plants are routinely used for the reconstruction of paleohydrological signals. The δ^2H signal that is recorded in leaf wax *n*-alkanes originates from plant source water δ^2H (often precipitation), with a relatively constant depletion in the heavy isotopologue during biosynthesis. In order to indicate the fractionation between source and product, enrichment factors (ε) are commonly used (Sachse *et al.*, 2012). In most stable isotope studies, the net fractionation between source water (δ^2H) and lipid stable isotope signature (δ^2H_{wax}) is referred to as the apparent fractionation (ε_{app}). In addition to biosynthesis, the apparent fractionation is influenced by environmental factors, such as moisture availability (resulting in soil and plant evapotranspiration), as well as the plant's physiology, i.e., the type of vegetation (Chikaraishi and Naraoka, 2003; Smith and Freeman, 2006; Hou *et al.*, 2007; Sachse *et al.*, 2012; Tipple *et al.*, 2013). In the study of Chikaraishi

et al (2003), the ε_{app} values for C_3 plants were -117±27‰ and -116±13‰ for angiosperms and gymnosperms respectively. For C_4 plants the ε_{app} value was -132±12‰. In a more recent study of Liu et al (2019), a large dataset crossing different latitudes was analyses, where a relatively constant average ε_{app} $-116 \pm 5‰$ ($n = 941$) was found.

The δ^2H_{wax} values of *n*-alkanes are used for the reconstruction of past hydrological conditions, due to the observation that the δ^2H in long chain (C_{29}, C_{31}) *n*-alkanes (δ^2H_{wax}) correlates with mean annual precipitation δ^2H (Huang, Shuman, Wang and Iii, 2004; Sachse, Radke and Gleixner, 2004b; Polissar and Freeman, 2010; Garcin *et al.*, 2012). As such, the δ^2H_{wax} values of plant biomarkers can be used to record the isotopic composition of precipitation. As a result, the isotopic signature of the source water is recorded in plant-derived lipids, indirectly reflecting the precipitation δ^2H in the plant δ^2H_{wax} (Sauer *et al.*, 2001; Sachse, Radke and Gleixner, 2004; Smith and Freeman, 2006; Hou, D'Andrea and Huang, 2008). Numerous studies on δ^2H_{wax} in soils that traverse altitudinal transects have been published with the aim to explore the suitability of δ^2H_{wax} as a paleo-elevation proxy (Jia *et al.*, 2008; Peterse *et al.*, 2009; Luo *et al.*, 2011; Bai, Fang and Tian, 2012; Ernst *et al.*, 2013; Nieto-Moreno *et al.*, 2016; Coffinet *et al.*, 2017; Herrmann *et al.*, 2017). The general conclusion is that relatively stable climate conditions are favorable for an optimal functioning of these proxies and serve as a promising tool for the reconstruction of paleo-elevation. However, numerous factors influencing the relationship between δ^2H_{wax} and elevation are not yet understood.

As a second chapter of my thesis I will focus on the use of δ^2H_{wax} in soils along altitudinal gradients, and if they can provide us with information on which secondary (climatic) factors that control the offset between δ^2H_{wax} and δ^2H_{water}, and therefore possibly impact paleoclimate/paleoelevation studies.

1.4.3. brGDGTs

Another important type of biomarker applied in paleostudies is the distribution of branched Glycerol Dialkyl Glycerol Tetraethers (brGDGTs) in sediments. These are membrane lipids produced by soil bacteria and can show variation in the number (4-6) of methyl branches attached to their alkyl backbone, the position of these methyl branches (5 or 6 position), and the number (0-2) of internal cyclizations (Weijers *et al.*, 2006, 2007; Schouten *et al., 2013)*. The relative distribution of brGDGTs in soils serves as an indirect recorder of the mean annual temperature (MAT) and the pH of the soil in which they are produced, which makes them a suitable proxy as a continental paleothermometer (De Jonge *et al.*, 2014a).

Mean annual air temperature generally decreases with elevation, due to the adiabatic cooling of air, functioning as an indirect measure of elevation. The potential of brGDGTs to track adiabatic cooling was first illustrated in a study at Mt Kilimanjaro, where a good relation was found between brGDGT-derived MAT and altitude (Sinninghe Damsté *et al.*, 2008). Subsequently, good relations between brGDGT signals and MAT were found along the southeastern margin of the Tibetan Plateau (Wang *et al.*, 2017), Mt Gongga (Peterse *et al.*, 2009) and Mt Meghalaya (Ernst *et al.*, 2013), among others. Outside of East Asia, this relationship has also been found in the Andes (Nieto Moreno *et al.,* 2016) and Africa (Coffinet *et al.*, 2017; Jaeschke *et al.*, 2018). However, the correlation between MAT_{mr} and mean annual temperature still shows a substantial amount of scatter, suggesting that the brGDGT proxy is affected by additional parameters. Several of those have been identified, for example soil moisture content (SMC) and precipitation amounts/aridity (Dirghangi *et al.*, 2013; Ernst *et al.*, 2013; Menges *et al.*, 2014; Wang, Liu and Zhang, 2014; Dang *et al.*, 2016), as well as soil and vegetation type (Davtian *et al.*, 2016). This can increase the uncertainties in the temperature-elevation relationship and, hence, the proxy's robustness in recording elevation. In order to improve the potential of the brGDGT – elevation relationship, a more thorough research needs to be done in order to unravel the specific relations between MAT and elevation.

To assess possible sources of scatter in the individual relations of soil *n*-alkane δ^2H and brGDGTs with elevation, and thus the suitability of these proxies in paleoelevation reconstructions, both proxies were applied in parallel at several altitudinal transects. This revealed, for example, that the rain belt surrounding Mt Kilimanjaro likely disturbed the relation between soil *n*-alkane δ^2H and elevation due to a D-depletion in the precipitation and consequently in the soil *n*-alkanes (Peterse *et al.*, 2009). A similar spatial heterogeneity in precipitation was shown at Mt Kenya and Mt Rungwe, resulting in weak or absent relationships between the soil *n*-alkane δ^2H and elevation (Coffinet *et al.*, 2017). Nevertheless, the combined application of brGDGTs and soil *n*-alkane δ^2H in the Andes, Mt Meghalaya and the Southern Alps in New Zealand did show the expected orography effect on temperature and precipitation (Ernst *et al.*, 2013; Nieto-Moreno *et al.*, 2016).

In our current study, the individual relations of brGDGT-derived MAT and δ^2H_{wax} with altitude by using a combination of field and remote-sensing data are further validated. In a second step, the proxies (δ^2H_{wax} and brGDGTs) are combined and we investigate whether this combination reduces potential uncertainties in the elevation estimates.

1.5. $\delta^{18}O$ and $\delta^{13}C$ in soil carbonates as a proxy for climate evolution

The lateral variations in modern climate along the SHF can be linked to vegetation patterns, which can be used to indirectly show the influence of the monsoon (humid versus dry areas) in this region. Temperature and precipitation during growing seasons are major factors that influence vegetation, where C_3 plants are generally dominantly present in humid climates and C_4 plants in water stressed and warm conditions (Ehleringer 1988).

The isotopic oxygen signature in pedogenic carbonates has been applied to reconstruct paleoelevation, in a similar manner as the relationship between δ^2H_{wax} and elevation (see paragraph 1.3.). In addition, by combining stable

oxygen isotopes with carbon isotopes in carbonates, paleovegetation reconstructions have been carried out for the Himalayas (Quade, Cerling and Bowman, 1989; Quade and Cerling, 1995; Quade *et al.*, 1995). The $\delta^{13}C$ isotopic signature in (bulk) organic matter can be used to differentiate between C_3- and C_4-dominated vegetation, which relies mostly on the observation that C_4 plants are mainly grass species (Farquhar, Ehleringer and Hubick, 1989; Diefendorf and Freimuth, 2017). Due to differences in carbon isotope fractionation between C_3 and C_4 plants during carbon fixation. C_3 plants are more depleted in ^{13}C relative to C_4 plants ((Farquhar, Ehleringer and Hubick, 1989; Hayes, 1993; A. Hobbie and Werner, 2004)) and C_4 plants are more adapted to conserve water and reduction of photorespiration in drier climates.

Using the $\delta^{13}C$ signature originating from bulk soil and soil carbonates therefore allows to track vegetation as an indirect measure of monsoon intensity. Applying this technique on sedimentary sections that date back on geological timescales, makes it possible to determine if the climate was cool and humid (favoring C_4 vegetation) or warm and dry (favoring C_3 vegetation). $\delta^{13}C$ values of soil carbonates and soil organic matter have been used to reconstruct changes in vegetation and climate (Jay, Cerling and Bowman, 1989; Quade and Cerling, 1995; Singh *et al.*, 2013). However, similar to lipid $\delta^{2}H$, the relationship between $\delta^{13}C$ and C_3/C_4 vegetation can be subject to influences from varying climatic parameters, pCO_2, ecosystems, and plant physiology (Diefendorf and Freimuth, 2016).

In the last chapter of this thesis I will focus on the use of $\delta^{13}C$ and $\delta^{18}O$ values in Miocene sediments, and how they can yield further insight into how the vegetation evolution in the Himalaya took place and under what climatic conditions this happened.

1.6. Research Questions

In this thesis, I address the following research questions:

1. What are the different hydrological components (varying moisture sources, precipitation, snow, and glacial melt) that contribute to the temporal and spatial isotopic signature (δ^2H and $\delta^{18}O$) of surface waters in the Himalaya?

2. What are the main processes that influence lipid biomarker δ^2H values, as well as brGDGT compositions, in the Himalaya and what implications does this have for paleoelevation studies?

3. How is the evolution of the monsoon climate, precipitation, and C_4 plants recorded in the isotopic composition ($\delta^{13}C$ and $\delta^{18}O$) of pedogenic carbonates and organic matter?

The thesis is structured in 3 chapters, in which all three questions are addressed. In chapter 2, the first research question is addressed. Here, we focus on unraveling the different hydrological components that contribute to the isotope signature of surface waters over an altitudinal gradient in two Himalayan catchments using an approach combining stable isotope chemistry and satellite-derived climate data (e.g., TRMM-derived rainfall and AMSR-derived SWE). Moreover, we analyzed two one-year-long surface water isotope time series, which were sampled at weekly intervals in high elevation catchments. These data are compared to temporal satellite data in order to test if snowmelt in the spring has a significant impact on surface water isotope compositions.

In chapter 3, the second research question is addressed. Here, we carry out a multiproxy analysis of soil samples along four altitudinal gradients in the Himalaya and assess the ability of δ^2H to record source water in soil *n*-alkane δ^2H and hence elevation. These different altitudinal transects have varying

precipitation regimes (200–4,0000 mm/year), relative influences of different moisture sources (Indian Summer Monsoon (ISM), Western Disturbances (WD)), and vegetation cover. These factors make it a suitable study area to identify secondary controlling factors that alter the relationship between source water δ^2H and soil *n*-alkane δ^2H, not only on an altitudinal basis but also on a lateral, i.e., east to west, basis (Figure 1.2.). To assess the fidelity with which the biomarker proxies record climate along the elevation gradient are additionally supported and validated with remotely sensed data, such as SMAP-derived root zone soil moisture content and TRMM-derived rainfall to analyze the larger spatial patterns.

In Chapter 4, we address research question 3, where we focus on the evolution of climate and vegetation during Miocene times, recorded in the sedimentary pre-Siwalik and Siwalik groups. Soil carbonates were analyzed for their $\delta^{18}O$ and $\delta^{13}C$ compositions to track vegetation as a signal of monsoon intensity and seasonality on a timescale of 20 Myr^{-1}. In this chapter, I carried out the analysis and interpretation of the biomarkers.

Ultimately, a final summary and synthesis and outlook about the main research questions will be presented in chapter 5, together with the research implications for paleoclimate and a future scientific outlook.

1.7. Background and setting

1.7.1. Study Area

My research focuses on multiple Himalayan river catchments over a large altitudinal gradient, which are also located along an extensive (~1,250 km) east–west transect (northwest India to eastern Nepal)(figure 1.1.). The Sutlej, Alaknanda, Khudi and Arun rivers are trans-Himalayan rivers that not only individually cover a large elevation (and therefore climate) gradient, but are also located resp. increasingly further from the moisture source (Bay of Bengal). Studying surface water isotope ratios and how these are recorded in bulk organic matter, carbonates, biomarkers and compound specific isotope ratios along a large altitudinal gradient provides the ideal environment to study large variations in climatic conditions (temperature, vegetation, and precipitation) with increasing elevation.

The Himalaya serves as a water supply for nearly one billion people living downstream in India, Nepal, and Bangladesh. Water is transported through some of Asia's major rivers, such as the Indus, Ganges, and Tsangpo-Brahmaputra (Immerzeel *et al.*, 2009; Bookhagen and Burbank, 2010). The geologic evolution of the Himalayas had a major influence on regional climate, which in turn may have influenced erosion rates, precipitation patterns, and vegetation (Yin and Harrison, 2000; Bookhagen *et al.*, 2006).

Since the Indo-Asian collision, major fault zones have accommodated continued convergence along the Himalayan range: the Southern Tibetan Detachment System (STDS), Main Central Thrust System (MCT), Main Boundary Thrust fault (MBT), and the Main Himalayan Frontal Thrust (MFT) as the most southern fault (Gansser, 1964; Yin and Harrison, 2000). The here studied trans-Himalayan rivers, the Sutlej, Alaknanda, Khudi, and Arun all dissect one or more of these major Himalayan geological units.

The Sutlej and Alaknanda catchments are located in India while the Khudi and Arun are in Nepal. The Sutlej is the westernmost river catchment studied in this thesis (Figure 1.1) and also has the largest drainage area of all

four catchments. The drainage area of the Sutlej is ~55,000 km^2, of which ~60% is located on the Tibetan Plateau (Wulf, Bookhagen and Scherler, 2016). The Sutlej River is the largest tributary of the Indus River and has a mean catchment elevation of 4,825 m asl with a catchment-elevation range of 480 to 6,970 m asl.

1.7.1.1. Studied Catchments

Bordering the Sutlej catchment to the southeast is the Alaknanda river catchment, which is one of the headwaters of the Ganges river system. The drainage of the Alaknanda catchment is ~10,000 km^2 and has a mean catchment elevation of 3,148 m asl (ranging from 346–7,495 m asl).

The Khudi catchment is the smallest catchment in this study and drains a total area of only ~137 km^2. The mean catchment elevation of the Khudi is 2,603 m asl with a range of 785–4,159 m asl.

The easternmost catchment studied in this dissertation is the Arun river catchment. The Arun catchment has an approximate size of 33,000 km^2 and drains into the Sapta Kosi, which drains ultimately into the Bay of Bengal. The Arun has a mean catchment elevation of 4,562 m asl, with a range of 193–8,806 m asl.

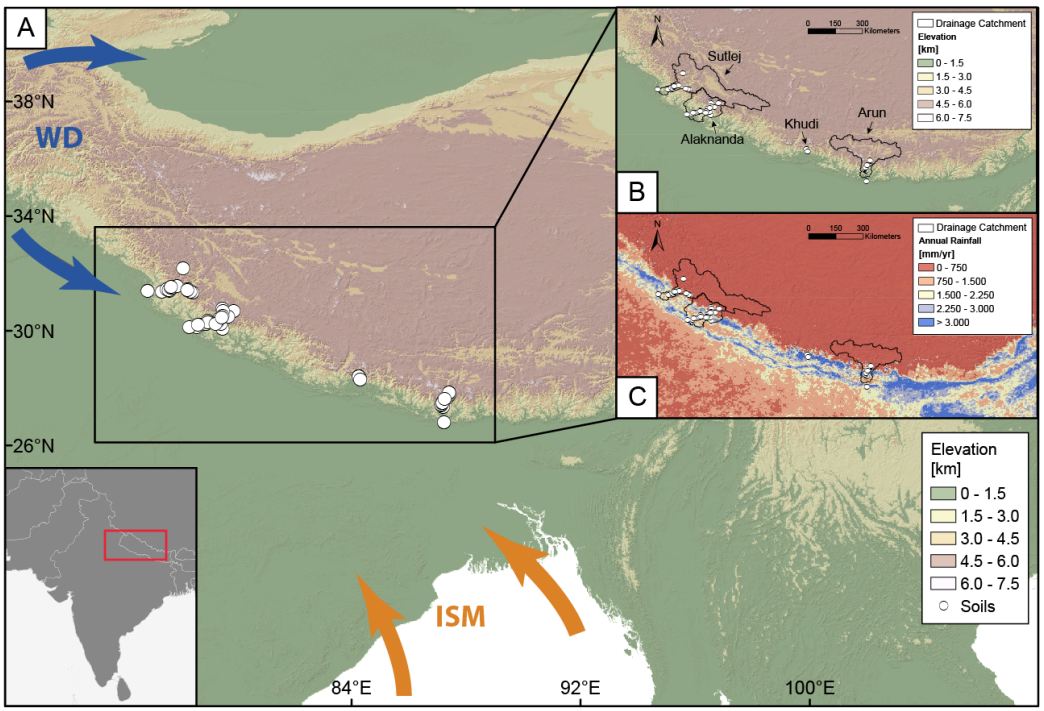

Figure 1.1: Topographic overview of the Himalaya (SRTM V3, (Jarvis et al., 2008), A, B: Topographic overview of the Southern Himalayan Front (SHF), indicating the four altitudinal transects, C: Precipitation amounts were derived from the TRMM 2B31 data product (mean annual average from 1998–2010 (Bookhagen and Burbank, 2010; Huffman et al., 2014)). WD indicates Western Disturbances and ISM indicates Indian Summer Monsoon. White circles indicate sampling locations for surface waters and soils.

1.7.2. Climate

1.7.2.1. Himalayan climate

The Himalaya is the Earth's largest and tallest mountain range that creates an extreme climatic gradient between tropical climate in the foreland and alpine conditions at the highest elevations. Precipitation patterns vary because the Higher Himalaya acts as an orographic barrier between the humid sections in the foreland and the arid sections at higher altitudes (Bookhagen and Burbank, 2010). The precipitation regime in the Himalaya is dominated by two independent systems: the Indian Summer Monsoon (ISM) and the Western Disturbances (WD), which strongly interact with each other (Bookhagen, Thiede and Strecker, 2005; Bookhagen and Burbank, 2010) (Figure 1.1). As monsoonal moisture travels along the SHF (Southern Himalayan Front) and collides with the two high mountain orographic barriers, heavy orographic rainfall occurs in the central Himalaya, resulting in

a 2-belt rainout pattern (Figure 1.1.C) (Bookhagen and Burbank, 2010) (see also paragraph 1.3.). The influence of ISM precipitation that originates from the Bay of Bengal decreases west of the Sutlej valley, after which rainfall is mainly dominated by the WD (Bookhagen and Burbank, 2010). In winter (Dec.–Mar.), the WD brings precipitation in the form of rain and snow, which originates in the Mediterranean, Black, and Caspian seas (Lang and Barros, 2004; Wulf, Bookhagen and Scherler, 2010; Cannon *et al.*, 2016; Norris *et al.*, 2016). Vegetation across the orogen is influenced by both the decreasing temperature from low to high elevation and the decreasing amount of moisture from east to west (Singh and Singh, 1987).

River discharge in the Himalaya is closely coupled with summer rainfall in non-glaciated catchments. In higher elevation catchments in the Himalayan interior, however, snow and glacial melt contribute up to 50% of the annual runoff (Bookhagen and Burbank, 2010; Wulf, Bookhagen and Scherler, 2016). The climatic control on Himalayan river discharge and glaciers varies from east to west. The monsoon weakens from east to west, creating more arid conditions at lower elevations in the west, which results in glacial meltwater as a major component of river discharge in these regions (Rees and Collins, 2006).

1.7.2.2. Climate gradients in the studied catchments

Average annual rainfall amounts show a large altitudinal variation but also a large difference between the four studied river catchments is observed (Fig. 1.1.C). The ISM results in relatively wet regions in eastern India and Bangladesh, which become drier west of the Sutlej valley. In the Sutlej (elevation range 475 – 3,533 m), lower elevation catchments (< 3,000 m asl) receive rainfall amounts between 1,500 and 2,000 mm/year (Bookhagen and Burbank, 2010), which decreases to < 500 mm/year at higher elevation sample sites (> 3,000 m asl). Rainfall between May and October (ISM source) contributes to 38.1% of the total river discharge in the Sutlej River while the annual snowmelt contribution to discharge has been estimated in the range of 57–67% (Singh and Jain, 2007; Wulf, Bookhagen and Scherler, 2016). Temperature also decreases with increasing elevation, ranging between 9.7

and 25.4°C, with an average of 19.7°C (2000–2014 yearly average, MOD11C3, (Wan and Hulley, 2015).

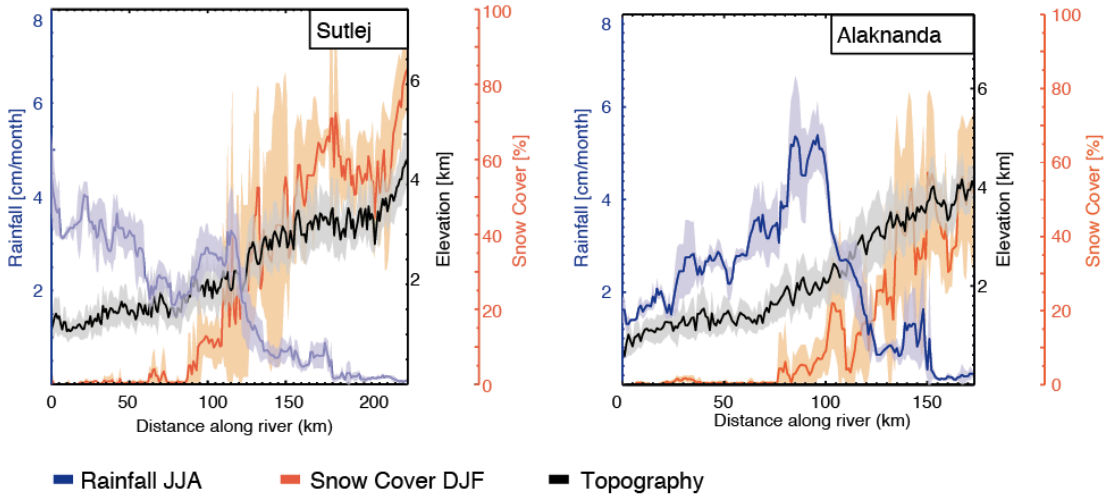

Figure 1.2. 10-km wide swath profiles along Sutlej and Alaknanda rivers in the NW Himalaya. 12-year-average JJA mean TRMM 2B31 precipitation in blue (Bookhagen and Burbank, 2010); 2-year-average (2012-2014) MODIS MYD10CM DJF mean snow cover in orange (Hall and Riggs, 2016), and topography in black with 1-σ standard deviation (gray).

In the Alaknanda (elevation range 346 - 3,155 m), rainfall amounts vary between 300 and 2,600 mm/year and, due to the two-step rise in relief, consist of two rainout belts (at ~500 and ~2,000 m, Fig. 1.1C), which is a phenomenon described in Bookhagen & Burbank (2006). On average, glacial melt has been estimated to comprise 32% of the total surface water discharge (Maurya *et al.*, 2011). Average annual temperatures vary between a minimum of 7.1°C and a maximum of 26.8°C, with a mean annual temperature of 19.8°C (Wan and Hulley, 2015).

The Khudi (elevation range 2,155 – 4,085 m) receives > 3,900 mm/year, which is the highest amount of annual rainfall of the four transects. Despite the steep elevation gradient, there is little precipitation variation in the Khudi catchment, which is mainly due to its location in the second orographic rainout belt of the Himalaya (Bookhagen and Burbank, 2006). The average annual temperature in the catchment varies between 7.5 and 19.5°C, with an average of 13.1°C.

The Arun (elevation range 225 - 2,580 m) catchment shows a range of annual rainfall amounts between 2,000 and 4,000 mm/year. This does not

take into account the very arid Tibetan Plateau area, where precipitation amounts decline to < 300 mm/year. The snowmelt contribution to the annual discharge has been estimated at 24.5% (Bookhagen and Burbank, 2010). The precipitation pattern in the Arun exhibits the same two-belt rainout pattern as the Alaknanda transect (at ~500 and ~2,000 m). Average temperatures in the catchment vary between 3.5 and 26.7°C, with an annual average of 16.3°C.

2. Identifying seasonal snowmelt in the western Himalaya using stable isotopes of modern surface waters and remote sensing

Iris van der Veen[1], Hima J. Hassenruck – Gudipati[3], Taylor Smith[1], Eric Deal[2], Henry Wichura[1], Manfred R. Strecker[1], Bodo Bookhagen[1], Dirk Sachse[4]

[1]Universität Potsdam, Institut für Erd- und Umweltwissenschaften, Karl-Liebknecht-Str. 24-25, 14476 Potsdam-Golm, Germany
(*Correspondence: veen@geo.uni-potsdam.de)
[2]University of Grenoble, ISTerre, BP 53, F-38041 Grenoble, France
[3]Department of Geological Sciences, The University of Texas at Austin, 2275 Speedway, M.S. C9000, Austin, Texas 78712, USA
[4]GFZ German Research Centre for Geosciences, Section 4.6: Geomorphology, Organic Surface Geochemistry Lab Potsdam, Germany

Hydrological Processes, 2020
Revised manuscript HYP-20-1016 submitted on October 30, 2020

Abstract

Global change affects seasonal and annual water storage, especially in high-mountain settings. Discharge from these areas consists of waters from rain, glacial melt, and snowmelt; however, their relative contributions are often unknown. Here, we present a new surface-water δ^2H, $\delta^{18}O$, and *d*-excess dataset from the Western Himalaya to distinguish seasonal water sources and their climatological drivers. The dataset consists of 135 post-monsoon season samples from three river catchments (Sutlej, Beas, and Alaknanda) covering an altitudinal gradient from 457 to 4,417 m asl and two one-yearlong isotope datasets with a weekly sampling interval at 1,900 and 3,285 m asl. We observe that δ^2H values of stream waters sampled in both the Sutlej and Alaknanda elevation transects show a significant negative

correlation with mean-catchment elevation. Both the lower Sutlej (<4,000 m asl) and Alaknanda regions showed a lapse rate of -8.8‰ km^{-1}, while the high-elevation Spiti and Sutlej have a significantly higher lapse rate (-32.7‰ km^{-1}). We argue that Rayleigh distillation processes caused by orographic uplift of Indian Summer Monsoonal (ISM) moisture drive the lapse rate in the lower elevations. In the higher elevations, the isotopic data reflect higher input of westerly-derived winter precipitation, as well as snow and glacial meltwater input affected by post-depositional processes such as sublimation. In the seasonal time series of surface-waters, an increase in *d*-excess during the peak snowmelt season was observed, coinciding with an areal decrease in remote-sensing derived snow-cover data, enabling the use of d-excess as a tracer for snow/ice melt. Our data further indicate a substantial component of snow and ice-melt contribution to annual discharge in high-elevation catchments during spring. In the scope of current climate change and increasing temperatures, these findings can be used to monitor snowmelt timing and the different contributing factors that determine the hydrological budget of Himalayan rivers.

Keywords: stable isotopes, Himalaya, snowmelt, remote sensing, *d*-excess, Indian Summer Monsoon

1. Introduction

The Himalaya supplies water for nearly a billion people living downstream in Nepal, India, and Bangladesh through some of Asia's major rivers such as the Indus, Ganges, and Tsangpo-Brahmaputra (Immerzeel *et al.*, 2009; Bookhagen and Burbank, 2010). In the northwestern Himalaya, future changes in hydrology have been predicted under the influence of global climate change, where increasing temperatures at high elevations may temporarily increase the relative contribution of snowmelt to surface-waters (Winiger *et al.*, 2005; Immerzeel *et al.*, 2009; IPCC, 2014; Smith and Bookhagen, 2018). The Himalayan mountain belt exhibits spatially heterogeneous precipitation patterns due to complex topography and

multiple, interacting moisture sources (Bookhagen and Burbank, 2010). Regional hydrology is complicated by the existence of extensive water reservoirs in the form of groundwater, snow, and glacial ice (Karim and Veizer, 2002; Immerzeel *et al.*, 2009; Bookhagen and Burbank, 2010; Andermann *et al.*, 2012; Wulf *et al.*, 2016). A more refined understanding of the spatial and temporal changes of water contributions from these different sources and drivers of change is essential to predict varying water budgets under climate-change scenarios.

Stable isotope ratios (expressed as δ^2H and $\delta^{18}O$ values) of meteoric waters are commonly used as tracers of atmospheric and hydrologic processes and thus can be employed to understand processes in the global hydrological cycle (Dansgaard, 1964; Gat, 1996; Fröhlich, 2001). For example, stable isotopes have been used to constrain temporal and spatial variability in precipitation or to differentiate between different moisture sources (Rohrmann *et al.*, 2014). These techniques have also been applied to surface-waters for hydrograph separation (Karim and Veizer, 2002; Maurya *et al.*, 2011), paleoclimate reconstructions from ice cores (Petit *et al.*, 2004), and marine and lacustrine sediment cores (Sarkar *et al.*, 2015). Moreover, stable isotopes are also used as an input for hydrological modeling and weather models, which requires a sound understanding of isotope-fractionation processes (Bowen and Revenaugh, 2003; Norris *et al.*, 2016).

Surface waters from streams are often used to track catchment-integrated precipitation signals, in particular in remote mountainous areas, where meteorological stations are scarce (Hren *et al.*, 2009). Numerous studies which relied on stable isotopes obtained from stream waters have been carried out along altitudinal gradients in the Himalaya to constrain moisture sources (Garzione *et al.*, 2000; Karim and Veizer, 2002; Hren *et al.*, 2009; Maurya *et al.*, 2011; Bershaw *et al.*, 2012). These studies have generally observed a linear relationship between $\delta^2H/\delta^{18}O$ values of meteoric waters and elevation, with decreasing δ^2H values at higher elevations, due to decreasing temperatures and progressive rainout processes (Poage and Chamberlain, 2001; Rowley *et al.*, 2001; Hren *et al.*, 2009; Bershaw *et al.*,

2012). However, observations show increasing scatter of δ^2H and $\delta^{18}O$ values on the Tibetan Plateau (Hren et al., 2009; Bershaw et al., 2012), some data suggesting an increase toward more positive values (Bershaw et al., 2012), likely reflecting additional processes and/or water sources are relevant in the lee of the orographic barrier. In particular, post-depositional alteration (snow and glacial melt) and the relative input of different water sources have been suggested to affect the isotopic composition of these stream waters (Lechler and Niemi, 2012; Racoviteanu *et al.*, 2013; Biggs *et al.*, 2015).

The combined measurements of δ^2H and $\delta^{18}O$ lead to the second-order proxy parameter *d*-excess, which is used to provide additional constraints on hydrological processes, due to differences in the sensitivity of stable H and O isotopes to hydrological processes (Gat and Confiantini, 1981; Fröhlich, 2001; Risi *et al.*, 2013). *D-excess* has for example been used to distinguish between moisture sources and assess atmospheric circulation shifts in the Himalaya (Sengupta and Sarkar, 2006; Pang *et al.*, 2012), but also to study isotopic effects during snow formation and snow melt (Moser and Stichler, 1974; Jouzel and Merlivat, 1984; Stichler *et al.*, 2001). However, due to different environmental processes influencing *d*-excess, its interpretation remains complex. A significant influence on *d*-excess by sublimation in snowpack has been observed, resulting in isotope enrichment in the snow/glaciers (Moser and Stichler, 1974; Stichler *et al.*, 2001), which subsequently is propagated into surface-waters due to melting processes (Lechler and Niemi, 2012).

In this study, we aim to constrain the different hydrological components that contribute to the isotopic signature of surface-waters over an altitudinal gradient in three Himalayan catchments. We combine stable-isotope chemistry and satellite-derived climate data including MODIS snow cover (Hall and Riggs, 2016), Tropical Rainfall Measurement Mission (TRMM) precipitation (Huffman *et al.*, 2014), and Advanced Microwave Scanning Radiometer Earth Observing System (AMSR-E) derived Snow Water Equivalent (SWE) data (Wentz *et al.*, 2014). Additionally, we analyze two one-year-long, surface-water isotope time series with weekly sampling intervals

from different locations and compare them to satellite data to test if snowmelt in spring has a significant impact on the surface-water isotope composition.

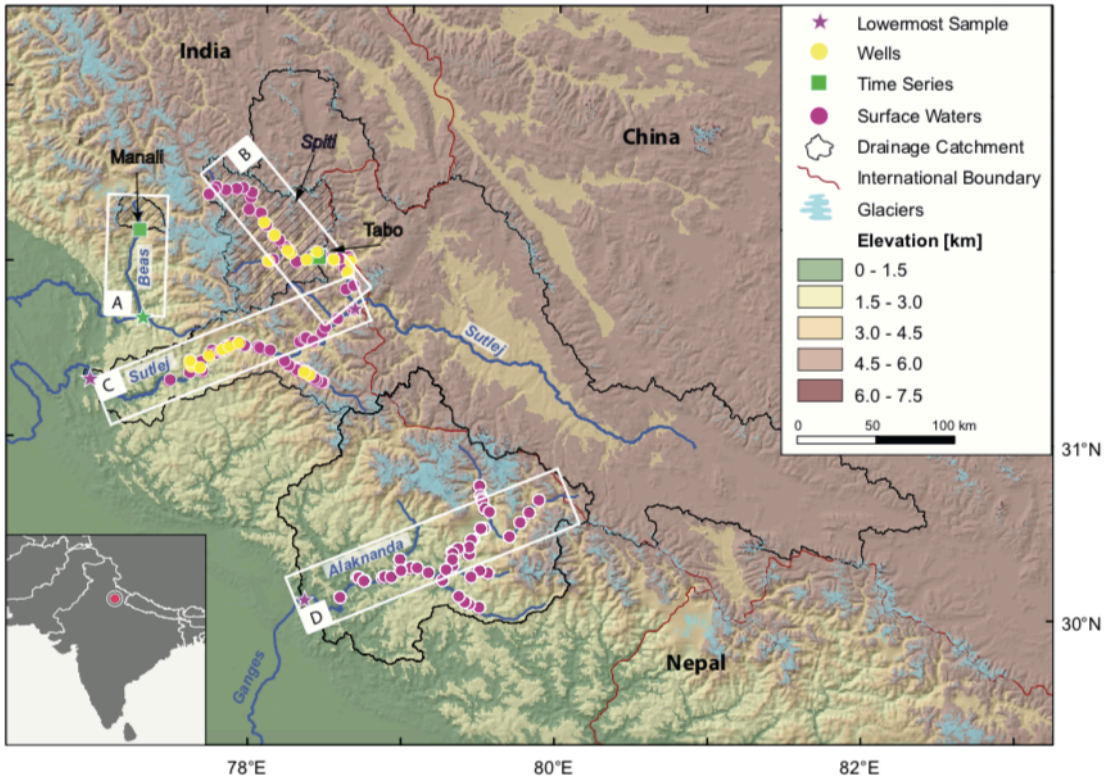

Figure 2.1: Topographic overview of study area. SRTM V4.1 DEM (Jarvis *et al.*, 2008) with river names in blue; pink circles are surface-water samples; yellow circles are well samples; green squares are locations of the one-year long river water time series with weekly sampling interval. The Spiti and Beas catchments are outlined by hatched polygons; light-blue shaded areas are glaciers from the GLIMS dataset (Pfeffer *et al.*, 2014). White rectangles indicate areas over which the swath profiles (elevation, rainfall and snow cover) were determined, and labeling corresponds to the swath profiles shown in Fig. 2. The lowermost sample in the river from which the swath profiles were determined is indicated with a star. Red lines indicate international borders.

2. Geographic setting and climate of the study area

The study area consists of three river catchments located in the western Himalaya (Fig. 1): the Sutlej, Beas, and Alaknanda rivers. The Sutlej and Beas rivers drain into the Indus catchment, while the Alaknanda River drains into the Ganges River system. Alongside the large altitudinal range covered by these catchments (between ~500 and ~7,000 m asl), temperature, glacial coverage, snow cover and snow-water equivalent (SWE), and monsoon precipitation are spatially and temporally heterogeneous (Fig. 2). In previous

studies, the Indus catchment was found to be highly dependent on glacier and snowmelt in order to maintain its baseflow (Ives and Messerli, 1990; Immerzeel *et al.*, 2009; Smith and Bookhagen, 2018). Both the Indian Summer Monsoon (ISM) and the Winter Westerly Disturbances (WWD) influence the precipitation regime of the Sutlej, Beas, and Alaknanda catchments. ISM rainfall contributes 57.1%, 30.6%, and 52.4% of the annual precipitation during the monsoon (JJA) in these catchments, respectively (leaving snowfall out of consideration). These estimates are based on satellite TRMM (Bookhagen and Burbank, 2010) and rain-gauge data (Wulf *et al.*, 2010); the main source of this rainfall is moisture sourced from the Bay of Bengal (Bookhagen and Burbank, 2010).

Average WWD rainfall (DJF) contribution to the Sutlej, Beas, and Alaknanda catchments is estimated to be 8%, 13.6%, and 6.6% of mean annual rainfall, respectively (TRMM 12-year average,(Bookhagen and Burbank, 2010). Large rainout belts can be found along the southern Himalayan front due to orographic lifting of ISM moisture, and ISM rainfall penetrates only episodically farther north into the valleys (Bookhagen *et al.*, 2005a; Wulf *et al.*, 2016).

The Sutlej River is the largest tributary of the Indus River, with an area of approximately 52,000 km^2 (upstream from the most distant downstream point, see Fig. 1). The Sutlej catchment has a mean elevation of 4,825 m asl, with the upper 60% of the area being located on the Tibetan Plateau and an overall elevation range of 480 to 6,970 m asl. The largest tributary of the Sutlej River is the Spiti River, which flows in a southeastward direction, located in the higher elevations (2,550 to 6,709 m asl) of the catchment. The ISM-derived rainfall between May and October contributes 38.1 % of the total river discharge in the Sutlej River, while the total annual snowmelt contribution to discharge was estimated to be between 57 % and 67 % (Singh and Jain, 2007; Wulf et al., 2016). More specifically, in the lower Sutlej catchment (<4,000 m asl), annual rainfall reaches 1,800 mm, of which 50 % falls in summer (JJA) during the ISM (Bookhagen and Burbank, 2010). The upper Sutlej catchment (>4,000 m asl) only receives a maximum of 200

mm/yr, of which only 20% falls in summer (TRMM 12-year average,(Bookhagen and Burbank, 2010). In the Spiti catchment, rainfall ranges between 40–200 mm/yr. The ISM-derived rainfall between May and October contributes 38.1 % of the total river discharge in the Sutlej River, while the total annual snowmelt contribution to discharge was estimated to be between 57 % and 67 % (Singh and Jain, 2007; Wulf *et al.*, 2016). The glacial cover in the entire Sutlej catchment is 3.5 %, while the Spiti sub-catchment has a glacial cover of 6.7 % (Pfeffer *et al.*, 2014).

Bordering the lower Sutlej catchment to the northwest is the Beas catchment (cf. Fig. 1), with a size of 5,300 km^2, of which the glacial coverage is 6.7% (Pfeffer *et al.*, 2014). The Beas catchment receives an average of 1,100 mm/yr of rainfall, of which 30% falls in JJA, and 13% in DJF (TRMM 12-year-average,(Bookhagen and Burbank, 2010). The average snow and glacial melt component of the Beas river discharge has been estimated to be 5% in the period between 1990 and 2004 (Kumar *et al.*, 2007).

The Alaknanda catchment is located southeast of the Sutlej catchment, and has a size of 10,000 km^2 (calculated upstream from the most distant downstream point; see Fig. 1). The lower Alaknanda and its tributaries receive 2,800 mm of annual rainfall (55 % of it during JJA), while in the upper tributaries rainfall amounts are below 350 mm/yr (TRMM 12-year-average,(Bookhagen and Burbank, 2010). The Alaknanda catchment has an average glacial coverage of 10.4 %, and glacial melt has been estimated on average to be 32 % of the total surface-water discharge (Maurya *et al.*, 2011).

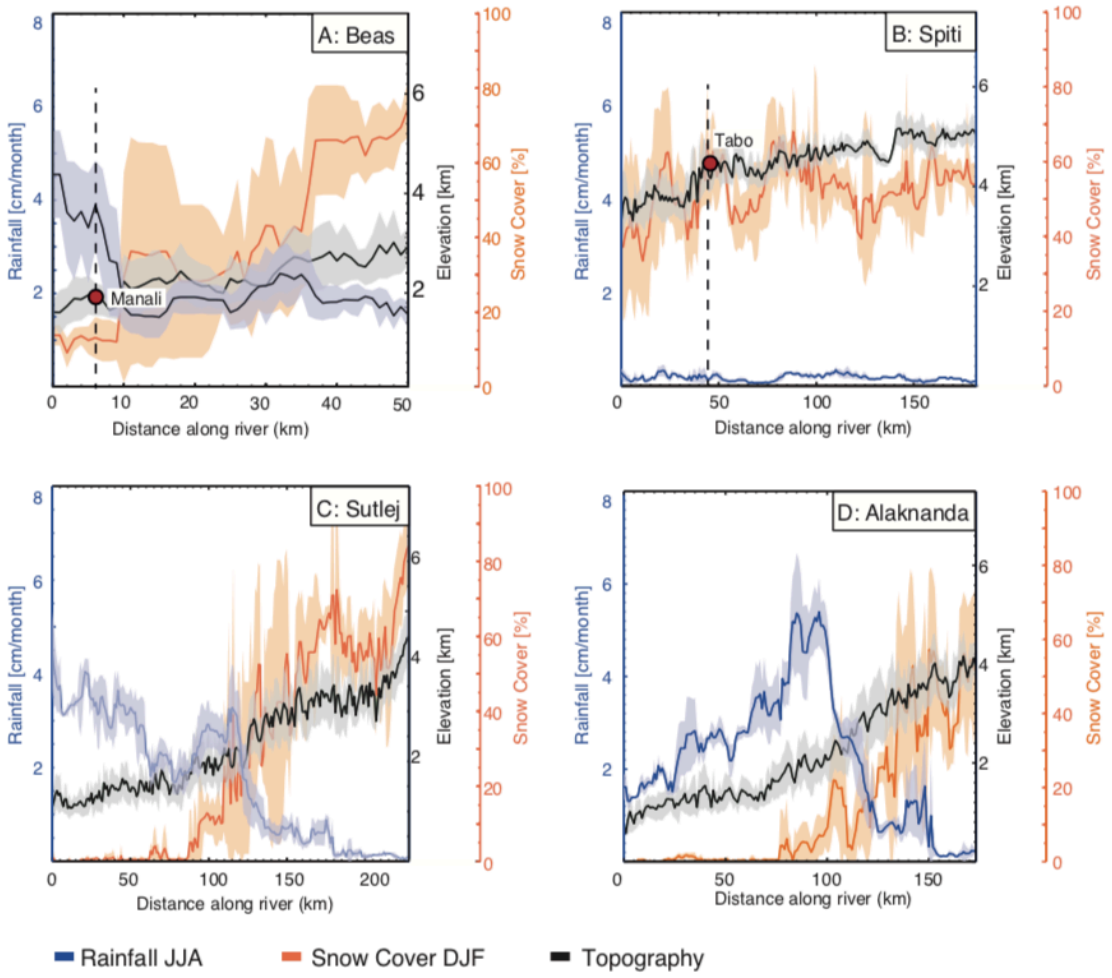

Figure 2.2: 10-km wide swath profiles along three rivers in the NW Himalaya (Spiti and Sutlej visualized as separate catchments; cf. Fig. 1); 12-year-average JJA mean TRMM 2B31 precipitation in blue (Bookhagen and Burbank, 2010); 2-year-average (2012-2014) MODIS MYD10CM DJF mean snow cover in orange (Hall and Riggs, 2016), and topography in black with 1-σ standard deviation (gray). Red dots indicate location of villages where one-year long sampling has taken place.

3. Methods

3.1. Sampling methods

Water samples from main rivers and their major and minor tributaries in the Sutlej catchment were collected in September 2014 during the post-monsoon season. The Alaknanda area was only sampled during the post-monsoon season in October 2014. There were no significant precipitation events during both fieldwork campaigns. In addition, water from water pumps for drinking water in the Sutlej catchment was sampled to assess the isotopic composition of local groundwater. All pump samples were located

within ~100 m of the river and were reported to vary in depth between 35 and 70 m by the irrigation and public health authorities of the state of Himachal Pradesh. Weekly sampling of surface-water was carried out at two locations in the Sutlej/Spiti (Tabo, 32.091918°N, 78.382793°E, 3,280 m asl) and Beas catchments (Manali, 32.205024°N, 77.189648°E, 2,050 m asl) in 2013/2014 (Fig. 1). Each sample was filtered through a 0.45 µm syringe filter in the field and stored in 2 ml vials. The surface-water samples were taken between September 2013 and September 2014.

3.2 Stable water isotope measurements

The hydrogen and oxygen stable isotope composition of waters were measured on a Picarro Cavity Ringdown Spectrometer L2140-I at GFZ Potsdam in Germany. The stable isotope composition is reported using the δ-notation relative to the Vienna Standard Mean Ocean Water (VSMOW) standard as:

$$\delta[‰] = \left(\frac{R_{Sample}}{R_{Standard}} - 1\right)[Equation1]$$

In which *R* represents the ratio of heavy isotopes relative to light isotopes ($^{18}O/^{16}O$ and $^{2}H/^{1}H$), and all values are reported in ‰. In addition, we calculate the second-order isotopic parameter *d*-excess, which is defined by (Dansgaard, 1964):

$$d - excess[‰] = \delta^{2}H - 8{\times}\delta^{18}O[Equation2]$$

The instrument precision was 0.08 ‰ for $\delta^{18}O$ and 0.5 ‰ for $\delta^{2}H$ based on long-term standard measurements. Samples were injected 10 times, in a volume of 1 µl, while the first three injections were discarded for each sample, to avoid any memory effect. The measurements were normalized using a two-point calibration from VSMOW2 and SLAP2 standards, provided

by the IAEA. The 1-s standard deviation was determined from the seven measurements of the $\delta^{18}O$ and $\delta^{2}H$ isotopic values.

3.3 Topographic and climatic remote-sensing data processing

The watersheds and their corresponding mean-catchment elevations were determined using the 90-m SRTM Digital Elevation Model (SRTM V4.1 DEM; (Jarvis *et al.*, 2008); swath data (see Figure 2) were created using TopoToolbox (Schwanghart and Scherler, 2014). Seasonal and annual rainfall were determined using the Tropical Rainfall Measurement Mission (TRMM) 2B31 data product, averaged over the 1998-2012 period (Bookhagen and Burbank, 2010), with a spatial resolution of ~5 km. The monthly snow-cover data between December 2012 and 2014 was obtained from the Moderate Resolution Imaging Spectroradiometer (MODIS) dataset MYD10CM (Hall and Riggs, 2016), with a spatial resolution of 0.05° (~5 km). Snow Water Equivalent (SWE) was obtained from the AMSR2 satellite (Wentz *et al.*, 2014; Smith and Bookhagen, 2016), with a spatial resolution of 0.25° (~25 km). The melt rate was determined from the instantaneous slope (1-month window) of the monthly catchment summed SWE volume, to quantify the change in SWE in the catchment. In order to determine the percentage of glacial coverage in each catchment, the Global Land Ice Measurements from Space (GLIMS5) dataset was used (Pfeffer *et al.*, 2014).

3.4. Statistical data evaluation

To determine turning points in the elevation-isotope relationships we used a mean-shift model (Chen and Gupta, 2012). We determined locations of significant shifts in the series mean using a simple cumulative sum of differences between values and the data mean. We then identified breakpoints where a piecewise fit better explains the relationship between elevation and isotopic signature or *d*-excess than a simple linear regression.

3.5. Rayleigh model

A Rayleigh distillation model was developed to predict the evolution of precipitation water δ^2H values during rainout from ISM moisture moving up the valleys, which was modified after (Rowley *et al.*, 2001)) and Rowley (2007). This model describes the progressive isotopic depletion of the remaining reservoir in atmospheric moisture during transport, from which condensation occurs (Rowley *et al.*, 2001). The model variables and a more extensive description of the model can be found in the Supplementary Material.

4. Results

4.1. Surface-water stable oxygen and hydrogen isotope ratios

Measured $\delta^{18}O$ values varied between -6.6 ‰ and -15.5 ‰ in the Sutlej surface-waters, and -8.0 ‰ and -14.6 ‰ in the Alaknanda surface-waters (Figure 3). The $\delta^{2}H$ varied between -37.4 ‰ and -112.4 ‰ in the Sutlej and -51.6 ‰ and -102.2 ‰ in the Alaknanda. The slope of the $\delta^{18}O$ vs. $\delta^{2}H$ relationship in the Sutlej (8.25) catchments falls relatively close to the slope of the Global Meteoric Water Line (GMWL), while the slope in the Alaknanda catchment (7.07) is lower than the GMWL. The GMWL has been defined as: $\delta^{2}H = 8.17 (\pm 0.06) \times \delta^{18}O + 10.35 (\pm 0.65)$ ‰ (Rozanski *et al.*, 1993). The intercept of the Sutlej LMWL (18.08±1.01) is substantially higher compared to the GMWL (10.35±0.65), while the Alaknanda intercept (3.3±1.13) is substantially lower compared to the GMWL.

In both the Alaknanda and Sutlej catchments, $\delta^{2}H$ and $\delta^{18}O$ values showed a significant negative linear correlation with mean catchment elevation (Figure 4). Isotope values of surface waters were compared to mean-catchment elevation, since the source of the surface water integrates over the entire upstream catchment. In the Sutlej, there was a larger amount of scatter between $\delta^{2}H/\delta^{18}O$ and mean-catchment elevation, which was especially noticeable in samples with mean-catchment elevations above 4,000 m asl. The isotopic-lapse rate for $\delta^{2}H$ in the Sutlej was -8.8±1.8 ‰ km^{-1} (from 0 to 4,106 m asl) and -32.7±8.6 ‰ km^{-1} (from 4,106 to 6,000 m asl). The $\delta^{2}H$ lapse rate of the entire Sutlej elevation-transect was -17.4±0.1 ‰ km^{-1}. In the case of $\delta^{18}O$ versus elevation, the lapse rates for the lower Sutlej, upper Sutlej, and entire Sutlej were -1.5±0.2 ‰ km^{-1}, -3.9±1.2 ‰ km^{-1} and -2.2±0.1 ‰ km^{-1}, respectively. In the Alaknanda, no significant breakpoint was found using a mean-shift model in $\delta^{2}H$, and the isotopic lapse rate in all surface-water samples in the catchment was -8.8±0.1 ‰ km^{-1} for $\delta^{2}H$. In $\delta^{18}O$ versus elevation in the Alaknanda, a lapse rate of -0.7±0.3 ‰ km^{-1} was found in the lower Alaknanda (from 0 to 2,574 m asl) and -1.6±0.2 ‰ km^{-1} in

the upper Alaknanda (>2,574 m asl). The lapse rate for the entire Alaknanda transect was -1.3±0.07 ‰ km^{-1}.

In general, most of the isotope values were situated within the mean and standard deviation of the Rayleigh distillation model (Fig. 4, see Tab. 1 and supplementary material for model and parameter details). This shows that the data are controlled by Rayleigh distillation; describing the partitioning of isotopes between two reservoirs, as one reservoir decreases in size (in this case the cloud travelling up the orogen). The high-elevation samples of the Sutlej samples fall above the Rayleigh model, suggesting non-Rayleigh processes in these catchments.

In addition to δ^2H and $\delta^{18}O$, *d-e*xcess values were determined (Figure 5). In the Sutlej, *d*-excess values increased from 12.3 ‰ to 18.5 ‰, up to mean-catchment elevations of 3,800 m asl in the Baspa River tributaries, where snow and glacial cover is high. Between 3,800 and 5,300 m asl, the *d*-excess values showed a decrease from 18.5 ‰ to values as low as 8.5 ‰ (Figure 5). In the Alaknanda catchment, values ranged from ~10 ‰ in the lower Alaknanda tributaries to ~15 ‰ in the upper Alaknanda. A significant positive correlation between *d*-excess (equation 2) and mean-catchment elevation was observed in the Alaknanda surface-waters, but not in the complete dataset of the Sutlej surface-waters ($R^2_{Sutlej\ \ Spiti}$<0.1 and $R^2_{Alaknanda}$=0.65, p<0.001). In the Sutlej surface waters, a positive correlation was observed between *d*-excess and mean-catchment elevation in the surface waters up to elevations of the calculated breakpoint at 4,153 m asl.

Water from the wells in the vicinity of the main stem in the Sutlej catchment showed isotopic δ^2H values comparable to the surface waters, between -49 ‰ in the lower Sutlej and -111 ‰ in the upper Spiti catchment (Fig. 6A). In a similar fashion, the *d*-excess of both the well and tributary samples were compared, and well samples show the same trend with elevation as the tributaries (Fig. 5A and 6B). In order to compare well samples and surface-water samples, both datasets were plotted versus sample-site elevation, since no information on the catchment size or elevation of the wells was available. The gap in well samples between 1,500

m and 2,500 m asl (Fig. 6A and B) was caused by an absence of wells in this elevation range.

A compilation of our surface-water data together with the available data in the Himalaya and on the Tibetan Plateau is shown in figure 8 (Hren et al 2009, Meese et al 2018). In figure 8B, the Rayleigh distillation is shown with the same curve as figure 4A and 4C. In figure 8C the *d*-excess values of surface-waters are plotted with mean catchment elevation. The same increasing amount of scatter above 4,000 m asl as in the Sutlej and Alaknanda dataset is shown in the compiled dataset.

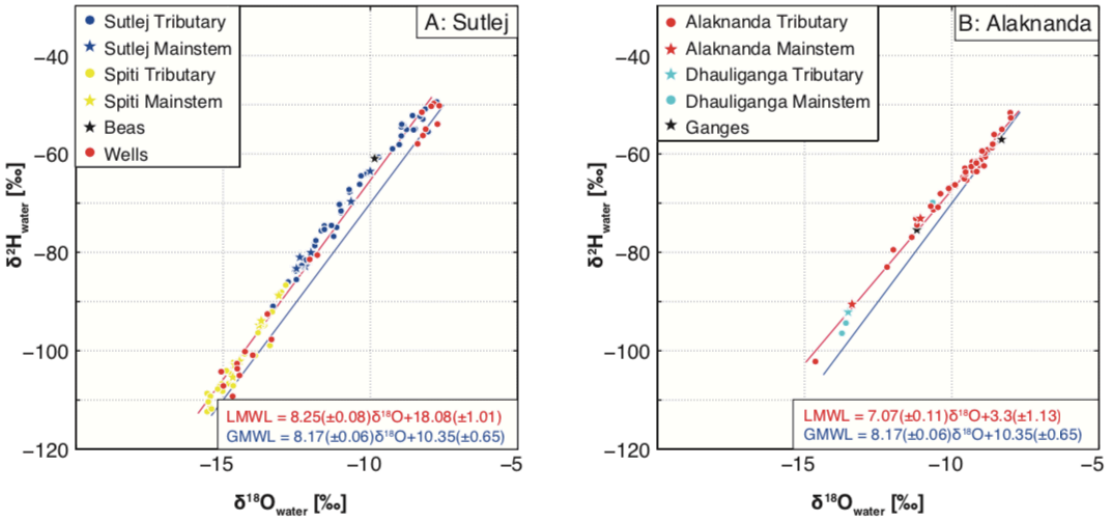

Figure 2.3: δ²H values versus δ¹⁸O values in surface-waters for the Sutlej and Alaknanda catchments. The blue line indicates the Global Meteoric Water Line (GMWL; (Rozanski *et al.*, 1993), and the red line indicates the Local Meteoric Water Line (LMWL).

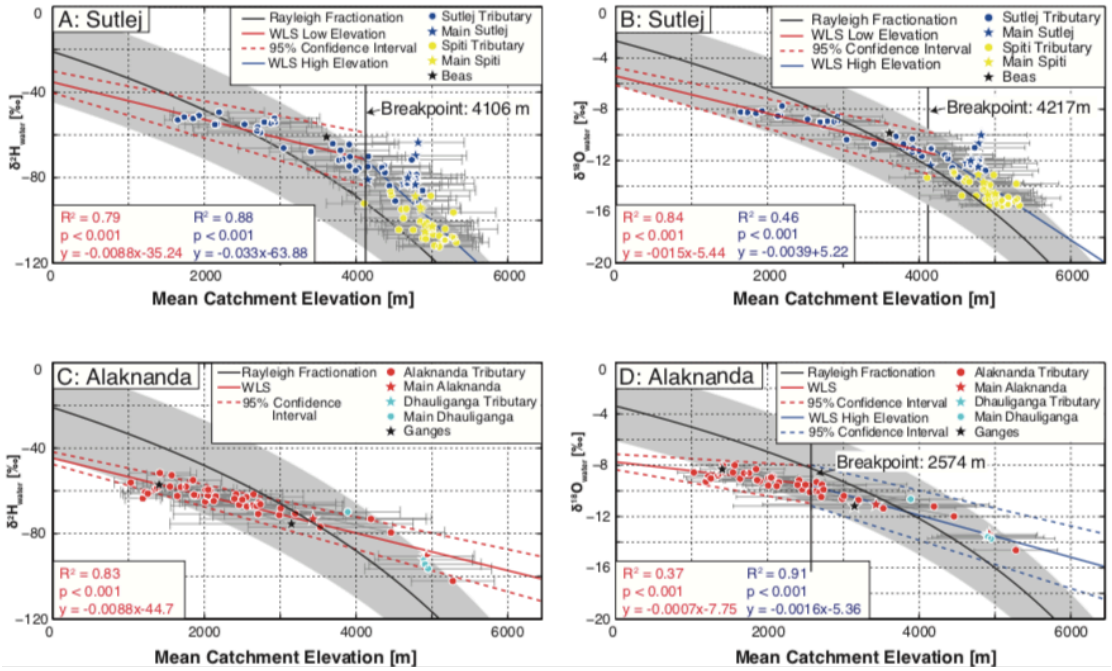

Figure 2.4: $\delta^{2}H/\delta^{18}O$ values in surface-waters versus mean-catchment elevation in the Sutlej (A, B) and Alaknanda (D, C) catchments in 2014. Tributaries are indicated with circles, main-stem samples with stars. The x-error bars show the standard deviation of the mean-catchment elevation in each catchment. Analytical uncertainties of stable-isotope measurements (y-error bars) are too small to show. R^2 and *p* values were determined using a weighted least squared regression (WLS, solid line), red dashed line is the WLS 95 % confidence interval. The Rayleigh fractionation curve (gray shading) is the standard deviation of the variation in model results based on the possible ranges of initial conditions has been calculated according to (Rowley *et al.*, 2001). In order to determine breakpoints in the elevation relationships we used a mean-shift model, and locations of significant shifts in the series mean were determined using a simple cumulative sum of differences between values and the data mean. A significant change in slope was found for the Sutlej at 4,106 m asl, but no significant breaks were found for the Alaknanda surface-water samples.

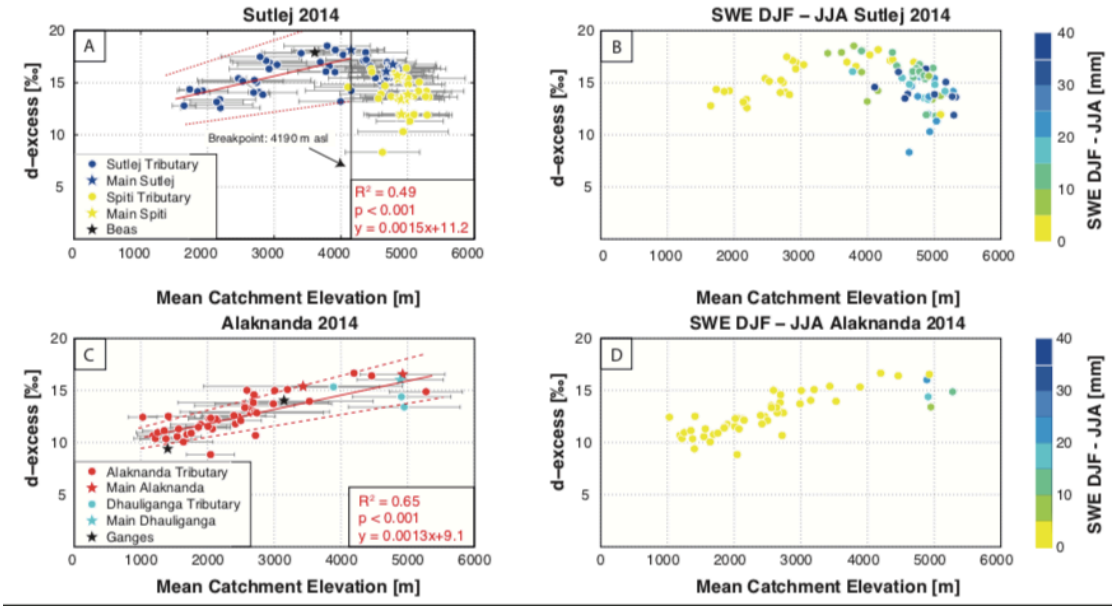

Figure 2.5: *d*-excess values of surface-waters in the Sutlej (A, B) and Alaknanda (C, D) catchments. Circles indicate tributaries, and stars indicate main-stem samples. B and D show the correlation between *d*-excess and mean-catchment elevation, in which symbols are colored by the absolute differences between satellite-derived Snow Water Equivalent (SWE) in DJF and JJA per catchment, indicating the amount of snowmelt generating runoff in the catchments. Regressions in A and C were

calculated with a weighted least square regression, where the dotted line shows the 95% confidence intervals. X-error bars show the standard deviation of the mean elevation in each catchment, y-error bars are too small to show. In order to determine breakpoints in the elevation relationships we used a mean-shift model, and locations of significant shifts in the series mean were determined using a simple cumulative sum of differences between values and the data mean. A significant breakpoint was found for the Sutlej at 4,190 m asl, but no breakpoint was found for the Alaknanda catchment.

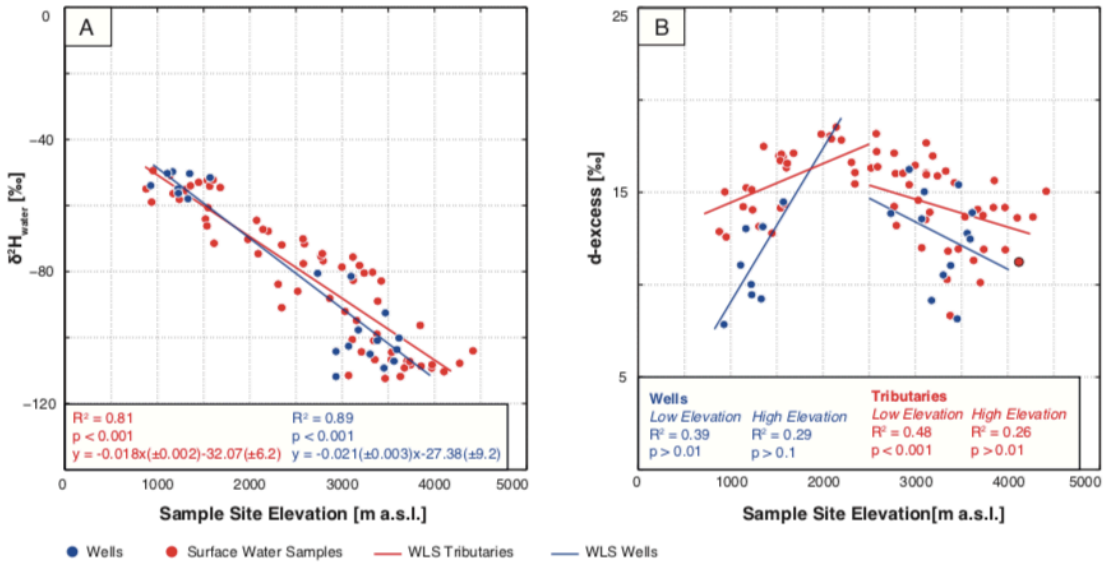

Figure 2.6: A. δ·H values of surface- water samples from tributaries in the Sutlej and Spiti catchments plotted alongside deep well samples from the Sutlej and Spiti catchments. B. *d*-excess values of surface- water samples from tributaries in the Sutlej and Spiti catchments plotted alongside deep well samples from the Sutlej and Spiti catchments. Note that the x-axis shows sample-site elevation (and not mean-catchment elevation as shown in Figure 4). Regressions (solid line) were determined with a weighted least square regression.

4.2. Time series

In the weekly samples from the Spiti River (Fig. 1) δ^2H values ranged between -109.5 ‰ in May 2014 and -101.26 ‰ in February 2014 and *d*-excess values varied from 3.7–20.9 ‰. In the Beas River δ^2H values varied from -72.1– -49.5 ‰, and *d*-excess from 17.6–21.6 ‰, and (Fig. 7B and D). The δ^2H time series showed a relatively stable signal throughout the year, with incidental isotopic excursions of ~5 ‰ (Figure 7B).

d-excess in the Spiti River exhibited values below 15 ‰ in fall/winter but increased towards 20 ‰ over the spring/summer months. In February 2014 there is one large negative excursion, where the *d*-excess values were measured at 3,7 ‰, (±0.9). Snowmelt was highest between February and May, where the largest increase in *d*-excess was observed (Fig. 7D). However, there is a shift in *d*-excess at the onset of satellite-derived data on

snowmelting, where the maximum is reached only 3 months later (early July). The duration of both the snowmelt increase and *d*-excess increase is ~4 months.

D-excess values in the Beas catchment showed a similar, but more subdued trend compared to the Spiti surface-waters (Fig. 7A and C). From fall of 2013 to spring of 2014, values fluctuated between 17 ‰ and 19 ‰, after which there was an increase to a maximum value of 22 ‰ during the summer months. Even though the Beas catchment is significantly smaller and has lower SWE amounts, the timing of the *d*-excess increase coincides with the *d*-excess increase in the Spiti catchment (Fig. 7C). The δ^2H amounts showed an increase in values during spring with 5–10 ‰ negative excursions from spring 2014 to early fall.

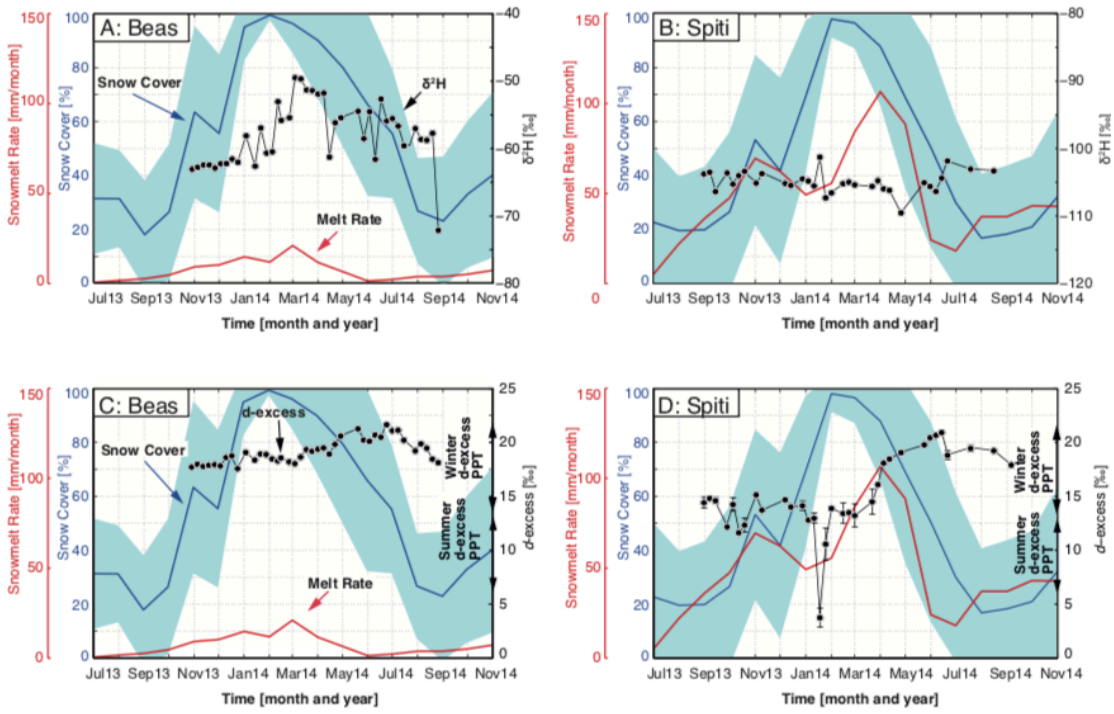

Figure 2.7: δ·H and *d*-excess time series for the Spiti catchment (Tabo; B and D), and Beas catchment (Manali; A and C) of weekly surface-water data sampled in 2013 and 2014, indicated by black circles. Red line indicates the snowmelt-rate curve, determined from the instantaneous slope (1-month window) of the monthly catchment-summed Snow Water Equivalent (SWE) volume (Wentz *et al.*, 2014). The blue line represents the snow cover in % in the catchment (MYD10CM data product, with the corresponding standard deviations (Hall and Riggs, 2016). Winter precipitation *d*-excess was determined from 18 precipitation samples (Tian *et al.*, 2007; Kumar *et al.*, 2010), and summer precipitation *d*-excess was based on 36 precipitation samples (Tian *et al.*, 2007; Kumar *et al.*, 2010). Note that the y-axis for δ·H in A and B are plotted on different scales.

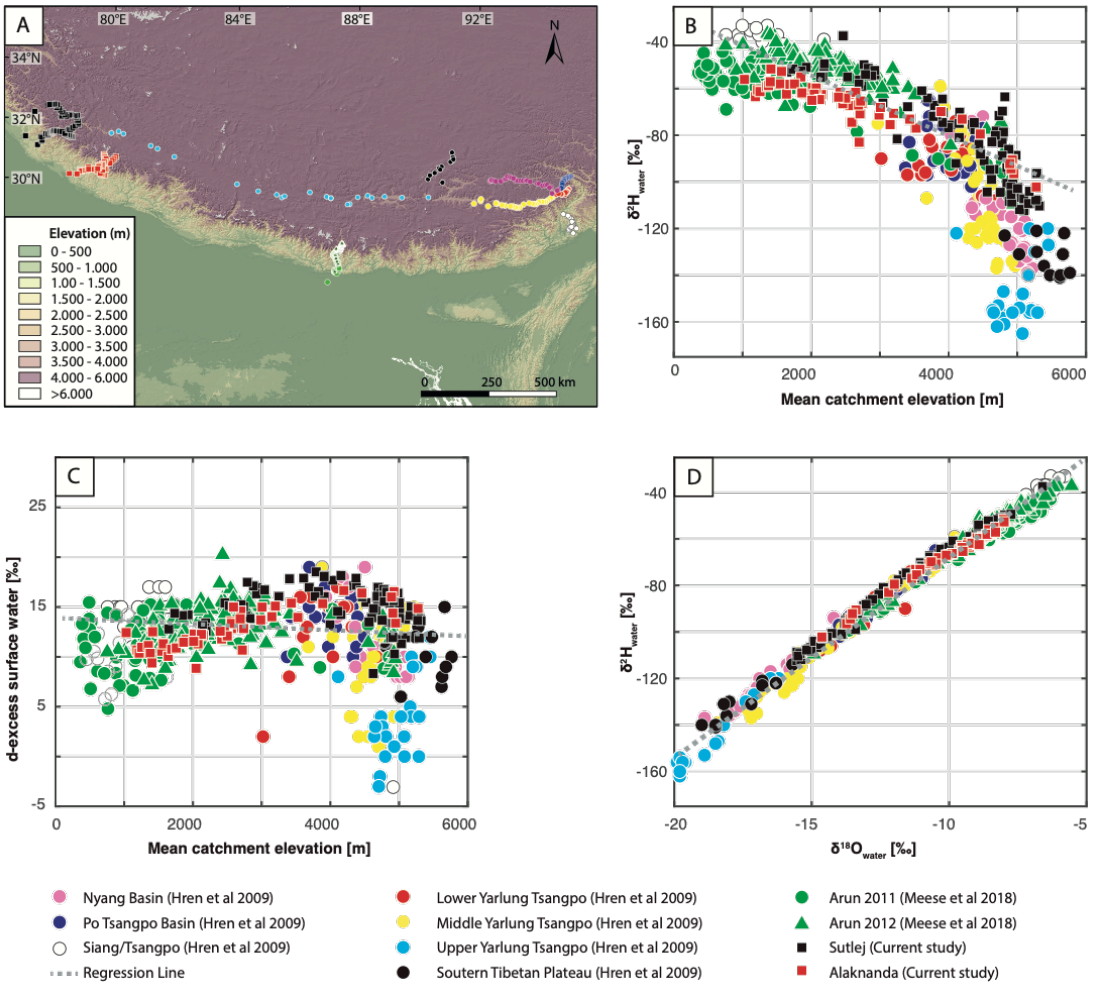

Figure 2.8: A: Topographic overview of study area. SRTM V4.1 DEM (Jarvis *et al.*, 2008). B: Overview of δ·H values in surface-waters versus mean-catchment elevation in the Sutlej, Alaknanda and nearby Himalayan surface water studies from Meese et al 2018 and Hren et al 2009. C: *d*-excess values in surface-waters versus mean-catchment elevation in the Sutlej, Alaknanda and nearby Himalayan surface water studies from Meese et al 2018 and Hren et al 2009. D: δ·H values versus δ·O values in surface-waters for nearby Himalayan surface water studies from Meese et al 2018 and Hren et al 2009.

5. Discussion

5.1. Controls on surface-water isotope composition

For a rigorous interpretation of the spatial and temporal distribution of surface-water δ^2H values, the relative importance of different processes affecting isotope ratios needs to be understood. In the monsoon-dominated parts of the catchments, precipitation will likely be the main source of surface-waters, either directly as surface runoff, or indirectly as groundwater discharge. Importantly, based on well data from the study area, the isotopic composition of groundwater is identical to that of surface waters during sample collection, suggesting that aquifers are mainly recharged by monsoonal precipitation (Fig. 6).

5.1.1. Local meteoric water line versus global meteoric water line

The slope of the Local Meteoric Water Line (LMWL) in the Sutlej (8.25 ‰ km^{-1}) is just outside of the error range of the GMWL (Figure 3A; (Rozanski *et al.*, 1993), and close to previously observed slopes in the vicinity of the study area of 8.5 ‰ km^{-1} (Hren *et al.*, 2009; Varay *et al.*, 2017). However, the intercept of the Sutlej LMWL (18.08±1.01) is significantly higher compared to the GMWL (10.35±0.65). High slope and intercept in LWML have been previously observed in studies located in this area (Pande *et al.*, 2000; Hren *et al.*, 2009; Rai *et al.*, 2016; Varay *et al.*, 2017). The high intercept has been attributed to input from precipitation in the form of snow, originating from the WWD. As such, the high intercept in the Sutlej LMWL is most likely a consequence of the high percentage of glacial and snow-meltwater input to the river.

The LMWL slope and intercept in the Alaknanda surface waters is lower compared to the GMWL and the LMWL in the Sutlej (Fig. 3B). Low LMWL slope and intercept have been identified before at two locations in the Alaknanda region: 5.4 ‰ km^{-1} from a time series in Rishikesh (Maurya *et al.*, 2011), and varying between 5.6 ‰ km^{-1} and 7.0 ‰ km^{-1} from a timeseries in

the Yamuna river, located in between the Sutlej and Alaknanda catchment (Dalai *et al.*, 2002). In the case of the Alaknanda catchment, it is shown that the relatively low slope and intercept are mainly caused by the most negative samples in both $\delta^{18}O$ and $\delta^{2}H$, which are the high-elevation (>3,000 m asl) samples in the catchment.

5.1.2. Stable isotope fractionation along elevation gradients

The significant correlation between surface-water $\delta^{2}H$ values and mean catchment elevation (Figure 4) in both the Sutlej and the Alaknanda catchments supports the notion that the isotopic signature of the surface-water is mainly controlled by Rayleigh-rainout processes of a monsoonal moisture source. At elevations >3,000 m asl, the Rayleigh curve steepens, which is generally also reflected in the surface-water samples of the Sutlej, and in the few high-elevation samples in the Alaknanda catchment. This effect is due to the increase in fractionation factor between the vapor and liquid state with decreasing temperature, causing the rainout to be more depleted in the heavier isotopologues (Clark and Fritz, 1997).

In the high-elevation Sutlej catchment, the surface-water $\delta^{2}H$ values from the Spiti river generally showed more negative values compared to the downstream Sutlej at the same mean catchment elevation. This is likely due to the orientation of the river (flow direction NW-SE) and an effective orographic barrier that shields the Spiti valley from ISM moisture approaching from the south (Figure 1, swath profile B). Despite similar mean-catchment elevations of these samples, the Spiti catchment receives lower rainfall amounts during summer (Fig. 2B and C; (Bookhagen *et al.*, 2005b). The Sutlej surface waters reflect a more pronounced monsoon-precipitation signature, while the more negative $\delta^{2}H$ values of the Spiti samples may originate from a higher relative input of both snowmelt (cf. Fig. 2; Wulf et al., 2016) and groundwater recharge.

The $\delta^{2}H$-lapse rate of -8.8 ‰ km^{-1} in both the Alaknanda surface waters, and the low-elevation Sutlej samples are comparable to the lapse rate of -8.3 ‰ km^{-1} observed in Arun River surface waters, located in eastern

Nepal, closer to the Bay of Bengal (Hoffmann *et al.*, 2016), and in agreement with modeling of Rayleigh rain-out processes (Fig. 4). In particular, the upper catchment surface-water samples in the Sutlej/Spiti catchment are characterized by a steeper lapse rate of -32.7 ‰ km^{-1} (Fig. 4A), as is observed in the Rayleigh distillation model. The steeper slope is most likely caused by the aforementioned increase in fractionation factor, and the distillation of the isotopes from a decreasing reservoir (Clark and Fritz, 1997). While the overall trends of lapse rates agree between the model and samples, the exact numbers vary for lapse rates both above and below 4,100 m asl. Several other processes that can influence the slope at the higher elevation sample sites are for example sublimation, evaporative processes, or the higher additional contribution of snow and glacial melt.

5.1.3. Alaknanda and Sutlej surface waters in a regional setting

A compilation of all surface-water lapse rates determined a global lapse rate of $\delta^{18}O$ with elevation of -2.8 ‰ km^{-1} (Poage and Chamberlain, 2001). The lapse rates in both the entire Alaknanda and Sutlej elevation transects are lower than the global lapse rate (-1.3 ‰ km^{-1} for the Alaknanda and -2.1 ‰ km^{-1} for the Sutlej). However, this global surface-water study observes a significant higher scatter in the Himalaya, caused by complex precipitation patterns (Poage and Chamberlain, 2001) or by the aforementioned increase in fractionation factor, and influence of secondary processes.

In the Alaknanda transect, a breakpoint is observed in the $\delta^{18}O$ elevation transect, which is mainly controlled by the high-elevation Alaknanda and Dhauliganga surface-water samples. In the LMWL, both the high-elevation samples in the Sutlej and Alaknanda plot closer relative to the GMWL, compared to the samples in the mid-range. Evaporative enrichment in the high-elevation catchment samples could have caused the offset between $\delta^{18}O$ and $\delta^{2}H$, resulting in a breakpoint in the $\delta^{18}O$ dataset, but not in the $\delta^{2}H$ dataset.

Other studies in the Western Himalaya have found lower $\delta^{18}O$ lapse rates than the global lapse rate of -2.8 ‰ km^{-1} as well: -1.6 ‰ km^{-1} (Ramesh

and Sarin, 1992), -1.4 ‰ km^{-1} (Bartaya *et al.*, 1995) -1.9 ‰ km^{-1} (Dalai *et al.*, 2002) -0.9 ‰ km^{-1} (Pande *et al.*, 2000), -1.9 ‰ km^{-1} (Jeelani *et al.*, 2010), -1.3 ‰ km^{-1}, (Bershaw *et al.*, 2012), -2.1‰ km^{-1} (Biggs *et al.*, 2015). The lapse rates in both $\delta^{18}O$ and $\delta^{2}H$ from surface waters in the Alaknanda and Sutlej catchment agree with the lapse rates that have previously been observed in the area.

D-excess values in the surface waters can provide information on second-order processes influencing the isotopic signature of the surface waters. In the surface waters of both the Alaknanda and Sutlej catchments *d*-excess showed an initial increase (1.3-1.5 ‰ km^{-1}, respectively) up to elevations of ~4,000 m asl in the Alaknanda catchment, after ~4,000 m asl there is no further increase. The initial decrease can be explained by Rayleigh fractionation: *d*-excess increases with increasing elevation due to the progressive cooling of the air mass. This results in higher *d*-excess values than the typical ISM-derived values in the range of 8-11 ‰ (Gat and Carmi, 1970; Karim and Veizer, 2002; Maurya *et al.*, 2011; Bershaw *et al.*, 2012). Above 4,000 m asl *d*-excess values show a relative high amount of scatter compared to the lower elevations, coinciding with a large amount of snow present in the catchments (Fig. 5 and Fig. 8), and the possible influence of continental moisture recycling, as is also observed in other studies along the Himalayan mountain range (Voss et al., 2020; Ren et al., 2017; Varay et al., 2017; Hren et al. 2009).

5.1.4. Influences of snow and glacial meltwater

Since the catchments above 4000 m have larger amounts of snow present during winter and summer (Fig. 5B and D) and receiving significant snowmelt flux into the surface waters in spring and summer, we explore the possibility that the low *d*-excess values are indicative of snow and ice melt input.

While *d*-excess of snow and ice is usually dependent on the source of the precipitation, post-depositional processes such as sublimation can alter the *d*-excess of snow and glacial ice (Moser and Stichler, 1974; Jouzel and

Merlivat, 1984; Whillans and Grootes, 1985; Gat, 1996; Stichler *et al.*, 2001; Lechler and Niemi, 2012). A sublimation experiment in a snowpit on high-altitude glaciers in the Andes resulted in a decrease of *d*-excess in the firn-surface snow from ~18 ‰ to ~7 ‰ over a timespan of 3.5 days (Stichler *et al.*, 2001) caused by the higher moisture deficit of the ambient air paired with the high surface temperatures. In addition, sublimation of snow during melting processes can result in lower *d*-excess values in snowmelt and therefore also surface waters (Moser and Stichler, 1974; Lechler and Niemi, 2012). Snow and glacial melt has been estimated to contribute 32 % of surface-waters in the Alaknanda catchment (Maurya *et al.*, 2011) and 70 % - 90 % in the Sutlej (depending on location) in spring (Wulf *et al.*, 2016). Therefore, if the snowmelt carries a different isotopic signature, a significant effect on the surface-water isotope composition can be expected.

In summary, the complexity of high-elevation precipitation and post-depositional processes influencing *d*-excess in snow and glaciers makes it challenging to explain trends in *d*-excess in this study. However, the decrease in *d*-excess in catchments with increasing elevation above 4,153 m asl (Fig. 5) cannot be reconciled with a simple Rayleigh-rainout process of ISM moisture. The addition of sublimated snowmelt with low *d*-excess to surface water in high-elevation catchments (>4,000 m asl) could be a potential cause for the observed decrease in *d*-excess values. Sublimated snowmelt from high-elevation catchments is expected to be a significant contributor to streamflow in the post-monsoon period (Wulf *et al.*, 2016).

5.2. Seasonal controls on the surface-water isotope composition

Two seasonal yearlong datasets of surface-water isotopes were obtained from the Spiti (Tabo, 3,280 m asl) and the Beas (Manali, 2,050 m asl) catchments. In the Beas catchment (Fig. 7A) δ^2H values become less negative in early spring, but are approximately stable over the rest of the year, suggesting small seasonal changes with contributions from sources

with a different isotopic signature (e.g., precipitation, groundwater recharge). No clear seasonal trends were observed in the Spiti time series (Fig. 7B).

The observed increase in *d*-excess during early spring in both the Beas and Spiti catchment coincides with an increasing melt rate, suggesting a snowmelt input into the surface waters (Fig. 7). As previously mentioned, the input of precipitation from a dominantly westerly source mainly falling in the winter months could be the cause of systematic seasonal variability in stream water *d*-excess values. This effect will mainly be observed during spring, when fresh unaltered snowmelt is added to the surface waters due to melting processes, resulting in higher *d*-excess values, as is observed in the Spiti, and to a lesser degree in the Beas time series (Fig. 7). However, the recycling of continental moisture has been previously found as an alternative process to also contribute to higher *d*-excess values in Himalayan high-elevation surface waters (Dalai *et al.*, 2002; Hren *et al.*, 2009; Bershaw *et al.*, 2012).

Our dataset shows an increase in *d*-excess during early spring in both the Beas and the Spiti catchment, following the decrease in snow cover and increase in melt rate (Fig. 7). It is therefore conceivable that this increase is due to the detected increased input of snow and ice melt during spring and summer (Wulf *et al.*, 2016) when little to no precipitation falls (Fig. 2B). Moreover, snowmelt was calculated to constitute 48 % of the discharge in the Sutlej River in the period of May-Oct (Bookhagen and Burbank, 2010). These measurements were made downstream of the Spiti river (~275 km), making it likely that the Spiti snowmelt percentage in the river is higher than this ((Wulf *et al.*, 2016). In addition, remote-sensing products based on SWE suggest that the melt rate in the main Spiti River increased from 50-60 mm/month in winter (DJF) to 100 mm/month in spring (MAM) and the total snow cover of the catchment decreased from a maximum of 100 % in winter to a minimum of 20 % after summer (Fig. 7). The first increase in melt rate in the catchment is observed in February and the subsequent increase in *d*-excess is observed in April. The delayed signal in *d*-excess could result from

the low snow decrease of 10-15 % between February and April. In May and June the snow cover decreases from 80% to 40% (Fig. 7D).

For the Beas catchment, the SWE-derived snowmelt rate increases from ~15 mm/month in winter to ~25 mm/month in spring, and the total snow cover in the catchment decreases from a maximum of 100 % in winter to a minimum of <20% after summer. The percentage of glacial coverage in these catchments is comparable, but the Spiti River has a significantly higher snow cover area and higher absolute SWE amounts compared to the Beas catchment in 2014 (60.4 mm and 8.4 mm, respectively), and subsequently a higher snowmelt volume during spring.

The absolute increase in *d*-excess during summer in the Beas is smaller than in the Spiti, possibly reflecting the smaller amount of snow in the catchment, reflected in the magnitude of the *d*-excess excursion (Fig. 7C). Moreover, studies report that the Beas River is mainly fed by rainfall (Kumar *et al.*, 2007), with snowmelt contribution to surface-waters in the order of 16.5 % in May-Oct (Bookhagen and Burbank, 2010).

After snow cover and the snowmelt rate have declined to a minimum, no immediate response in the *d*-excess values of the surface waters is observed (Fig. 7C and D). One possible explanation for this phenomenon could be groundwater recharge. In Nepal, a post-monsoonal drainage of groundwater is reported (Andermann *et al.*, 2012) with a response time of 30-45 days. If the groundwater in the high-elevation catchments is recharged with snowmelt during the pre-monsoon period, this could also explain the observed delay in *d*-excess response in the surface waters (Fig. 7C and D). After April until July there is still a strong loss of snow cover, resulting in a continuous input from snow and glacial meltwater, causing the *d*-excess in the rivers to stay elevated for a longer period.

Alternatively, (Wulf *et al.*, 2016)) showed at three locations in the Sutlej catchment that the snowmelt component of the surface waters is larger in spring until summer, while glaciers melt later in the season during summer and fall. The *d*-excess values measured in glaciers in the Himalayas in summer and fall show a large range, but exhibit *d*-excess values high enough

that could cause the prolonged high *d*-excess signal in the time series (15.5±5.0 ‰, see Supplementary Material Tab. 3; (Nijampurkar and Rao, 1992; Pande *et al.*, 2000; Rai *et al.*, 2016).

In summary, we argue that in both the Beas and the Spiti catchments the higher *d*-excess in the river during spring and summer was related to increased input of meltwaters from westerly-derived fresh snow (i.e. not yet influenced by post-depositional processes, such as sublimation) derived from high-elevation catchments. As soon as temperatures in the catchments increased above zero degrees, high *d*-excess fresh snowmelt is added to the surface water, causing the *d*-excess of the river to increase. The timing of this effect is supported by results obtained from the MODIS snow cover and AMSR SWE remote-sensing data products with a time lag of ~3 months and is consistent with previous estimates of groundwater-turnover time.

5.3. Two-member mixing model for *d*-excess

In order to test if the isotopic signature in the surface-water is caused by the influence of snowmelt, a simple two-member mixing model was applied. Assuming the Nov-Feb period reflects baseflow conditions of the river with low snowmelt contribution, and the May-Oct period reflects a mixture of rainfall, snowmelt and baseflow, the isotopic signature of the snowmelt can be estimated using a two-component mixing model (see more detailed description in the Supplementary Material):

$$d_{snow} \times Q_{snow} + d_{baseflow} \times Q_{baseflow} = d_{snow+baseflow} \times Q_{snow+baseflow} \qquad \text{[Equation 3]}$$

In which *d* is the *d*-excess value, and *Q* the percentage of the total discharge represented by snowmelt from Bookhagen and Burbank (2010), baseflow or a mixture thereof. Solving for the *d*-excess values of snow, yields a *d*-excess value of ~24.4±5.1 ‰ for the Spiti river, and ~27.3±2 ‰ for the Beas river (more details in the Supplementary Material), which falls in the range of

reported winter precipitation in the Himalaya (Tian *et al.*, 2007; Kumar *et al.*, 2010). In the percentages of snowmelt published by (Bookhagen and Burbank, 2010), we assume there is a 10 % error in the discharge, because there is an annual change in river discharge depending on SWE stored in the catchments. Large interannual changes in discharge caused by changes in SWE amount have been shown in the Sutlej catchment (Wulf *et al.*, 2016).

The two-member mixing model for *d*-excess supports our hypothesis regarding higher *d*-excess values in spring is caused by input of meltwater from westerly-derived fresh snow from high-elevation catchments.

6. Conclusion

Surface-water stable isotope ratios (δ^2H, $\delta^{18}O$, and *d*-excess values) over a 4 km altitudinal gradient have been measured in the Sutlej, Beas, and Alaknanda catchments in the western Himalaya during the post-monsoon season in 2014. Based on our analysis, we make the following key observations:

First, the isotopic lapse rate in $\delta^2H/\delta^{18}O$ in the low-elevation Sutlej (<4,000 m asl) and Alaknanda samples are similar (δ^2H: -8.8 ‰ km^{-1}, $\delta^{18}O$: -1.5 ‰ km^{-1}), while the high elevation Sutlej/Spiti area records a significantly higher lapse rate (δ^2H: -32.7 ‰ km^{-1}, $\delta^{18}O$: -3.9 ‰ km^{-1}). The significant negative correlation between $\delta^2H/\delta^{18}O$ values and mean-catchment elevations in the surface waters of the Sutlej and Alaknanda suggests that the isotopic signature is mainly controlled by Rayleigh distillation at low elevations. The higher lapse rate in the high-elevation Sutlej catchment, combined with the decrease in the *d*-excess signal and increased scatter, is most likely caused by a an increase of evaporative processes and the higher relative contribution of sublimated snow and glacier melt to the surface waters during the post-monsoon season.

Second, the increase in *d*-excess in the high-elevation time series in spring reflects the impact of runoff from snow-covered areas on the surface waters. The contribution of fresh snowmelt to surface waters can be verified with independent remote-sensing data products, such as passive microwave

(AMSR-E) derived snow-water equivalents and snow cover based on optical data (MODIS), which can be used to understand seasonal variability in water-source contribution. After the snowmelt rate decreases to a minimum at the end of summer, there is no direct response in the *d*-excess values in the surface-waters, which could be caused by meltwater originating from glaciers. The use of *d*-excess as a tracer for glacier and snowmelt in combination with remote-sensing data products will be useful in river-monitoring studies in the Himalaya or other high mountain ranges, in order to assess the interannual variation in glacier and snowmelt contribution.

Third, analysis of time series with a longer duration in combination with an extensive sampling of end-member components can improve the current knowledge on melting processes and the constraining of hydrological components in high-elevation catchment surface-waters. Moreover, given the scope of current climate change and increasing temperatures, and its impact upon high-mountain regions, it is important to monitor the timing of snowmelt and the different contributing factors that determine the hydrological budget of Himalayan rivers.

Acknowledgements

This study was funded by the Marie Curie ITN (iTECC), and additional funding provided by the University of Potsdam to M. Strecker and B. Bookhagen. D. Sachse was supported by the Emmy-Noether grant (SA1889/1-1). We acknowledge N. Hovius and C. Andermann at the GFZ Potsdam for insightful discussions, and B. Hoffmann, University of Potsdam for assistance with the catchment statistics. We thank Dr. Vikrant Jain for assistance with sample handling, and H. Wulf for contribution of isotope values of snow. *NCEP_Reanalysis 2 data provided by the NOAA/OAR/ESRL PSD, Boulder, Colorado, USA, from their Web site at http://www.esrl.noaa.gov/psd/.*

3. Validation and calibration of soil δ^2H and brGDGTs along (E-W) and strike (N-S) of the Himalayan climatic gradient

Iris van der Veen[1], Francien Peterse[2], Jesse Davenport[3], Bernd Meese[1], Bodo Bookhagen[1], Christian France-Lanord[3], Ansgar Kahmen[4], Hima J. Hassenruck – Gudipati[6], Ananta Gajurel[7], Manfred R. Strecker[1], Dirk Sachse[5]

[1]Universität Potsdam, Institut für Erd- und Umweltwissenschaften,
Potsdam-Golm, Germany
(*Correspondence: Veen@geo.uni-potsdam.de)

[2]Department of Earth Sciences, Utrecht University, the Netherlands

[3]Geochemistry, Centre des Recherche Petrographiques et Geochimiques (CNRS-CRPG), Vandœuvre-lés-Nancy France

[4]University of Basel, Botanical research, Basel, Switzerland

[5]GFZ German Research Centre for Geosciences, Section 5.1: Geomorphology, Organic Surface Geochemistry Lab Potsdam Germany

[6]Department of Geological Sciences, The University of Texas at Austin, 2275 Speedway, M.S. C9000, Austin, Texas 78712, USA

[7]Tribhuvan University, Tri-Chandra College, Central Department of Geology, Kathmandu, Nepal

Published in Geochimica et Cosmochimica Acta, 2020
Issue 290
Pages 408 – 423
DOI: 10.1016/j.gca.2020.09.014

Abstract

Reconstructing the timing of mountain range uplift and the evolution of high-altitude plateaus is important when attempting to understand potential feedbacks between tectonics and climate at geological timescales. This requires proxies that are able to accurately reconstruct elevation during different time periods in the past. Often, the sensitivity of climatic parameters to elevation gradients, recorded in geological archives such as soils, is used to estimate paleoelevations. However, most proxies reflect an indirect response to elevation change, adding uncertainties to reconstructions. In this study, we aim to identify those sources of uncertainty with respect to elevation reconstructions and test if the combined application of two such proxies, i.e., stable isotopes (δ^2H) of plant waxes in modern soils and surface waters and bacterial membrane lipids (brGDGTs) in soils, which can potentially reduce uncertainties in the estimation of (paleo-) elevation. We performed this study in four Himalayan catchments (from west to east: Sutlej, Alaknanda, Khudi, and Arun), of which each individual catchment is subject to a unique precipitation regime, relative influences of moisture sources, and vegetation cover. In total, we analyzed 275 surface water samples, 9 precipitation samples, 131 xylem water samples, and 60 soil samples, which were collected between 2009 and 2014.

The following key observations were made: Soil n-C_{31}-alkane δ^2H values (δ^2H_{wax}) in the Sutlej, Alaknanda, Khudi, and Arun generally record surface water δ^2H values, confirming that the first-order control on the plant wax isotopic signature is precipitation δ^2H and, therefore, the elevation in orogenic settings. We identified aridity as the factor that introduces scatter to this relationship. BrGDGT-derived Mean Annual Temperature (MAT) correlates in a statistically significant manner with sample site elevation and a 14-year annual average of remotely sensed land-surface temperature, showing that the main process influencing the brGDGT distribution is the adiabatic cooling of air.

In an effort to combine these proxies to improve uncertainties in elevation reconstruction, elevations were inferred from both the δ^2H_{wax} and brGDGT distributions. Arid, high elevation sites appear to underestimate actual sample site elevations using δ^2H values while sites subject to high (>23–25°C) annual temperatures overestimate the actual sample site elevation using brGDGT distributions. Elevations inferred from both proxies under such paleoclimatic conditions should be interpreted with caution. Elevations derived from the brGDGT distribution appear to most accurately reconstruct elevation. However, we show that the difference in elevation between the two proxies, described by the proposed $\Delta_{Elevation}$ parameter, can provide information on the hydrological conditions of the soil's depositional environment. In conclusion, we emphasize that knowledge of the sample site's climatic conditions are essential to reconstruct elevation from paleoarchives. In particular, knowledge of moisture availability and annual air temperatures are important, as these have been found to cause the largest scatter in the observed data.

1. Introduction

The uplift of mountain ranges has been a key interest in climate and tectonic studies due to its impact on atmospheric circulation patterns, erosion, and precipitation patterns (Zhisheng et al. 2001; Clift et al. 2008). For example, the uplift of the Himalayan mountain range has played a key role in the onset and intensification of the Indian (ISM) and East Asian (EASM) monsoons, as well as in changing the global carbon cycle due to increasing weathering of freshly exposed bedrock (Dettman et al. 2003; Molnar & England 1990; Quade et al. 2007; Poulsen et al. 2010; Garzione et al. 2000a). Testing these scenarios, uplift histories, and comparison with coeval climatic records are needed.

To reconstruct mountain range paleoelevation, we use proxies that record the persistent hydrological and climatological gradients preserved in geological archives. These proxies include numerous stable isotope and lipid biomarker approaches, such as $\delta^{18}O$ in pedogenic carbonates (Garzione et al.. 2000b; Quade et al. 2007), leaf wax $\delta^{2}H$ (Zhuang et al. 2014; Bai et al. 2015; Peterse et al. 2009; Polissar et al. 2009, Jia et al 2008), and branched tetraether membrane lipid distributions (Ernst et al. 2013; Wang et al. 2017, Sinninghe Damsté et al. 2008). These aforementioned proxies are all based on climatic parameters that are observed to co-vary with elevation, and hence indirectly record elevation. Rayleigh distillation processes during rainout result in a negative relationship between the isotopic composition ($\delta^{18}O$ and $\delta^{2}H$) of precipitation and elevation (Dansgaard 1964; Gat et al. 2000). Temperature generally decreases with increasing elevation. The $\delta^{2}H$ values in *n*-alkanes derived from higher terrestrial plants have shown a strong relationship with mean precipitation $\delta^{2}H$ values, which have been used for paleohydrological and paleoelevation reconstruction (Sauer et al. 2001; Huang et al. 2004; Sachse et al. 2004; Smith & Freeman 2006; Hou et al. 2008). The potential of leaf wax $\delta^{2}H$ to record elevation has initially been shown at Mt Gongga in China (Jia et al. 2008) and later at Mt Shennongjia, Mt. Wuyi and Mt Tianshan (Luo et al. 2011), and Mt Meghalaya (Ernst et al.

2013). These studies reflect that soil δ^2H_{wax} records overall δ^2H from precipitation, and thus indirectly records the elevation.

Even though $\delta^{18}O$ and δ^2H values in precipitation primarily correlate with elevation, locally or seasonally varying processes and climatic conditions, such as heterogenic precipitation patterns, complex topography, and the relative influence of multiple moisture sources, can distort the general linear elevation relationships (e.g. Rohrmann et al. 2014; Hren et al. 2009; Galewsky 2009).

Similarly, mean annual air temperature (MAT) generally decreases with elevation due to the adiabatic cooling of air, and is therefore also an indirect measure of elevation. This temperature change can be reflected by distributional changes in branched glycerol dialkyl glycerol tetraethers (brGDGTs) (Weijers et al. 2007). BrGDGTs are membrane lipids produced by soil bacteria, which vary in the number (4-6) of methyl branches attached to their alkyl backbone, the position of these methyl branches (5 or 6 position), and the number (0-2) of internal cyclizations, depending on the MAT and pH of the soil in which they are produced (Weijers et al. 2007; De Jonge et al., 2014b). As such, MAT can be reconstructed based on the molecular signature of brGDGTs in an environmental sample (Weijers et al., 2007; De Jonge et al., 2014a; Naafs et al., 2017). The ability of brGDGTs to track adiabatic cooling was first illustrated in a study at Mt Kilimanjaro, where a good relation was found between brGDGT-derived MAT and altitude (Sinninghe Damsté et al. 2008). Subsequently, good relations between brGDGT signals and MAT were found along the southeastern margin of the Tibetan Plateau (Wang et al. 2017), Mt Gongga (Peterse et al. 2009), and Mt Meghalaya (Ernst et al. 2013), among others. Outside of East Asia, this relationship has also been found in the Andes (Nieto Moreno et al 2016) and Africa (Coffinet et al 2014, 2017; Jaeschke et al., 2018).

Nevertheless, the latest global temperature transfer functions still contain a substantial amount of scatter, indicating that the brGDGT temperature proxy is influenced by additional climatic parameters, such as soil moisture content (SMC) and precipitation amount/aridity (Peterse et al., 2012;

Dirghangi et al. 2013; Menges et al. 2014; Wang et al. 2014; Dang et al. 2016; Naafs et al. 2017), but possibly also by soil and vegetation type (Davtian et al. 2016) and the co-occurrence of brGDGT-producing microbial communities with distinct temperature relationships (De Jonge et al., 2019; Dearing Crampton-Flood et al., 2020). These effects can introduce uncertainties in the relationship between brGDGT signals and temperature, and thus the proxy's robustness in recording elevation.

To assess possible sources of scatter in the individual relations of soil *n*-alkane δ^2H and brGDGTs with elevation, and thus the suitability of these proxies in paleoelevation reconstructions, both proxies were applied in parallel at several altitudinal transects. This revealed, for example, that the rain belt surrounding Mt Kilimanjaro likely disturbed the relation between soil *n*-alkane δ^2H and elevation due to a D-depletion in the precipitation and consequently in the soil *n*-alkanes (Peterse et al. 2009, Zech et al 2015). A similar spatial heterogeneity in precipitation was shown at Mt Kenya and Mt Rungwe, resulting in weak or absent relationships between the soil *n*-alkane δ^2H and elevation (Coffinet et al. 2017). Nevertheless, the combined application of brGDGTs and soil *n*-alkane δ^2H in the Andes, Mt Meghalaya, and the Southern Alps in New Zealand did show the expected orography effect on temperature and precipitation (Nieto-Moreno et al. 2016; Ernst et al. 2013, Zhuang et al 2015).

In this study, we further validate the individual relations of brGDGT-derived MAT and δ^2H_{wax} with altitude using a combination of field and remote-sensing data. In a second step, the proxies are combined and we investigate whether this combination reduces potential uncertainties in the elevation estimates. Specifically, we analyze the stable isotopic composition (δ^2H) of surface waters, xylem waters (i.e. the lipid H source), and long chain n-alkanes, as well as brGDGT signals in modern soils along four altitudinal gradients along the Himalayan orogeny. These altitudinal transects are subject to varying precipitation regimes, different degrees of aridity, relative influences of moisture sources, and vegetation cover, which allows a thorough investigation of the impact that different environmental factors have

on δ^2Hwax and brGDGTs. Combining the multiproxy data with satellite-derived climate products, we aim to identify the controlling secondary factors that potentially alter the relationship between source water δ^2H and δ^2Hwax, as well as physically measured MAT and brGDGT-derived MAT. Ultimately, we discuss how the offset between these parameters can potentially impact paleoelevation studies and the interpretation of these proxies in sedimentary archives.

2. Study area

The Himalayan mountain range separates the Tibetan Plateau from the Indian subcontinent, traversing 2,700 km along the range from the Karakoram in Pakistan in the northwest through India, Nepal, and Bhutan into the Arunachal Pradesh in the southeast. The range varies in width between ~ 400 km in the west and ~150 km in the east, containing several significant mountain peaks.

The Himalayan range acts as an orographic barrier separating the humid regions in the foreland and arid sections in the rain shadow, resulting in varying precipitation patterns along the Southern Himalayan Front (SHF). Two partly independent, but interfering climatic circulation systems dominate the precipitation regime in the Himalaya: the Indian Summer Monsoon (ISM) system and the Western Disturbances (WD)(Bookhagen & Burbank 2010; Cannon et al. 2014). The ISM moves along the SHF and transports moisture from the Bay of Bengal toward the northeast, causing heavy rainfall along the southern slopes of the mountain front during summer (Bookhagen et al. 2005). The second major moisture source is the WD, originating from the Caspian, Black, and Mediterranean seas, transporting winter precipitation between December and March (Cannon et al. 2014; Wulf et al. 2010; Dash et al. 2009). Spatially, the dominance of the ISM decreases from east to west, whereas the WD becomes particularly influential west of 78°E (Bookhagen & Burbank 2010). The Himalayan range creates an extreme gradient between the humid tropical climate in the foreland and alpine conditions at higher

elevations. The two major climatic gradients that strongly influence the vegetation cover and type along the orogen are the decreasing air temperature from low to high elevations and the decreasing amount of moisture from east to west (Singh & Singh 1987).

3. Methods

3.1. Elevation transects

Four transects from the northeast to the southwest were selected in the Sutlej, Alaknanda, Khudi Khola (hereafter referred to as Khudi), and Arun catchments, of which the first two are located in the western Himalaya in India and the latter two in central and eastern Nepal (Fig.1). These four transects each cover a large altitudinal gradient and consequently also span large ranges in precipitation, vegetation, and temperature (Fig. 2).

The Sutlej catchment elevation transect ranges from 475–3,533 m over a horizontal distance of ~170 km. The lower sites (< 3,000 m asl) receive 1,500–2,000 mm rainfall annually (cf. TRMM 2B31, Bookhagen & Burbank 2010), decreasing to < 500 mm/year at the higher sample sites (> 3,000 m asl) (Fig 2A). Mean Annual Temperature (MAT) in the catchment ranges between 9.7°C and 25.4°C, with an average of 19.7°C (2000–2014 yearly average, MOD11C3, Wan & Hulley 2015; Wulf et al. 2016). Concurrently, with the decrease in rainfall amount and the increase in elevation, the Enhanced Vegetation Index (EVI) shows that vegetation cover in the catchment decreases with elevation (Fig.2A).

The Alaknanda catchment transect ranges from 346 to 3,155 m with a horizontal distance of 160 km. Annual rainfall varies between 300 and 2,600 mm/year and consists of two rainout belts (at ~500 and ~2,000 m, Fig. 2B) due to a two-step rise in relief (Fig. 2B), as described in (Bookhagen & Burbank 2006). The 14-year average MAT in the catchment is 19.8 °C, ranging between 7.1 °C and 26.8 °C (Wan & Hulley 2015).

The Khudi, where the transect ranges from 2,155 – 4,085 m asl with a horizontal transect of ~13 km, receives rainfall amounts of >3,900 mm/year

(Fig. 2C). There is little variation in the amount of rainfall along the altitudinal transect due to its short distance. MAT varies between 7.5 °C and 19.5 °C with an average temperature of 13.1 °C.

The transect in the Arun valley ranges from 225 to 2,580m over a horizontal transect of 160 km. Annual rainfall amounts along the transect vary between 2,000 and 4,000 mm/year (Fig. 2D), showing a two-belt rainout pattern similar to the Alaknanda transect (at ~500 and ~2,000 m, Fig. 2D). MAT varies between 3.5 °C and 26.7 °C, with an average of 16.3 °C.

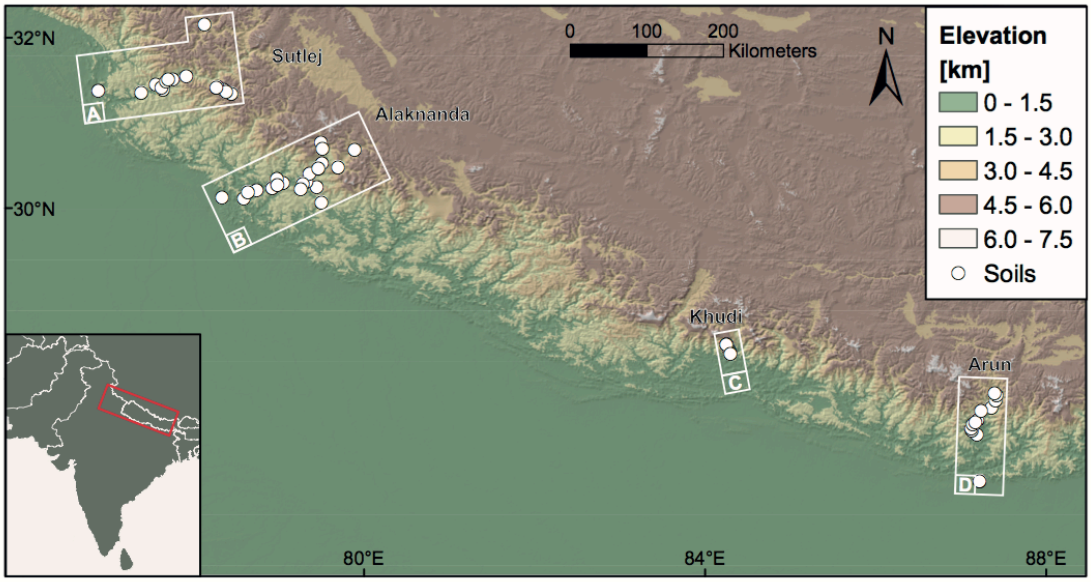

Figure 3.1: Topographic overview of the Himalaya (SRTM V3). White circles indicate the sample sites of the soils along four altitudinal gradients. White rectangles indicate areas over which the swath profiles were determined, and labeling corresponds to the swath profiles shown in Fig. 2.

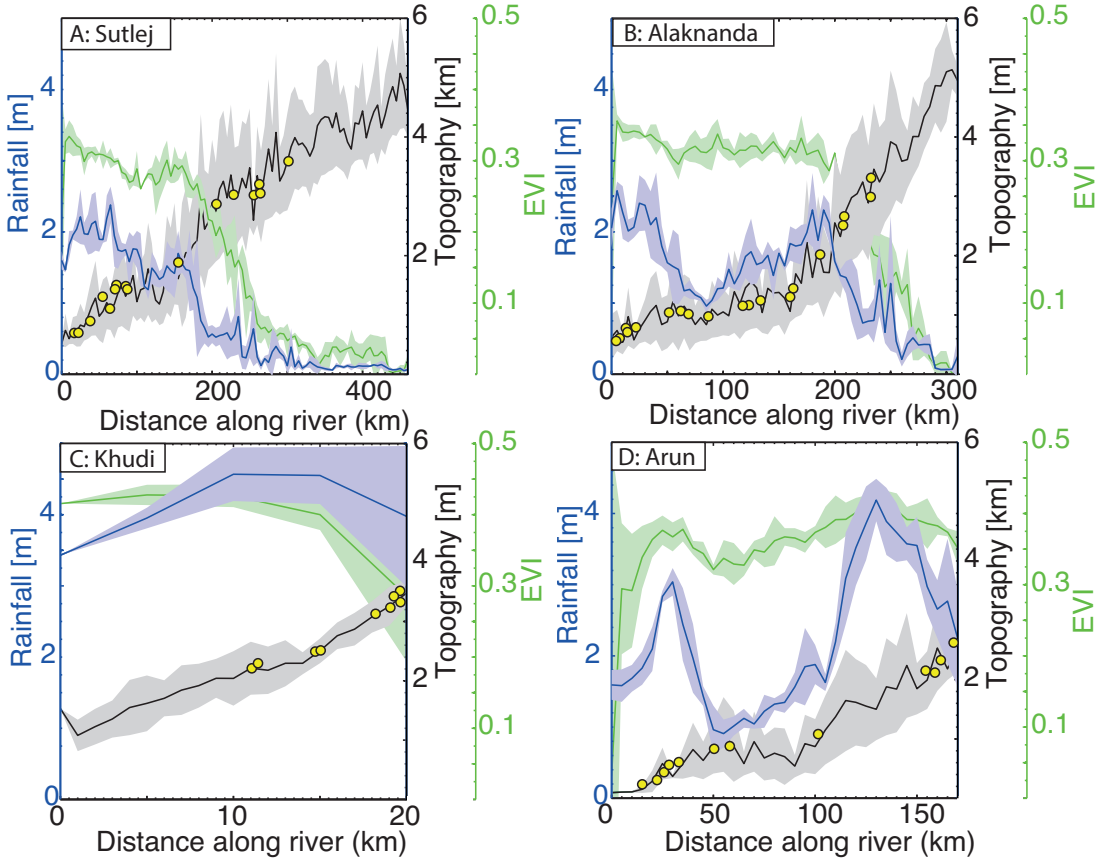

Figure 3.2: 10-km wide swath profiles along the four altitudinal transects in the Himalaya (cf. Figure 1). 12-year average JJA mean TRMM 2B31 precipitation in blue (Bookhagen & Burbank 2010), 17-year average (2000-2017) MODIS derived EVI in green (Didan 2015), and topography in black with 1-sigma standard deviation (gray)(USGS 2006). Yellow circles indicate soil sample sites along the elevation transects.

3.4 Sample collection

Soil (0-5 cm, without litter) and water samples in the Alaknanda and the Sutlej catchment were obtained in September/October 2014, whereas soils and water in the Arun catchment were collected both in September 2011 and October/ November 2012 (Hoffmann et al. 2016). In the Khudi Khola catchment, only soils were sampled at various depths in September 2009.

All soils were sampled adjacent to roads/paths in the catchments, which were checked for undisturbed soils. Soils were never sampled on steep slopes, but from the most horizontal part of the terrain. However, due to the generally steep terrain in the study area it is possible that geomorphic processes (e.g. creep and downslope transport) have transported material from higher elevations.

In total, 107 water samples and 17 soil samples in the Sutlej catchment, 52 water samples and 21 soil samples in the Alaknanda catchment, 10 soil samples in the Khudi Khola catchment, and 116 water samples and 12 soil samples in the Arun catchment were collected. In addition, 35 xylem water samples from dominating vegetation at sample sites in the Alaknanda, 33 in the Arun, and 63 in the Sutlej catchments were collected. At every xylem water sampling location, 9 branches were collected from 3 individuals of the same species. Per sample location, the 2 most dominant angiosperm species were sampled. Due to the large climatic gradient, it was not possible to sample the same species along the entire elevation transect. After collecting the branches, the bark was removed to prevent mixing between xylem water and phloem water, after which the peeled branches were placed in airtight containers. Xylem waters were extracted at a vacuum line at the university of Basel (Newberry et al. 2017). Extracted xylem water was measured on a TCEA-IRMS for $\delta^{18}O$ and $\delta^{2}H$ values. For the Khudi precipitation samples, rain gauges were installed at three stations allowing daily collection of rainwater in 2013 (time series data for the Ghalegaon station (IAEA). These stations are at Ghalegaon village

(2,103 m) on the western crest of the basin and two near the Khudi river at the Khudi Hydropower Intake station (968 m) and Probi village (1,456 m). At higher elevations between 2,500 and 4,050 m, cumulated rain waters were collected over long periods in sealed 40 liter plastic containers (DRUM) surmounted with a 15 cm funnel.

3.3. Analysis of δ^2H and $\delta^{18}O$ values of water samples

The surface water δ^2H and $\delta^{18}O$ values sampled in the Alaknanda and Sutlej catchment were measured on a Picarro Cavity Ringdown Spectrometer L2140-I at GFZ Potsdam, with a precision of 0.08‰ for $\delta^{18}O$ and 0.5‰ for δ^2H. For the Khudi precipitation samples, waters were analysed at CRPG laboratory (Nancy-France) using a Eurovector-Isoprime EA-IR-MS coupled with a chromium reactor. Samples were systematically repeated three times and external reproducibility was better than ±1‰. Samples were analysed with internal standards every five samples and calibrated using the V-SMOW, GISP, and V-SLAP standards. All samples were filtered through a 0.45 µm syringe and stored in 2 mL vials. The samples were injected 10 times, with a volume of 1 µl, and the first three injections were discarded for each individual sample, to avoid any memory effects. The measurements were normalized using a two-point correction using VSMOW2 and SLAP2 standards, provided by the IAEA.
The stable isotope composition is reported using the δ-notation relative to the Vienna Standard Mean Ocean Water (VSMOW) standard as:

$$\delta\ [‰] = \left(\frac{R_{Sample}}{R_{Standard}} - 1\right), \qquad (1)$$

where R is the ratio of heavy isotopes relative to light isotopes ($^{18}O/^{16}O$ and $^2H/^1H$). All values are reported in per mille ‰ (implying a factor of 1000).

3.4. Lipid extraction

The soil samples were freeze-dried and stored in pre-combusted (500°C) glass vials. Before extraction, all soil samples were sieved with a 2 mm sieve, and any leaves and large roots were removed to avoid any contamination from modern organic material. A total lipid extract (TLE) was extracted from the soil samples using an Accelerated Solvent Extractor (ASE) (Type Dionex ASE 350) using 9:1 dichloromethane:methanol as a solvent. Samples were initially separated into two fractions using columns containing 1.5–2 gram of precombusted silica gel. Samples were added to the top of the column, and then rinsed with 12 mL of hexane to obtain the hydrocarbon fraction. The GDGT fraction was obtained by subsequent rinsing with 1:1 dichloromethane:methanol.

3.5. Lipid analysis

The hydrocarbon fraction containing the *n*-alkanes was analysed on an Agilent GC MSD (Agilent 5975C MSD, Agilent 7890A GC with Agilent J&W HP-5 MS column, 30 m×0.25 m×0.25 µm film) coupled to an FID. A Thermo Scientific Delta V Plus IRMS coupled to a Trace 1310 GC (Agilent GC MSD (RESTEK, Rtx-5 Crossbond ms column, 30 m×0.25 mm×0.25 µm df. 5% diphenyl, 95% dimethyl polysiloxane) via an Isolink pyrolysis furnace operated at 1420°C was used at Potsdam University for the measurement of the *n*-alkane δ^2H values (δ^2H_{wax}). The H_3^+ factor was determined at the beginning of every sequence, and was constant (3.9±0.7) throughout the entire duration of the measurements, indicating stable conditions in the ion source. All samples were measured in duplicates, with a standard deviation of < 3‰, and a C_{10} – C_{40} standard measured in between every 10 samples. The δ^2H_{wax} values were all normalized to the VSMOW-SLAP scale, with the use of an external standard containing C_{16} to C_{30} alkanes (A-Mix, A. Schimmelmann, Indiana University, Bloomington). The dominant alkane in the majority of the samples was nC_{31}, which has been used to reflect $\delta^2H_{wax.}$

A known amount of internal standard (C_{46}-GDGT) was added to the GDGT fraction, after which it was filtered through a 0.45 µm PTFE filter using 99:1 (v/v) hexane:2-propanol. Samples were measured on an Agilent 1260 Infinity ultra high performance liquid chromatograph (UHPLC) coupled to an Agilent 6130 single quadrupole mass detector (MS) according to the method described by (Hopmans et al. 2016). The separation of the brGDGTs was performed on two silica Waters Acquity UPLC HEB Hilic (1.7µm, 2.1mm x 150mm) columns in tandem, preceded by a guard column of the same material. The $[M+H]^+$ ions were detected in selected ion monitoring mode.

3.6. Proxy calculation

The apparent fractionation (Sauer et al. 2001), ε_{app}, reflecting net fractionation between the source water (in this case the surface waters) and soil lipids, is defined as:

$$\varepsilon_{app} = \left(\frac{\delta^2 H_{alkane} + 1000}{\delta^2 H_{water} + 1000)} - 1 \right). \qquad (2)$$

All values are reported in per mille ‰ (implying a factor of 1000). Surface water δ^2H was used as a catchment integrated value of precipitation δ^2H (Hren et al. 2009; Kendall & Coplen 2001; Bershaw et al. 2012). In the case of soil samples in the Arun that were sampled in 2011, source water was determined from the relationship between surface waters from 2012 and sample site elevation of the 2011 soil sample.

Using the fractional abundances of the brGDGTs, the MAT was determined based on the degree of methylation of 5-methyl brGDGTs (MBT'_{5me}; De Jonge et al., 2014b):

$$MBT'_{5me} = \frac{(\mathrm{Ia} + \mathrm{Ib} + \mathrm{Ic})}{(\mathrm{Ia}+\mathrm{Ib}+\mathrm{Ic}+\mathrm{IIa}+\mathrm{IIb}+\mathrm{IIc}+\mathrm{IIIa})} \ . \qquad (3)$$

Temperatures derived from the GDGTs were calculated using the Bayesian regression model (BayMBT0) reported in Dearing Crampton-Flood et al. (2020), which are referred to as BayMBT MAAT hereafter. As prior input to

the BayMBT0 model, the temperatures derived from the MODIS satellite (paragraph 3.6) for each individual site were used and the prior standard deviation was set at 15 following Dearing Crampton-Flood et al. (2020). The Isomerisation ratio, (IR), was determined according to De Jonge et al. (2014b):

$$IR = \frac{IIa' + IIb' + IIc' + IIIa' + IIIb' + IIIc'}{IIa + IIb + IIc + IIIa + IIIb + IIIc + IIa' + IIb' + IIc' + IIIa' + IIIb' + IIIc'}. \quad (5)$$

3.7. Remote sensing Data

MAT was derived by averaging the monthly 0.05° (approximately 5,6 km) Land Surface Temperature (LST) from 2000 to 2014 from the Moderate Resolution Imaging Spectroradiometer (MODIS) MOD11C3 product, from its first availability in 2000 until the fieldwork period (Wan & Hulley 2015). Seasonal and annual rainfall was determined using the Tropical Rainfall Measurement Mission (TRMM) 2B31 data product averaged from 1998–2010, with a spatial resolution of ~5 km (Huffman et al. 2014; Bookhagen & Burbank 2010). The seasonal and annual Enhanced Vegetation Index (EVI) was determined using MOD13C2 (MODIS) by averaging data products from 2000–2017 (Didan 2015). Soil moisture in the root zone (0–100 cm) in m^3/m^3 was determined using the SMAP soil moisture SPL4SMGP data product (Reichle et al. 2016). Data were averaged from March–April–May (growing season), with a spatial resolution of 9 x 9 km. The aridity index was determined using the following equation:

$$Aridity\ Index = \frac{Mean\ Annual\ Precipitation}{Mean\ Annual\ Potential\ Evapotranspiration}, \quad (6)$$

where the mean annual precipitation derives from the aforementioned (TRMM 2B31) data product and mean annual potential evapotranspiration was determined using the Global PET dataset (Trabucco & Zomer 2009).

4. Results

4.1. Surface water and xylem water δ^2H values

In the Sutlej catchment, surface water δ^2H values ranged from –50‰ in the foreland to –112‰ in the high elevation catchments (Fig. 3A). The Alaknanda surface water δ^2H values ranged from –51 to –102‰ (Fig. 3B). The Arun surface water data ranged between –36 and–110‰ (Meese et al. 2018), which was sampled simulatneously with the soils and additional river sediments (Hoffmann et al. 2016)(Fig. 3C). The surface water δ^2H values in the Arun catchment ranged between –73 and –103‰. Surface water was sampled from both tributaries and main streams, resulting in the integration of a number of samples over a larger upstream catchment area (Table 2 Research Data). To take into account the upstream catchment sizes, surface water δ^2H values were compared using both the sample site elevation (Fig. 3) and mean catchment elevation (Fig. EA4, Electronic Annex). A negative correlation was observed between δ^2H and the mean catchment elevation in the Sutlej, Alaknanda, and Arun river catchments ($r = 0.89$, $p < 0.001$; $r = 0.91$, $p < 0.001$; and $r = 0.85$, $p < 0.01$, respectively). Moreover, a significant negative relationship was observed between surface water δ^2H and the sample site elevation in both the Sutlej and Alaknanda ($r = 0.78$, $p < 0.01$ and $r = 0.85$, $p < 0.01$, respectively)(Fig. 3A,B). The sample site elevation represents a more local δ^2H signal while the mean catchment elevation also integrates the upstream catchments of the surface waters. The isotopic lapse rates of the surface water in the Sutlej and Alaknanda catchments were 15.7 and –8.8‰ km^{-1}, respectively, when assuming a linear relationship between δ^2H and mean catchment elevation. The Arun dataset consists of surface water samples that were collected in 2011 and 2012. An extensive analysis on the factors that control the surface water δ^2H of the Arun has been previously published (Meese et al. 2018). The isotopic lapse rate of the surface waters in the Arun in 2011 and 2012 were –10.9 and –12.3‰ km^{-1}, respectively. However, since the 2011 lapse rate does not span the entire

length of the transect on which the soil samples were collected, only the 2012 dataset was used in this study.

In the Khudi catchment, we did not obtain a surface water δ^2H dataset, but do have access to a daily precipitation δ^2H dataset (Fig. 3C). A significant relationship was observed between the sample site elevation and precipitation δ^2H ($r = 0.92$, $p < 0.01$). We note that this water was only sampled during the monsoon, i.e., in the same period as the soil samples were collected.

Xylem water δ^2H of the Sutlej samples varied between –18.3‰ at 475 masl and –119.4‰ at 3,533 masl (Fig. 3), but showed an absolute difference between the minimum and maximum of 28‰ to 82‰ between individual sample sites. The smallest range in isotope values was observed at the second highest sample site (28‰) while the largest range in isotope values was observed at the highest sample site (55‰). In the Alaknanda, xylem water ranged between 7.1‰ at 346 masl and –74.3‰ at 651 masl. High variations in the xylem water δ^2H occur along the Arun catchment, where values range between –39.7 and –96.07‰.

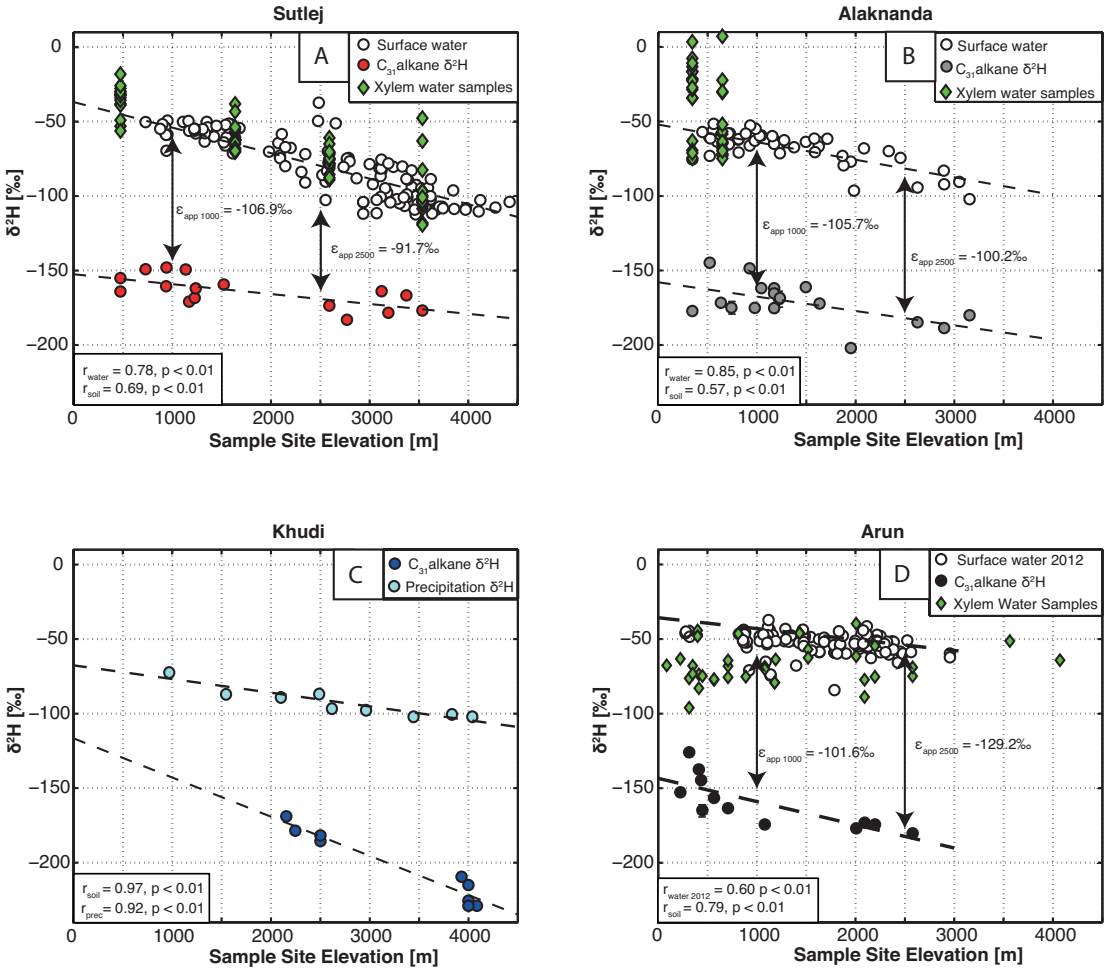

Figure 3.3: Soil δ·H of *n*C$_{31}$ (red, grey, blue, and black circles) and δ·H of tributary surface waters (white circles) and xylem waters (green diamonds) in the Sutlej, Alaknanda, Khudi and Arun catchment. ε$_{app}$ is calculated at different elevations according to equation 2. The precipitation δ·H in Fig. C is time series data from the Ghalegaon station (IAEA) http://www-naweb.iaea.org/napc/ih/IHS_resources_isohis.html. For the Arun dataset, five outliers were removed that do not represent the local precipitation signal. Thus, samples that showed a larger difference than 1,500 m between sample site elevation and mean catchment elevation were removed for this reason

4.2. Soil *n*-alkane isotopic composition

The most dominant alkane in the majority of the dataset (all Sutlej and Alaknanda samples) was *n*C$_{31}$. In the following analysis, we therefore refer to the *n*C$_{31}$ δ^{2}H values as δ^{2}H$_{wax}$. Along the Sutlej transect, δ^{2}H$_{wax}$ ranged between –148 and –183‰ over an altitudinal transect from 475–3,371 masl, the Alaknanda catchment δ^{2}H$_{wax}$ ranged between –129 and –202‰ over an

altitudinal transect from 346–3,100 masl, and finally the Arun catchment values ranged between –125 and 180‰ (Fig. 3). The Khudi Khola transect is significantly shorter and steeper than the other three catchments, such that the δ^2H_{wax} ranged between –169 and –229‰, with an altitudinal transect from 1,750–4,085 masl over a distance of ~13 km, whereas the Alaknanda, Sutlej, and Arun transects are each between 160–175 km long.

We observe a significant negative correlation between δ^2H_{wax} and sample site elevation along the Sutlej, Alaknanda, Khudi, and Arun transects (r_{Sutlej} = 0.69, p = 0.001, $r_{Alaknanda}$ = 0.57, p = 0.01, r_{Khudi} = 0.97, p = 0.001, r_{Arun} = 0.79, p = 0.01; Fig. 3). The δ^2H_{wax} with the elevation isotopic lapse rate was the lowest in the Sutlej at –6.7 (± 1.8)‰ km^{-1}, –9.6 (± 3.5)‰ km^{-1} for the Alaknanda, –15.6 (± 3.9)‰ km^{-1} for the Arun, and –26.3 (± 2.6)‰ km^{-1} in the Khudi Khola (Fig. 3).

The comparison of δ^2H of surface waters and δ^2H_{wax} in soils yielded a significant correlation in the Sutlej and Alaknanda catchment (r = 0.56, p = 0.01 and r = 0.58, p = 0.01, respectively)(Fig. 4A). In the Arun catchment, no significant correlation (r = 0.37, p > 0.01) between the δ^2H of surface waters and δ^2H of soils was observed. No values on surface water δ^2H and ε_{app} (see below) in the Khudi are reported, as no surface water samples were collected to pair with the soils.

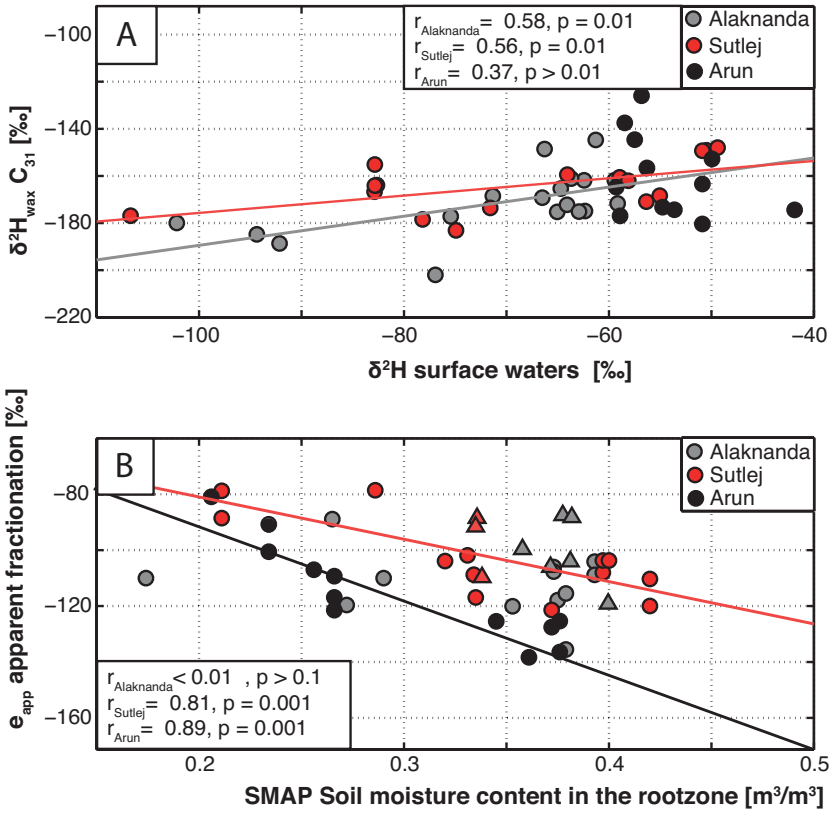

Figure 3.4: A. δH_{wax} nC_{31} plotted against the surface water δH of the tributaries nearest the soil location. Correlation coefficients and p-values were determined with a linear regression (red and grey lines). Only regressions that are statistically significant are shown. B: Apparent fractionation versus soil moisture content in the root zone (m^3/m^3) from March–May, derived from the Soil Moisture Active Passive (SMAP) soil moisture SPL4SMGP data product (Reichle et al. 2016). Circles indicate sample sites with a predominant angiosperm vegetation cover, and triangles indicate sample sites with predominantly gymnosperms. Red and black lines are the linear regressions. Only regressions that are statistically significant are shown.

4.3. Apparent fractionation

Values of the apparent fractionation ε_{app} (equation 2) in the Alaknanda, Sutlej, and Arun catchments have average values of –108.3, –102.1, and –112.3‰, respectively (Table 1, Research Data), but varied between –138.3 and –73.3‰ in the three transects.

A significant relationship was observed between ε_{app} and the soil moisture content in the root zone during spring (March–April–May; Reichle et al. 2016) in both the Sutlej and Arun catchment (Fig 4B). In the Sutlej, the correlation between the soil moisture content and ε_{app} for the entire transect

is significant ($r = 0.71$, $p = 0.001$). When only considering the sample sites that have predominantly *angiospermae* as vegetation cover, which are the main producers of n-alkanes (Bush & McInerney 2013; Diefendorf et al. 2011) as opposed to gymnospermae, a higher correlation between soil moisture content and ε_{app} was observed ($r = 0.81$, $p = 0.001$). In the Alaknanda and Sutlej, where ε_{app} was relatively stable along the entire transect, no significant relationship between soil moisture in the rootzone and ε_{app} was observed (Fig 4B).

4.4. BrGDGT thermometry

BayMBT MAAT derived from brGDGTs (equation 3) varied between 3.8°C and 23.9°C in the Sutlej, 6.1°C and 26.1°C in the Alaknanda, and 5.4°C and 20.2°C in the Khudi Khola catchments. One of the lowest sample sites (AK6) was located on a very steep north-facing slope, receiving little to no sunlight. As a result, the BayMBT MAAT for this location was lower than expected (7.8°C) for a sample at this elevation (523 m). We therefore identified this sample as an outlier (studentized residual t(21) = –10.13, adjusted Bonferroni p = 0.02). In all transects, a significant negative correlation between BayMBT MAAT and sample site elevation was observed (r_{Sutlej} = 0.92, p = 0.001, n = 16, $r_{Alaknanda}$ = 0.82, p = 0.001, n = 19 and r_{Khudi} = 0.85, p = 0.001, n = 10)(Fig. 5A). The associated temperature lapse rates in the Sutlej, Alaknanda, and Khudi were –5.1 ± 0.5°C km^{-1}, –5.8 ± 1.1°C km^{-1}, and –5.6 ± 1.1°C km^{-1}, respectively (Fig. 5A).

Correlating the BayMBT MAAT with the 14-year average annual MODIS-derived MAT (from its first availability in 2000 until 2014, when our fieldwork was carried out; Wan & Hulley 2015) for each sample location (Fig. 5B) resulted in a positive relation in all three catchments: the Sutlej catchment and the Khudi catchment both showed a highly significant correlation (r_{Sutlej} = 0.88, p < 0.001, r_{Khudi} = 0.87, p < 0.001, $r_{Alaknanda}$ = 0.80) between BayMBT MAAT and MAT (MODIS).

The modern lapse rates in the three catchments were determined by correlating the 14-year MODIS derived MAT with the sample site elevation (Fig. 5C). The associated temperature lapse rates in the Sutlej, Alaknanda, and Khudi were –5.1 ± 0.6°C km^{-1}, –5.4 ± 0.3°C km^{-1}, and –6.5 ± 0.4°C km^{-1}, respectively.

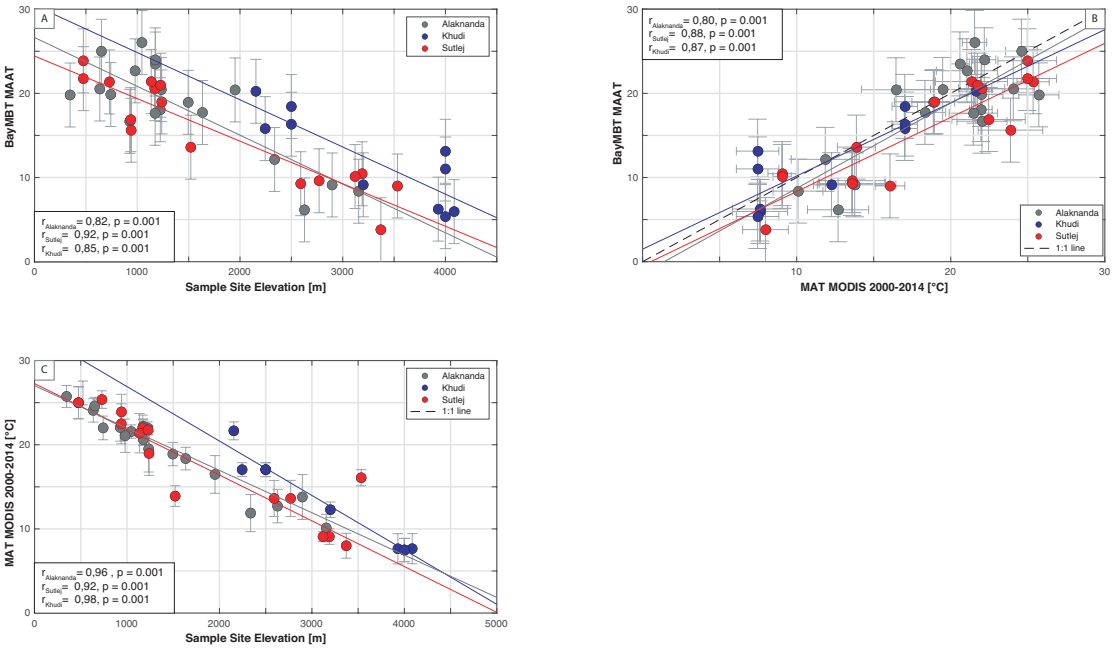

Figure 3.5: BrGDGT-derived MAT for the Sutlej, Alaknanda, and Khudi catchments. A: MAT (De Jonge, 2014b) versus sample site elevation. B: MAT versus a 14 year average MODIS derived MAT (2000-2014, Wan & Hulley 2015). C: MODIS MAT versus sample site elevation. Error bars represent the standard deviation from the 14-year mean MODIS temperature. Regressions were determined using a least-square weighted linear regression.

4.5. δ^2H and BrGDGT-derived elevation

To estimate elevation from δ^2H_{wax} data in a similar manner as in paleoelevation studies, we applied a Rayleigh distillation model to the dataset (Rowley 2007). This exercise was performed to assess the correlation between the actual elevation of the sample site and the modeled elevation derived from the Rayleigh distillation model. This model describes the progressive isotopic depletion of a reservoir in atmospheric moisture during transport (Rowley et al. 2001) and hence depicts the ideal scenario (under ideal conditions) at the point where a moisture packet encounters an orographic barrier, which results in isotopic depletion with altitude.

The δ^2H_{wax} -based elevation reconstructions correlate significantly with the actual sample site elevation along the three transects (Alaknanda, Sutlej, and Khudi), for which both δ^2H_{wax} and brGDGTs were measured (Fig. 6A). Due to the large uncertainties associated with the Rayleigh model, the standard deviations of the elevation estimates were at a magnitude of up to

2,000 m. Most samples plotted above the 1:1 line, indicating that the δ^2H_{wax} proxy generally overestimated sample site elevation. The extent of the overestimation was the largest in the lower Alaknanda (< 2,000 m asl), where reconstructed elevation can be up to 2,500 m higher than the actual sample site elevation (Fig. 6A).

BayMBT MAAT was translated to elevation using the MODIS 14-year average temperature lapse rate of each elevation transect (Wan & Hulley 2015). BrGDGT-based elevations were subsequently compared with the actual sample site elevation, showing a close resemblance in all three transects (Fig. 6B).

The difference in the estimated elevation from both the δ^2H_{wax} and brGDGT proxies can be visualized with the $\Delta_{Elevation}$ parameter (Fig. 6C). Soils that were sampled at arid sites (low aridity index) generally plotted under the 0-line while most of the Alaknanda and all of the Khudi samples plotted above this line.

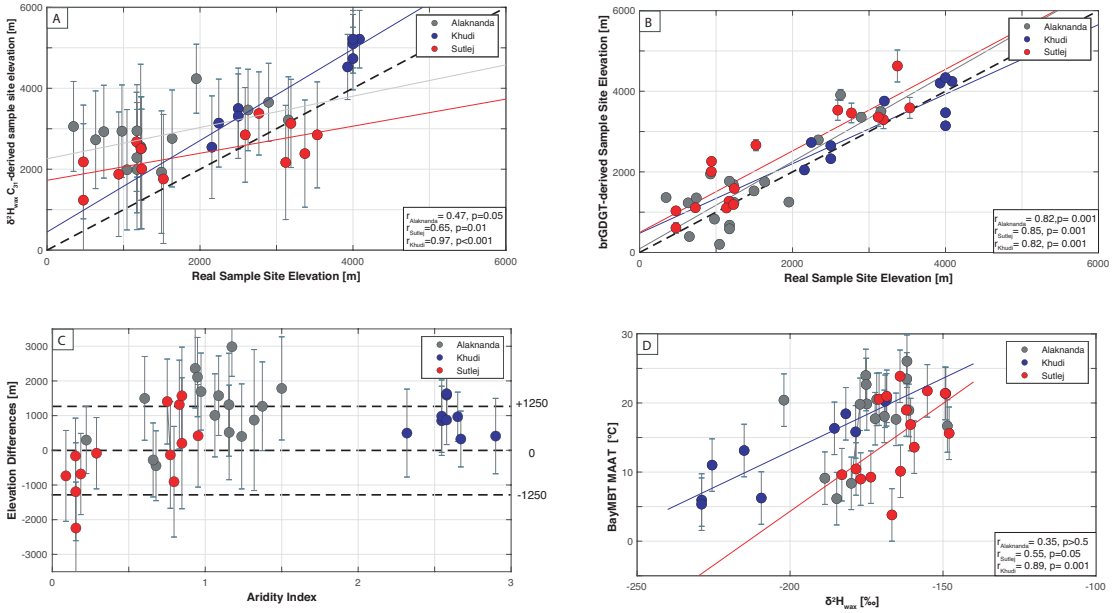

Figure 3.6: A: MAT versus δH_{wax}. B. BrGDGT-derived elevation versus actual sample site elevation. C. δH derived elevation versus actual sample site elevation. Regressions were determined by least square weighted linear regression. D. Absolute differences between brGDGT-derived and δH-derived elevation versus the Aridity index (equation 6). The data points represent the difference between the actual sample site elevation and the brGDGT or δH_{wax} derived sample site elevation. The standard deviations were determined by adding the brGDGT derived elevation standard deviation and δH_{wax}-derived elevation standard deviations using the equation $\sigma = \sqrt{\sigma^2_{\delta 2wax} + \sigma^2_{brGDGT}}$.

5. Discussion

5.1. Relationship between elevation and surface water δ^2H values, δ^2H_{wax}, and brGDGTs

To assess the robustness of δ^2H_{wax} and brGDGTs as a proxy for paleoelevation, the relative importance of all factors influencing these proxies other than changes in elevation must be determined. The four elevational transects along the southern Himalayan front are all characterized by different precipitation amounts, vegetation cover, and moisture sources, thus allowing us to investigate the impact of these variable parameters.

The δ^2H values of the surface waters in the Sutlej, Alaknanda, and Arun all show a significant correlation with the mean catchment elevation. Comparable lapse rates are observed in the Alaknanda and Arun surface waters (Alaknanda = –8.8‰ km^{-1}, Arun = –8.8‰ km^{-1})(Fig. 3) while the higher lapse rate in the Sutlej (Sutlej = –15.7‰ km^{-1}) can be explained by a larger relative contribution of snow and glacial melt from tributaries in the higher elevation regions of the catchment (Wulf et al. 2016; Maurya et al. 2011; Karim & Veizer 2002; Varay et al. 2017; Bookhagen & Burbank 2010). The uniform direction of the lapse rates indicates that the main process controlling surface water δ^2H values is the progressive rainout of a monsoonal moisture source, i.e., the altitude effect (Gat & Confiantini 1981). The remaining scatter in the relationship between surface water δ^2H and mean catchment elevation is possibly due to a combination of processes, such as evaporation, mixing of moisture sources with a different isotopic signature, blocking of moisture by topography, convective storms, seasonality, or contribution of snow and glacial melt, which have been observed in high elevation systems (e.g. Gat 1996; Dansgaard 1964; Rohrmann et al. 2014; Hughes et al. 2009; Lechler & Niemi 2012).

The δ^2H_{wax} shows the expected negative correlation with sample site elevation in all four transects, suggesting that the first order control on the plant wax isotopic signature is precipitation δ^2H (Fig. 3). However, the different degrees of correlation between δ^2H_{wax} and the elevation in the

different transects suggest that this relationship is subject to additional processes (see section 5.2.1. for more detail).

Comparing surface water δ^2H and δ^2H_{wax} yielded a significant correlation in the Alaknanda and Sutlej, but no significant relationship in the Arun (Fig. 4A). In the Arun catchment, no significant relation was found between δ^2H_{water} and sample site elevation (Fig. 3D), which subsequently results in the absence of a relationship between δ^2H_{water} and δ^2H_{wax}. The low elevation tributaries in this area reflect the isotopic composition of ISM rainfall while the higher elevation tributaries receive elevated portions of glacial meltwater and Winter Westerly Disturbances precipitation (Meese et al. 2018). In addition, Meese et al. (2018) point out a significant difference in the isotopic composition of surface water between the sampling years (2011 and 2012). This interannual variation may have contributed to the absence of a relation between δ^2H_{water} and $\delta^2H_{wax.}$ Scatter in the relationship between the surface water δ^2H_{water} and δ^2H_{wax} in the Sutlej and Alaknanda is most likely due to secondary processes. Surface water δ^2H reflects the isotopic signature of the upstream area, which is a mixture of precipitation, snow, and glacial melt. δ^2H_{wax} reflects a combination of source water isotopic compositions, in addition to climatic and plant physiologic drivers (Sessions et al. 1999; Chikaraishi & Naraoka 2003; Smith & Freeman 2006; Sachse et al. 2006; Feakins & Sessions 2010; Sachse et al. 2012). Our observation of an effect of moisture availability on ε_{app} (see paragraph 4.3.) suggests that this is one factor that weakens the relationship between surface water δ^2H and δ^2Hwax.

The significant correlation between BayMBT MAAT and both sample site elevation and MODIS-derived MAT indicates that the adiabatic cooling of air mainly controls the distribution of brGDGT in the soils (Fig. 5A,B). Nevertheless, BayMBT MAAT is at times below the expected modern temperature (derived from the MODIS MAT remote sensing product) at low elevation sample sites (Fig. 5B). This offset may in part be explained by the absence of field measured temperature data, instead replaced by a 14 year average remotely sensed MODIS MAT product (Wan & Hulley 2015). The accuracy of the MOD11C3 temperature product has been estimated to be <

1 K in the range from –10°C to +58°C (Wan & Li 2011), and the MODIS MAT and ground station lapse rates have been found to correlate well in previous studies in the Sutlej (Wulf et al. 2016). However, there is an ongoing discussion on what temperature data (e.g., soil or air temperature, mean annual or growing season temperature) best describes the variation in brGDGT distributions in soils (Naafs et al. 2017; Dearing Crampton-Flood et al., 2020).

5.2. Influence of water availability on soil *n*-alkane δ^2H and brGDGTs

5.2.1. Soil n-alkane δ^2H_{wax}

The environmental factors that influence plant δ^2H_{wax} and soil δ^2H_{wax} can be examined at two different levels. First, processes influencing a plant's moisture source (i.e., precipitation and, to a lesser degree, soil water) before it enters the plant. Second, processes that affect the isotopic composition of δ^2H_{wax} through the evaporation of leaf water from leaves (Smith & Freeman 2006; Liu & Yang 2008; Feakins & Sessions 2010; Lai et al. 2006; Kahmen et al. (2013b); Sachse et al. 2012).

To characterize the offset between the source water and lipid δ^2H, the apparent fractionation (ε_{app}) was calculated (Eq. 2). The apparent fractionation incorporates the influence of evapotranspiration, soil evaporation, and plant physiology, and is directly linked to the variation in the relative humidity and precipitation in the study area (Smith & Freeman 2006; Sachse et al. 2006). However, the ε_{app} in this study is used to describe the offset between the surface water δ^2H and δ^2H_{wax}. Surface water δ^2H is assumed to be an annual integrated precipitation δ^2H signal, but glacier/snowmelt, seasonality in precipitation, and evaporation may influence the isotopic signature of surface water δ^2H. Moreover, the apparent fractionation integrates both evaporative effects and biosynthetic fractionation, complicating attempts to decipher the degree of impact from both factors individually (Sachse et al. 2006; Smith & Freeman 2006; Feakins & Sessions 2010; Kahmen et al. (2013a); Sessions et al. 1999).

In the Sutlej, Alaknanda, and Arun catchments, the apparent fractionation changes with elevation (Fig. 3A, B, D). Unfortunately, along the Khudi elevation transect, no surface water samples coupled to the soil sampling locations were taken (Fig. 3C), preventing us from testing this relationship in this catchment. Values of apparent fractionation in the Sutlej, Alaknanda, and Arun are similar to the ε_{app} between soil alkane δ^2H and surface waters observed in other elevation transects on the SE Tibetan Plateau (Bai et al. 2015), but lower than other surface soil studies located on the Tibetan Plateau (Luo et al. 2011; Jia et al. 2008; Wang et al. 2017).

Soil evaporation enriches δ^2H in soil water and causes a decrease in the ε_{app} in arid regions (Smith & Freeman 2006; Polissar et al. 2010). A decrease in the apparent fractionation with increasing elevation is observed along the Sutlej and Alaknanda transect, which are the two transects that receive the lowest amount of precipitation at high elevation sample sites (Fig.2, 3). This decrease in ε_{app} with increasing elevation suggests that aridity has an effect on the soil δ^2H_{wax} values in the high elevation Sutlej and Alaknanda samples. The same pattern is observed when using xylem water δ^2H to calculate the ε_{app}; however, we regard surface water δ^2H values as better integrators (both spatial and temporal) compared to single plant xylem water values, which is supported by the observed scatter in the xylem water δ^2H values (Fig. 3).

In addition, in the Arun transect, a significant negative correlation was observed between ε_{app} and the Soil Moisture Content (Fig. 4B)(SMC; Reichle et al. 2016). A decrease in the apparent fractionation under drier conditions reflects increasing leaf and/or soil water evaporative ^2H-enrichment, which has been observed in previous studies (Kahmen et al. 2013b; Polissar et al. 2010; Schwab et al. 2015). Moreover, a higher correlation was observed between ε_{app} and SMC in the rootzone when only considering the soil sample sites with *angiospermae* in the Sutlej transect (Fig 4.B, circles). *Gymnospermae* modify their leaf waxes in a different manner (having higher photosynthetic discrimination) when subject to specific environmental stress, and display lower stomatal conductance for CO_2 and H_2O vapor in comparison with *angiospermae*, resulting in a different relationship between

surface water δ^2H and δ^2H_{wax} (Tipple et al. 2013; Pedentchouk et al. 2008; Diefendorf et al. 2011).

However, in the Alaknanda transect, no significant correlation between ε_{app} and any of the previously mentioned hydrological parameters was observed. This suggests that aridity is not the main controlling factor that determines ε_{app}, or that the surface water δ^2H values were not representative of the local conditions at the soil sampling sites in the Alaknanda. We relate the apparent fractionation to the soil moisture content to show that, in drier areas (low soil moisture content), the apparent fractionation is smaller. Therefore, we show that assuming a constant apparent fractionation, as is often done, is strictly not valid. Moreover, changes in climatic conditions during mountain range uplift, such as rainshadow development, should be taken into account when interpreting paleoelevation/paleoclimate records in such settings, as been introduced by Rohrmann et al. (2016)

5.2.2. BrGDGTs

In a similar manner as with the lipid δ^2H_{wax} proxy, confounding factors that may alter the brGDGT distribution in soils also influence the brGDGT temperature proxy. The most important factors that were found to have an impact on the relationship between brGDGTs and temperature are soil pH and moisture availability (Weijers et al. 2007). These influences become especially important in arid regions (MAP < 500 mm), where moisture availability appears to explain a larger part of the variation in the brGDGT distribution than temperature (Dirghangi et al. 2013; Wang et al. 2014; Menges et al. 2014; Peterse et al. 2012; Dang et al., 2016). Based on brGDGT distributions in a soil transect with a large range in moisture content (0–61%), Dang et al. (2016) suggested that 6-methyl brGDGTs especially respond to variations in the moisture content rather than to MAT. Consequently, they proposed that only sites where the contribution of 6-methyl brGDGTs is low, defined by an isomerisation ratio (IR; Eq. 5) < 0.5, can be used to reliably reconstruct MAT (Dang et al., 2016; Naafs et al.,

2017). Interestingly, for most sites (>75%) in the Alaknanda and Sutlej catchments the IR is significantly above 0.5, whereas the relationship between BayMBT MAAT and elevation, as well as between BayMBT MAAT and MODIS MAT, is good (Fig. 5). Moreover, there is no trend between SMC and the relative distribution of brGDGTs, suggesting that moisture content does not influence brGDGT distributions in Himalaya transects, and, more importantly, that the use of IR is generally not a valid method for discarding samples for (paleo-) temperature reconstruction (Table 4, Research Data).

5.3. Combination of brGDGTs and *n*-alkane δ^2H as a more robust elevation proxy

The dual application of brGDGTs and δ^2H_{wax} has been used to assess the effect that varying environmental conditions have on their potential as elevation proxies (Ernst et al. 2013; Nieto-Moreno et al. 2016; Wang et al. 2017; Hren et al. 2010; Peterse et al., 2009). Although these studies analyzed both proxies in the same set of samples, their performance has thus far only been assessed separately. Here, we test the potential of the actual combination of brGDGTs and δ^2H in an elevation context, with the aim to improve their use as a reliable paleoelevation proxy.

Both the δ^2H_{wax} and brGDGT proxy are used to reconstruct elevation, but the individual proxies record different processes that indirectly cause their changes with increasing elevation (i.e., Rayleigh distillation and adiabatic cooling of air). The strongest correlation between these proxies is found along the Khudi transect, suggesting that both proxies are suitable for elevation reconstruction in this catchment (Fig.6A). The Khudi transect is relatively short and does not encompass large changes in hydrology (i.e., it is generally wet, with a mean annual precipitation above 3,000 mm/year), as well as that environmental conditions vary less here than in the other transects. The Sutlej shows a significant correlation between δ^2H_{wax} and reconstructed MAT ($r = 0.55$, $p = 0.05$), but with a substantial amount of scatter, while in the Alaknanda no significant correlation ($r = 0.35$, $p > 0.5$)

was observed (Fig. 6D). The previously mentioned climatic conditions and geomorphological/physiological processes influencing either the δ^2H_{wax} or BayMBT MAAT may be the cause of this scatter.

In an attempt to combine these two proxies and observe to what extent this can improve elevation reconstruction reliability, we assessed the differences in estimated elevation between the proxies (Fig. 6C), where the difference is indicated as $\Delta_{Elevation}$:

$$\Delta_{Elevation} = \delta^2 H_{Elevation} - brGDGT_{Elevation}. \qquad (7)$$

To assess the influence of changing hydrological conditions, $\Delta_{Elevation}$ is compared to the aridity index (Eq. 6) of each sample location. The majority of the sites plot within a 1,250 m range from the 0-line, indicating that both proxies yield comparable elevation estimates that are less than 1,250 m offset (Fig. 6C), which is within the same range of error reported in studies that use these proxies to reconstruct paleo-elevation, e.g., the Sierra Nevada and Tibetan Plateau (Hren et al. 2010; Zhuang et al. 2014). In the trans-Himalayan transects of this study, the good relation between brGDGT-derived elevation and the actual elevation indicates that brGDGTs can be considered a good predictor of elevation (Fig. 6B). Nevertheless, brGDGTs increasingly overestimate sample site elevation towards the lowlands, likely as an artifact of proxy saturation, as MBT'_{5me} values near 1 at these sites (Table 4, Research Data). Hence, the MBT'_{5me} value can be used as an indicator of the accuracy of the reconstructed elevation for each site. On the other hand, δ^2H_{wax} is associated with large errors, primarily subject to influences from aridity and soil moisture availability.

In general, samples with negative $\Delta_{Elevation}$ values are located in areas that are either experiencing arid conditions, or located behind an orographic barrier, resulting in moisture blocking (Galewsky 2009; Hughes et al. 2009). Samples with a positive $\Delta_{Elevation}$ offset may be located in areas with high moisture, where the relationships between δ^2H_{wax} and elevation can become distorted by the amount effect, as shown in Peterse et al. (2009). This suggests that, in

a multiproxy study, the use of both δ^2H_{wax} and brGDGTs can provide information on the hydrological conditions of the (paleo-) soils using the $\Delta_{Elevation}$ parameter. For example, the formation of soils during arid conditions can result in large offsets between the reconstructed elevation and actual sample site elevation. We therefore suggest that soils that show a large negative offset ($\Delta_{Elevation}$ value outside of the 1,250 m error bars) between the δ^2H_{wax} and brGDGT proxies should be interpreted with caution, as these samples can be influenced by arid conditions during formation.

6. Conclusions

Both leaf wax *n*-alkane δ^2H values and brGDGTs primarily record a climatic parameter that changes with elevation, although additional processes influence these compositions. We found that the δ^2H_{wax} values in the Sutlej, Alaknanda, and Arun generally record surface water δ^2H values. Scatter in this relationship is attributed to the possibility that surface water δ^2H values did not represent the local conditions at the soil sampling sites, as well as the influence of aridity on the δ^2H_{wax} signature stored in soils. We confirm this via an observed dependency of the apparent fractionation between the soil δ^2H_{wax} and surface water δ^2H in the Sutlej catchment with soil moisture availability, as well as based on the vegetation type.

The BayMBT MAAT in the same three transects showed a high correlation with both sample site elevations and MODIS-derived MAT. To improve the accuracy of paleo-elevation studies, a combined approach between the δ^2H and brGDGT proxy could be applied. Large offsets (above 1,250 m) between elevations inferred from both proxies ($\Delta_{Elevation}$) should be interpreted with caution, and could be affected by moisture availability/aridity, the amount effect in precipitation, or originate from locations with high annual temperatures. In the case of a large offset, where MBT'_{5me} values are < 1, the proposed $\Delta_{Elevation}$ parameter can provide information on the hydrological setting of the depositional environment of these soils.

In conclusion, the results of this study show that both the δ^2H_{wax} and brGDGT proxies are optimal in a relatively stable climate (as the shorter Khudi transect suggests), but are significantly influenced by variable hydrology, i.e., increasing aridity (as is often the case in orogenic settings with high altitude plateaus). Our results contribute to the existing literature on organic proxies, showing that the application of a combined proxy approach could provide information on the hydrological characteristics of the depositional environment. The uncertainties in elevation estimates due to moisture availability and high temperatures emphasize that prior knowledge of the tectonic setting is crucial when reconstructing elevations.

Acknowledgements

A Marie Curie ITN (iTECC) funded Iris van der Veen and Jesse Davenport, Dirk Sachse was funded by a DFG Emmy Noether (SA1889/1-1) grant and the ERC Consolidator grant STEEPclim (grant no. 647035). NWO grant no. 834.11.006 enabled the purchase of the UHPLC–MS system used for GDGT analyses at the UU. Francien Peterse acknowledges financial support from NWO-Veni grant no. 863.13.0016. We thank Viktor Evrard and Thomas Rigaudier for technical lab support, Guillaume Morin for sampling soils in Nepal, and Tashi Jigmet for field assistance. We thank the editors for their time and valuable remarks and the three anonymous reviewers for their constructive comments.

4. Lateral variations in vegetation in the Himalaya since the Miocene and implications for climate evolution

Natalie Vögeli[1], Yani Najman[2], Peter van der Beek[1], Pascale Huyghe[1], Peter M. Wynn[2], Gwladys Govin[2], Iris van der Veen[3,4], Dirk Sachse[3,4].

[1] Université Grenoble Alpes, Institut des Sciences de la Terre (ISTerre), CS 40700, 38058 Grenoble Cedex 9, France

[2] Lancaster Environment Centre, Lancaster University, LA1 4YQ, UK

[3] GFZ German Research Centre for Geosciences, Earth Surface Geochemistry, Telegrafenberg, 14473 Potsdam, Germany.

[4] Department of Earth and Environmental Sciences, University of Potsdam, 14476 Potsdam, Germany.

Published in Earth and Planetary Science Letters 2017
Issue 471
Pages 1 – 9
DOI: 10.1016/j.epsl.2017.04.037

Abstract

The Himalaya has a major influence on global and regional climate, in particular on the Asian monsoon system. The foreland basin of the Himalaya contains a record of tectonics and paleoclimate since the Miocene. Previous work on the evolution of vegetation and climate has focused on the central and western Himalaya, where a shift in vegetation has been observed at ~7 Ma and linked to increased seasonality, but the climatic evolution of the eastern part of the orogen is less well understood. In order to track vegetation as a marker of monsoon intensity and seasonality, we analyzed $\delta^{13}C$ and $\delta^{18}O$ values of soil carbonate and associated $\delta^{13}C$ values of bulk organic carbon from previously dated sedimentary sections exposing the syn-orogenic detrital Dharamsala and Siwalik Groups in the west, and, for the

first time, the Siwalik Group in the east of the Himalayan foreland basin. Sedimentary records span from 20 to 1 Myr in the west (Joginder Nagar, Jawalamukhi, and Haripur Kolar sections) and from 13 to 1 Myr in the east (Kameng section), respectively. The presence of soil carbonate in the west and its absence in the east is a first indication of long-term lateral climatic variation, as soil carbonate requires seasonally arid conditions to develop. $\delta^{13}C$ values in soil carbonate show a shift from around -10 ‰ to -2 ‰ at ~7 Ma in the west, which is confirmed by $\delta^{13}C$ analyses on bulk organic carbon that show a shift from around -23 ‰ to -19 ‰ at the same time. Such a shift in isotopic values is likely to be associated with a change from C3 to C4 vegetation. In contrast, $\delta^{13}C$ values of bulk organic carbon remain at ~-23 ‰ in the east. Thus, our data show that the current east-west variation in climate was established at 7 Ma. We propose that the regional change towards a more seasonal climate in the west is linked to a decrease of the influence of the Westerlies, delivering less winter precipitation to the western Himalaya, while the east remained annually humid due to its proximity to the monsoonal moisture source.

1. Introduction

The Himalayan belt has a major influence on global and regional climate, by acting as an orographic barrier for air masses and humidity (Boos and Kuang, 2010; Molnar et al., 2010). Modern climate shows significant east-west variation in the Himalaya: both mean-annual and winter precipitation on the plains and foothills are higher in the east, while the west is characterized by more pronounced winter aridity (Figure 1; Bookhagen and Burbank, 2006; 2010). This variation is due to the two major atmospheric circulation systems influencing the climate of the Himalayan region: the Indian Summer Monsoon (ISM) and the Westerlies (Kotlia et al., 2015). The ISM takes up moisture in the Bay of Bengal and transports it towards the Himalaya during the northern-hemisphere summer months (e.g., Molnar et al., 2010), whereas the Westerlies bring moisture from the Mediterranean, Black and Caspian Seas and are most efficient in winter (Benn and Owen, 1998; Cannon et al., 2015).

Generally, the influence of the Westerlies is greater in the western part of the Himalayan region (Cannon et al., 2015; Caves et al., 2015; Kotlia et al., 2015). The proximity to the moisture source in the Bay of Bengal, makes the eastern Himalaya very humid (Bookhagen et al., 2010).

These lateral variations in modern climate are linked to vegetation patterns, in particular the relative importance of C3 versus C4 plants. C3 plants are favored in a cool and humid climate, whereas C4 plants prefer intense light, warm and water-stressed conditions (Ehleringer, 1988). An additional factor that possibly influences the evolution of C4 plants is growing season temperature and precipitation, favoring C4 plants in drier periods (Cotton et al., 2016). The distinct stable carbon-isotopic signature of C3 versus C4 vegetation allows paleo-vegetation to be tracked from the sedimentary record: pure C3 vegetation has $\delta^{13}C_{org}$ values between -22 ‰ and -30 ‰, whereas $\delta^{13}C_{org}$ values of C4 plants range from -10 ‰ to -14 ‰ (Cerling et al., 1997). The lateral variations in modern climate and vegetation are expressed by the signature of modern organic carbon transported in the foreland (Galy et al., 2008a; Fig. 1): sediments sampled from Himalayan tributaries at the mountain front have $\delta^{13}C_{org}$ values around -25 ‰, indicating dominance of C3 plants at higher elevations within the mountain belt. These values remain stable within the eastern Brahmaputra catchment, whereas they increase to values around -22 ‰ in the Western Ganga catchment (Fig. 1), implying laterally varying vegetation (from C4 in the west to C3 in the east) in the floodplain.

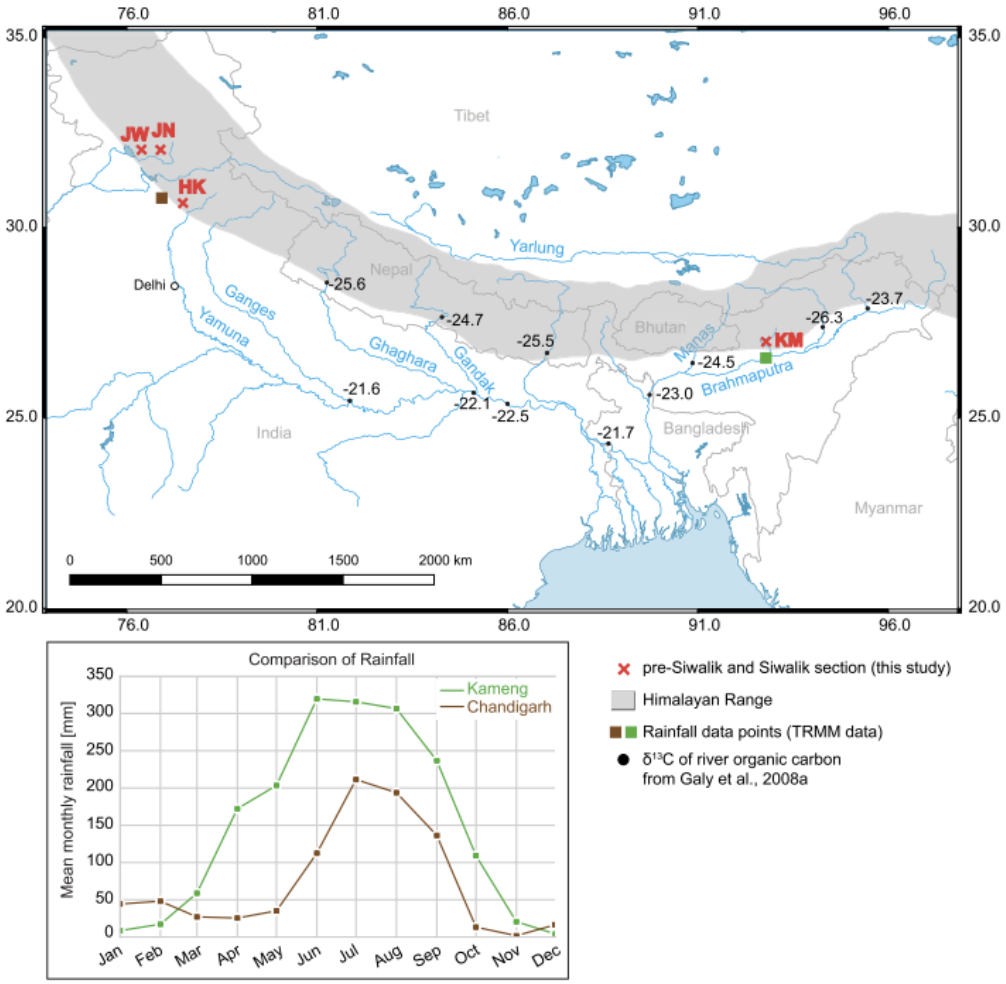

Fig. 4.1. Map of the Himalayan region, with δ¹³C of modern river organic carbon from Galy et al., 2008a. The Himalayan range is indicated schematically in grey. Sections are indicated in red: JW: Jawalamukhi; JN: Joginder Nagar; HK: Haripur Kolar; KM: Kameng. Lower plot shows comparison of modern annual precipitation data (TRMM) in proximity to the sampled sedimentary sections in the west and east. (For interpretation of the references to color in this figure legend, the reader is referred to the web version

An important question is when and why the modern spatial patterns in climate and vegetation were established in the Himalayan foreland. The onset of the ISM is dated back to at least the middle Miocene (Dettman et al., 2001) and possibly the Late Eocene (Licht et al., 2014). Likewise, the Westerlies have been argued to influence Asian climate since the Eocene (Caves et al., 2015). However, the evolution of regional climate and vegetation patterns will depend on the relative strength of these two systems through time, which remains largely unknown.

The foreland basin of the Himalaya contains a sedimentary record of vegetation and paleoclimate since Miocene times, within the continental

detrital pre-Siwalik and Siwalik Groups. The record of spatial and temporal variations in vegetation holds information on climate evolution, in particular patterns of atmospheric circulation, seasonality and the origin and transport of humidity (Hoorn et al., 2000; Sanyal et al., 2004; Gupta 2010, amongst others). Carbon and oxygen isotopic compositions of soil carbonates and soil organic matter from pre-Siwalik and Siwalik sediments in Nepal, Northwest India and Pakistan have been used to reconstruct changes in vegetation and climate during the Neogene (Quade et al., 1989, 1995a; Quade and Cerling, 1995; Sanyal et al., 2010; Singh et al., 2013). These records consistently show a shift in $d^{13}C$ values at ~7 Ma, which has been interpreted as a change from C3 to C4 vegetation, which was initially interpreted to be related to an intensification of the ISM (Quade et al., 1989). Steinke et al. (2010) suggest that this change was rather linked to an increase in aridity, and therefore a weakening of the ISM. A similar shift has also been recorded in the distal Himalayan-derived sediments of the Bay of Bengal (France-Lanord and Derry, 1994). It has been argued that the late-Miocene expansion of C4 plants is a global phenomenon due to a decrease in atmospheric pCO_2 (Cerling et al., 1997), global cooling and/or increased aridity (Herbert et al., 2016). Others, however, argue that pCO_2 was already at a level favorable for C4 plants during Oligocene times (Pagani et al., 2005; Beerling and Royer, 2011) and that the spread of C4 plants during the late Miocene should therefore have other, more regional triggers.

The focus of previous studies on Himalayan climate and vegetation records has been entirely on the western and central Himalayan foreland; no climate and vegetation data are available east of Nepal. In order to obtain better spatial insight into the evolution of the monsoon climate, precipitation patterns and the expansion of C4 plants along strike in the Himalaya, we present and compare new $\delta^{13}C$ and $\delta^{18}O$ data of pedogenic carbonate and organic matter from the northwestern and the poorly studied eastern Himalayan foreland basin. Lateral variations in the evolution of the vegetation yield further insight into how and under what climatic conditions C4 plants developed or not, suggesting that regional influences play a major role.

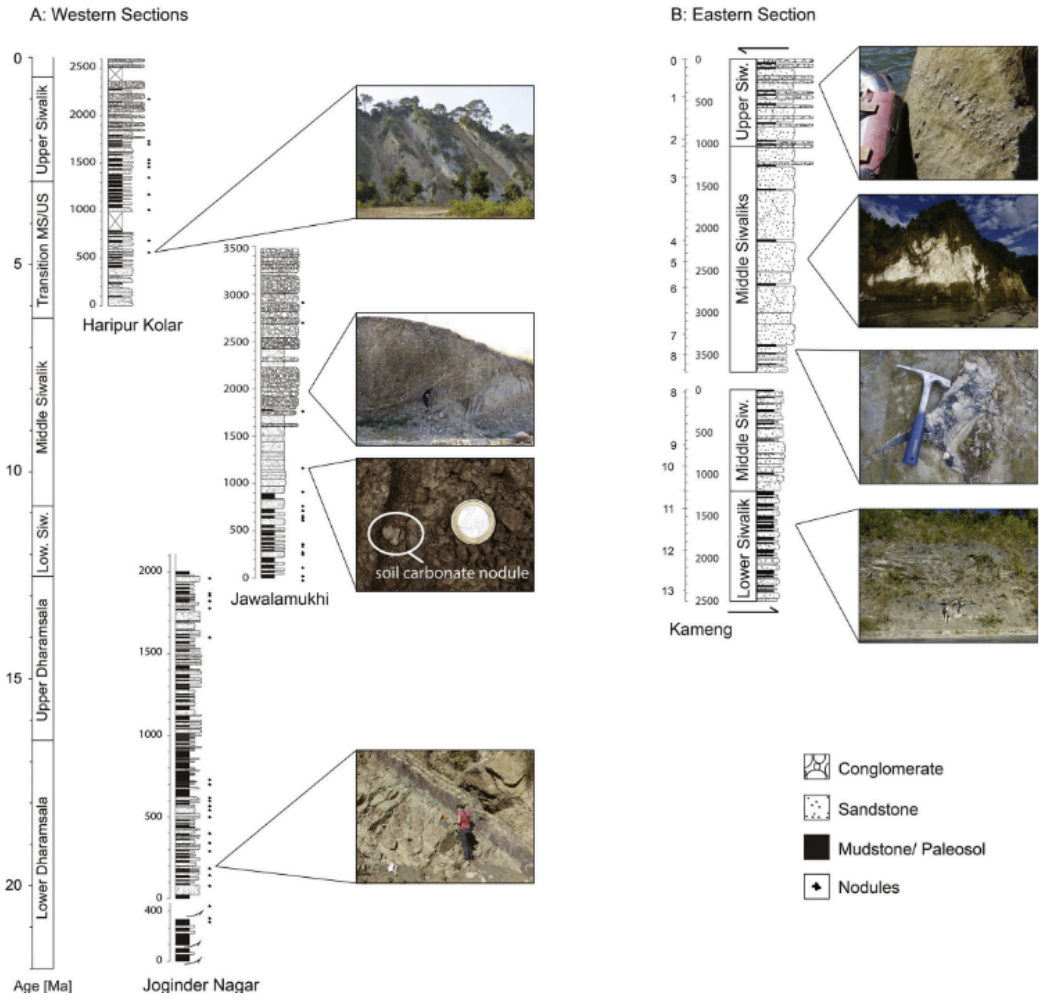

Fig. 4.2. Stratigraphy of sections of the Dharamsala and Siwalik Groups in the west (A) and in the east (B), with field photos showing sedimentological characteristics of different sub-groups

2. Setting

Neogene Himalayan foreland-basin sediments are composed of the fluvial Dharamsala Group of Late Oligocene and early Miocene age (Burbank et al., 1996), and the Siwalik Group deposited since the early Miocene. The Dharamsala rocks consist of continental fluvial, lacustrine or deltaic sediments, and contain fine-to medium grained sandstones, siltstones and overbank mudstones with soil carbonate nodules (Raiverman and Seshavataram, 1983). The sediments of the Siwalik Group are exposed nearly continuously along the front of the Himalayan range, with only minor age variation along strike (Burbank et al., 1996). They were deposited in the foreland before being incorporated in the foothills due to southward

propagation of deformation and onset of motion on the Main Frontal Thrust (MFT).

The Siwalik Group shows an overall coarsening- and thickening-upward trend, interpreted as recording increasingly proximal deposition (DeCelles et al., 1998), and is divided into the Lower, Middle and Upper Siwaliks (LS, MS, US). The LS were deposited by high-sinuosity streams (Nakayama and Ulak, 1999). The Middle Siwaliks (MS) are characterized by thickly bedded sandstones, which are medium- to coarse-grained and often rich in mica. The MS represent a depositional environment of large braided rivers. The Upper Siwaliks (US) consist of beds of conglomerates alternating with sandstone beds, deposited by gravelly braided rivers. Paleosols are developed throughout most of the Siwalik sections, with lateral and temporal variations in abundance: they are more abundant in the LS and in the west. Paleosols are characterized in western and central Himalayan sections by the presence of soil-carbonate nodules.

We sampled three sections exposing Dharamsala and Siwalik deposits in the western Himalaya; the Joginder Nagar (JN), Jawalamukhi (JW) and Haripur Kolar (HK) sections in Himachal Pradesh, and one Siwalik section in the eastern Himalaya; the Kameng River (KM) section in Arunachal Pradesh (Figures 1, 2). All sections have previously been dated by magnetostratigraphy (Meigs et al., 1995; Sangode et al., 1996; White et al., 2001; Chirouze et al., 2012). They span a time range of 20-1 Ma in the west and 13-1 Ma in the east. In the western sections, we collected paleosols and associated carbonate nodules, as well as fine-grained mudstone in zones without well-developed paleosols. Carbonate nodules are lacking in the Kameng section (Figure 2); therefore only mudstones, where possible from paleosols, were sampled. Additionally, modern river mud was sampled from riverbanks in proximity to the sections in both the west and the east. Modern river samples in the west (Beas River and Jner Khad River) were collected at an elevation of ~640 m within the sections, whereas the modern Kameng River sample was collected at an elevation of ~100 m downstream of the Siwalik.

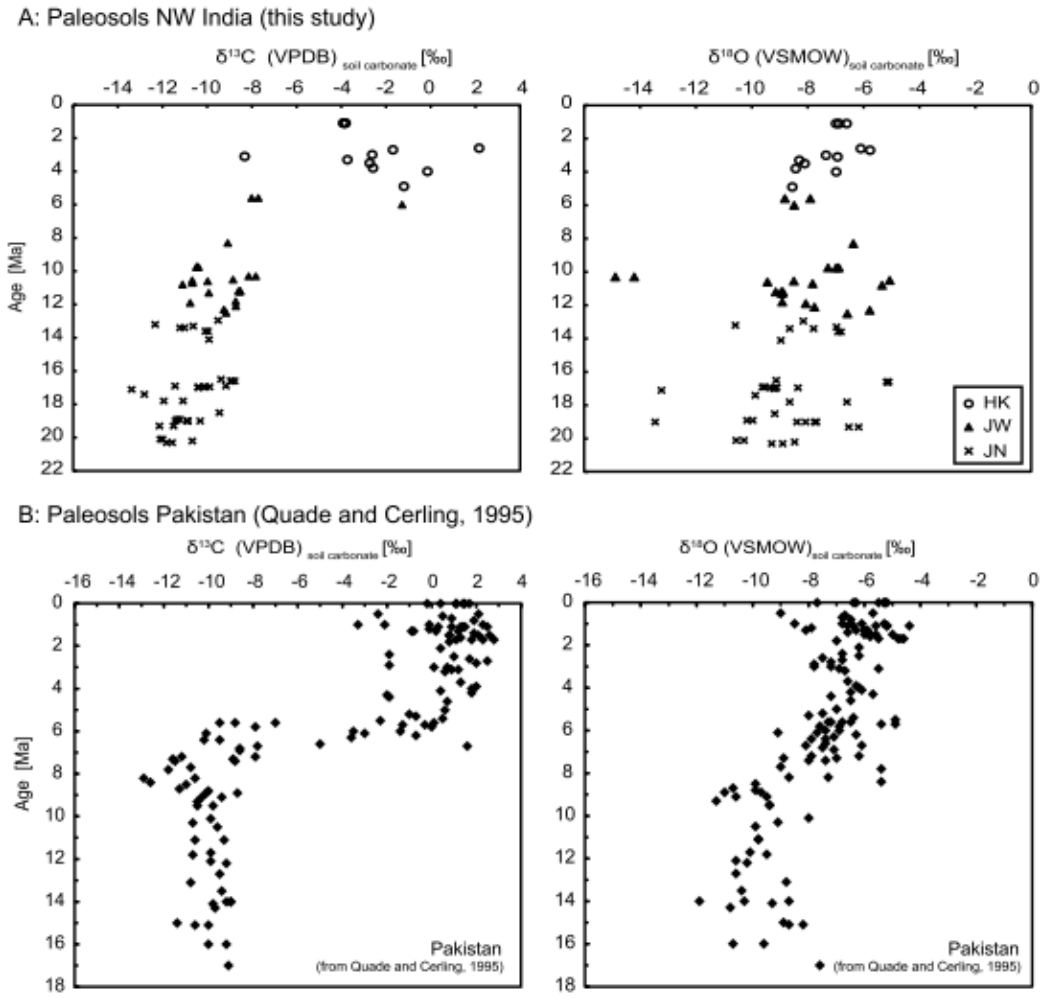

Fig. 4.3. A: δ13Csoil carb. and δ18Ovalues of soil carbonate in the western Himalaya. Different symbols indicate the different sections (HK: Haripur Kolar; JW: Jawalamukhi; JN: Joginder Nagar). B: δ13Csoil carb. and δ18Ovalues of soil carbonate in Pakistan from Quade and Cerling (1995).

3. Methods

$^{13}C/^{12}C$ and $^{18}O/^{16}O$ ratios (expressed as $\delta^{13}C$ and $\delta^{18}O$ values respectively) of soil carbonate nodules were determined using a multiflow analyser linked to an Isoprime 100 continuous flow mass spectrometer at the Lancaster University, UK. Approximately 600-700 µg of sample powder was drilled from each carbonate nodule and digested online at 90°C with dehydrated phosphoric acid in a He-flushed exetainer. Product CO_2 was analyzed for $\delta^{13}C_{CO2}$ and $\delta^{18}O_{CO2}$ and corrected against VPDB and VSMOW, respectively, using within-run analyses of international standards NBS18, LSVEC and CO-1. Within-run standard replication (1 s) was <0.1 ‰ for both C and O isotope

ratios. Sample replication based on separate drill aliquots of powder from the same carbonate nodule was <0.1‰ for $\delta^{13}C$ and <0.2 ‰ for $\delta^{18}O$ (1 s). $^{13}C/^{12}C$ ratios (expressed as $\delta^{13}C$ values) of bulk organic matter were determined using an Elementar Vario Micro elemental analyser linked to a VisION continuous flow mass spectrometer at the University of Lancaster. The carbonate content of each sample was removed by acid digestion using 1M ultrapure HCl and the resultant sample washed repeatedly using de-ionised water and centrifugation. Approximately 10 mg of each prepared sample was combusted within tin capsules at 960 °C to yield CO_2 for determination of $\delta^{13}C_{org}$. $\delta^{13}C$ values were corrected against VPDB using internal reference materials calibrated to international standards. Within-run $\delta^{13}C$ replication (1 s) was <0.2 ‰ for standards and <0.25 ‰ for samples.

4. Results

The three sections in Himachal Pradesh (Western Himalaya) provide a continuous age record over the past 20 Ma (Figure 3). Prior to ~7 Ma, $\delta^{13}C$ values of soil carbonate ($\delta^{13}C_{soil\ carb.}$) range between -8 ‰ and -13 ‰, whereas at ~7 Ma a shift towards more positive $\delta^{13}C$ values, ranging from +2 ‰ to -8 ‰, is observed (Figure 3; Appendix 1). $\delta^{18}O$ values range mostly from -11 ‰ to -4 ‰, except in the older part of the sections, where some values are as low as -14 ‰. A weak trend towards more positive $\delta^{18}O$ values over time is observed. As noted above, soil carbonate was not present in the eastern Himalayan section.

We additionally measured a continuous record of $\delta^{13}C$ in organic carbon ($\delta^{13}C_{org}$) in both the western and eastern sections (Figure 4; Appendix 1). In the west, a clear shift towards more positive $\delta^{13}C_{org}$ values is observed at ~7 Ma, synchronous with the $\delta^{13}C_{soil\ carb}$. Before 7 Ma, $\delta^{13}C_{org}$ values range between -23 ‰ and -27 ‰, while values are less negative, from -18 ‰ to -23 ‰, after 7 Ma. In the east, in contrast, $\delta^{13}C_{org}$ values remain constant between -29 ‰ and -23 ‰ since the middle Miocene and no shift towards more positive values is observed. Organic matter from modern river sediments show $\delta^{13}C$ values of approximately -26 ‰ and -23.5 ‰ in the west and in the east, respectively (Figure 4). Total Organic Carbon content

(TOC) in the western samples is mostly <0.5 % although samples from the JN can have up to 15% TOC (Figure 5). TOC of most Kameng samples is also <0.5 %, with some samples showing values up to 3%. There is no correlation between $\delta^{13}C_{org}$ values and TOC (Appendix 2).

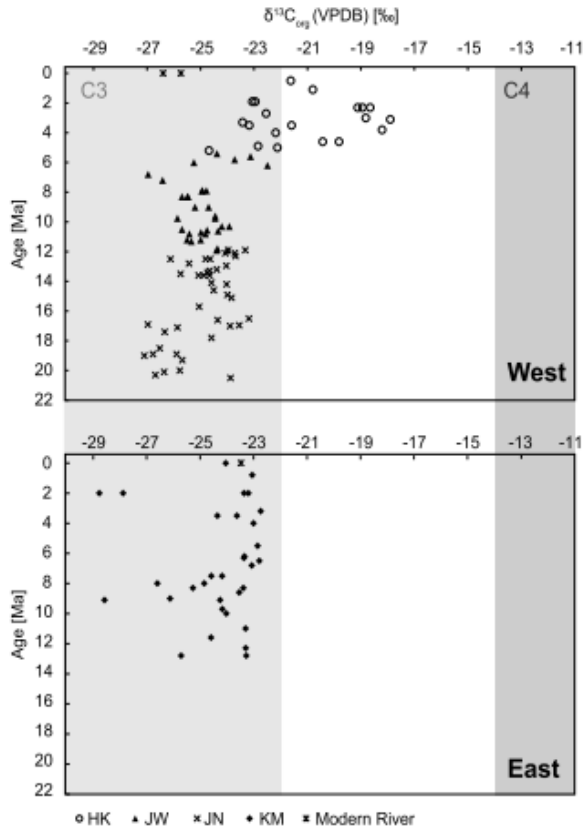

Fig. 4.4. δ13Corg of bulk organic carbon in the western (HK: Haripur Kolar; JW: Jawala- mukhi; JN Joginder Nagar) and the eastern (KM: Kameng) Himalayan sections. Light and dark grey shaded bars indicate δ13Corg values characteristic of C3 and C4 plants, respectively (Cerling et al. 1997)

5. Discussion

5.1. Modern river sediments and vegetation

The modern Ganga/Brahmaputra floodplain is widely used for agriculture and is therefore predominantly covered in C3 plants such as rice crops, and in the east by tea plantations (Blasco et al., 1996). This is not reflected by the organic carbon transported in the Ganga and Brahmaputra Rivers: $\delta^{13}C_{org}$ values of ~-21.9 ‰ in the modern Ganga floodplain are representative of a mixture of C4 and C3 plants, suggesting the presence of C4 plants in the west, whereas the modern Brahmaputra River carries organic carbon with $\delta^{13}C_{org}$ values of -23.0 ‰ in the range of C3 plants (Galy et al., 2008a).

Measured $\delta^{13}C_{org}$ values of modern river muds in both the west (Beas and Jner Khad River) and the east (Kameng River) are in the range of C3 plants. However, these modern river sediments were not collected in the floodplain but at the mountain front, where they will contain detrital organic carbon of C3 plants transported from higher elevations (Dobremez, 1978) and/or fossil organic carbon from Himalayan formations (Galy et al., 2008a), which both have a more negative isotopic signal. Dharamsala and Siwalik sediments were deposited further into the floodplain, and hence should carry a signal of floodplain vegetation.

5.2. Possible factors influencing the isotopic signal

Earlier studies (Quade et al., 1995a; Quade and Cerling, 1995; Singh et al., 2007; Sanyal et al., 2010) measured $\delta^{13}C$ on soil carbonate nodules, which can only be found in the western and central Himalayan Siwalik sections, and have consistently shown a change towards more positive values at ~7 Ma from Pakistan to Nepal (Quade et al., 1995a; Quade and Cerling, 1995). This change was interpreted in terms of a shift in vegetation, from initially dominated by C3 plants to containing C4 species. In order to compare the western and the eastern Himalaya in this study, we rely on $\delta^{13}C_{org}$ of bulk organic matter, as soil carbonate nodules are absent in the east. In both the western and the eastern sections, $\delta^{13}C_{org}$ values range between -23 ‰ and -29 ‰ before 7 Ma, indicating vegetation dominated by C3 plants. After 7 Ma, $\delta^{13}C_{org}$ in the western sections demonstrates an isotopic shift to values enriched in ^{13}C (~-19 ‰), suggesting that a component of the organic matter comprises C4 species. Carbonate nodules from western Himalayan sections analyzed in this study show a trend similar to $\delta^{13}C_{org}$, demonstrating a shift from C3-dominated vegetation composition, to an increasing proportion of C4 species in the younger sections. In the east, in contrast, $\delta^{13}C_{org}$ values stay in the range of C3 plants throughout the sedimentary succession (Figure 4). In modern soils, carbonate precipitates in equilibrium with soil CO_2 (Cerling et al., 1989) following an isotopic enrichment in ^{13}C of 10.36 ‰, (Cerling et al., 1989). Diffusional effects cause soil-respired CO_2 to be further

enriched in ^{13}C by 4.4 ‰. The total fractionation between soil organic matter and soil carbonate is ~14 ‰, at 25°C to ~17 ‰ at 0°C (Cerling et al., 1989). $\delta^{13}C_{soil\ carb.}$ values show a greater (~ +10‰) shift towards more positive values after 7 Ma than the $\delta^{13}C_{org}$ values (~ + 6 ‰; Figure 6). This discrepancy in the absolute value of the isotopic shift to signatures more enriched in ^{13}C likely reflects the nature of carbonate nodule production and organic matter source. Whereas soil carbonates reflect only the soil CO_2 characteristics and temperature during formation, the $\delta^{13}C_{org}$ values are more susceptible to bias by inherited and transported material.

Although $\delta^{13}C_{org}$ is usually interpreted to represent isotopic values of vegetation in the floodplain at the time of sediment deposition, it can potentially be biased by several factors, such as input of (likely C3 plant dominated) organic carbon from high elevations (Dobremez, 1978) and/or input of fossil organic carbon. The amount of fossil organic carbon present in Himalayan river sediments was estimated using the radiocarbon content of total organic carbon (TOC) of modern suspended and bedload sediments (Galy et al., 2008a; 2008b). Galy et al. (2008b) estimated the total amount of fossil organic carbon transported in the Ganga and Brahmaputra Rivers between 0.02 and 0.03 %. Sediments of the sampled sections mostly have TOC values >0.1 % (Figure 5) suggesting that the proportion of fossil carbon should be low, <30 % at most, if the modern amounts of transported fossil organic carbon can be extrapolated to the past. $\delta^{13}C_{org}$ of fossil organic carbon from Himalayan source rocks varies from -28 to -14.6‰ (Galy et al., 2008a); it is therefore unclear what the effect of varying proportions of fossil organic carbon on the observed $\delta^{13}C_{org}$ signal would be. However, we have no reason to assume the influence of fossil carbon to be very different from east to west and our data suggest this influence to be rather constant over time (see below). It is therefore unlikely that the spatial and temporal variations in $\delta^{13}C_{org}$ values could be explained by variable fossil organic carbon content.

Additionally, the efficiency of oxidation of organic carbon and hence the replacement of inherited carbon by floodplain carbon can influence the

$\delta^{13}C_{org}$ signal in modern river sediments (Galy et al., 2008a; 2011). Organic-carbon oxidation varies between the Ganges and Brahmaputra foreland basin, being more efficient in the Ganges floodplain due to different hydrological settings: the Ganges is a meandering river, whereas the Brahmaputra is a braided river with a narrower floodplain (Galy et al., 2008a). Oxidation of inherited organic carbon from vegetation at higher altitudes, hence with a C3 signal, is efficient in the Ganges floodplain (Galy et al., 2008a), as shown by the proportion of C4 organic matter increasing downstream in the Ganges floodplain (Figure 1). This pattern is not present in the Brahmaputra floodplain, suggesting that the influence of inherited carbon could therefore be greater in the Brahmaputra. Even though paleosols are less developed in the east, high TOC values indicate the presence of organic matter acquired from surface organic litter during pedogenesis (Figure 5). Degradation of organic matter in soils could have an influence on the $\delta^{13}C_{org}$: detrital organic matter has a ~1-2 ‰ more negative $\delta^{13}C$ signal than soil organic matter (von Fischer and Tieszen, 1995 and references therein). The more negative $\delta^{13}C$ values in the Kameng section could therefore be explained by the presence of more detrital organic matter. Differences in floodplain dynamics during transport and a greater influence of inherited organic carbon could possibly bias the signal but are unlikely to cancel out the entire C4 signal in the eastern Himalaya.

Further information on different organic carbon sources could potentially be derived from lipid biomarker analysis (i.e. compound-specific C- and H-isotope analysis; Freeman et al. 2001; Sachse et al., 2012). We extracted n-alkanes from samples of both the western and the eastern sections (see Appendix 3), but unfortunately n-alkane preservation was generally low in the sediments. Moreover, evidence of diagenetic overprinting was found in sediments with a sufficient concentration, evidenced by an absence of the predominance of odd carbon numbered n-alkane chain lengths (expressed as the carbon preference index, CPI), which is prevalent in modern plant and sediment samples. In modern plant material and immature sediments, CPI values are generally significantly >3 and up to 20,

whereas we found values around 1 in the Kameng samples, indicating diagenetic overprinting or addition of fossil carbon at the time of sedimentation. As a result of this, compound-specific hydrogen and carbon stable isotopic values would likely have been altered towards less negative values (Radke et al., 2005). While diagenetic overprinting could also have affected bulk $\delta^{13}C_{org}$ values by homogenizing the isotopic signal (Cerling et al., 1984; Bera et al., 2010), our CPI data remained uniform at values around 1 from the base of the section until ca. 2 Ma, indicating a similar degree of overprinting in these samples. Since we did not find any change in bulk $\delta^{13}C_{org}$ values corresponding to changes in CPI values, we argue that any potential overprinting affected all samples equally and as such relative changes can still be interpreted from bulk $\delta^{13}C_{org}$ values. In addition, the samples presented in Figure 3 are in the same isotopic range as modern soil carbonate nodules, indicating that diagenesis is unlikely to have influenced the isotopic values of the sedimentary samples.

The isotopic values of pedogenic carbonate are in equilibrium with soil CO_2 derived from irreversible oxidation of organic matter in a diffusion-controlled soil system at different temperatures. The isotopic equilibrium factor is dependent on temperature, hence if pedogenic carbonate precipitates in equilibrium with soil CO_2, $\delta^{13}C_{soil\ carb}$ should be enriched by ~14 ‰ at 25 °C and by 17 ‰ at 0 °C, respectively (Cerling et al. 1984, 1989). Carbonate nodules and their corresponding organic matter of the Dharamsala and Siwalik paleosols plot mostly at temperatures between 0 and 25°C and are therefore not isotopically altered by diagenesis (Figure 6), but rather formed within this soil temperature range. Samples below the 0°C line could reflect an inconsistency in the enrichment of ^{13}C in soil carbonate nodules compared to the co-existing organic matter. Most of the samples plotting under the 0°C line show a strong C4 signal, and the offset between $\delta^{13}C_{org}$ and $\delta^{13}C_{soil\ carb.}$ in these samples is greater than expected from isotopic equilibrium considerations. A possible explanation for this enhanced offset could be that the carbonate nodule formed in a sediment body (e.g. another paleosol horizon) that was separate from the parent organic matter.

Alternatively, organic matter may be more influenced by inherited organic matter from C3 vegetation, whereas the $\delta^{13}C_{soil\ carb}$ would more directly represent the local vegetation cover. However, this inconsistency does not reflect a diagenetic overprint, as it is found in the youngest samples, where diagenesis is least likely to occur.

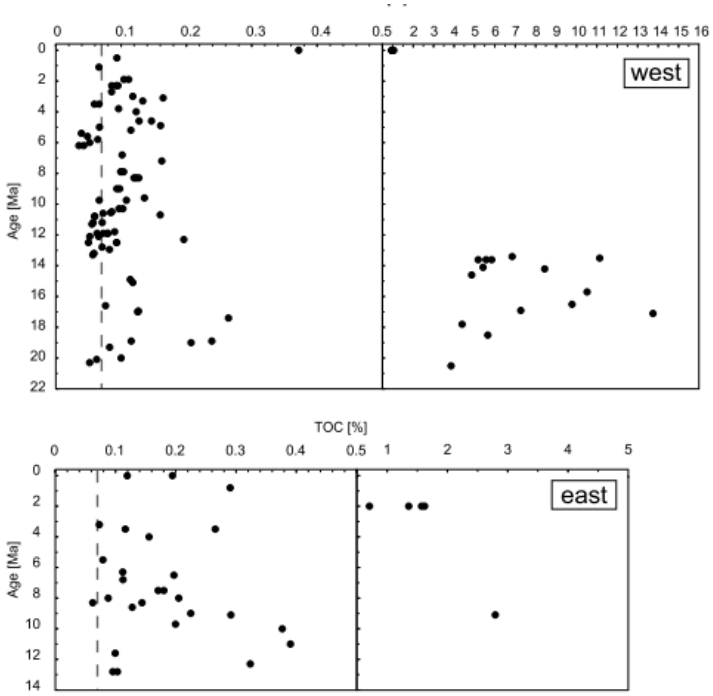

Fig. 4.5. Total organic carbon content (TOC) vs age [Ma], zoomed in to values below 0.5% on the left and values above 0.5% on the right. TOC values above 0.07% indicate dominant biogenic Corg, from soil organic matter and floodplain vegetation, rather than detrital and fossil Corg (Galy et al., 2008b).

$\delta^{18}O_{soil\ carb}$. values of the three western sections show a slight change towards more positive values (Figure 3), comparable to $\delta^{18}O$ values of the Surai Khola section in Nepal (Quade et al., 1995a). Only $\delta^{18}O_{soil\ carb.}$ values from Pakistan show a clear shift from values < -8 towards more positive values at ~8-6 Ma (Quade and Cerling 1995). In contrast, samples from this study already show $\delta^{18}O_{soil\ carb.}$ values > -8 before 7 Ma (Figure 3). A change in $\delta^{18}O_{soil\ carb.}$, which forms in-situ from soil water, can be associated with a change in either soil temperature ($\delta^{18}O_{soil\ carb.}$ being positively correlated with mean annual temperature; Cerling, 1984) and/or precipitation source: $\delta^{18}O$ values of precipitation of moisture transported from the Bay of Bengal are generally lighter (more negative) than $\delta^{18}O$ values of moisture transported by the

Westerlies (Caves et al., 2015 and references therein). The isotopic change over time was measured on samples of three separate sections (Figure 2) at different longitudinal locations; therefore the isotopic signature from precipitation may be location specific rather than representing change over time. However, there is no clear shift in $\delta^{18}O_{soil\ carb.}$ values going from one section to another (Figure 3), suggesting this effect to be minimal. As all sediments were deposited in the foreland, the influences of any altitudinal effects (Dansgaard, 1961) can also be excluded.

The coarsening-upward trend of sedimentary rocks throughout the sections reflects a change in depositional environment and location in the foreland basin, which varies from a distal floodplain for the Dharamsala and Lower Siwaliks to deposition closer to the mountain front in the Upper Siwaliks. At different locations in the foreland basin, the source of precipitation may vary from moisture influenced by the Westerlies, to moisture sourced from the ISM. More positive $\delta^{18}O_{soil\ carb.}$ values over time could therefore indicate an increasing influence of Westerlies with respect to ISM moisture sources, and/or a trend towards a warmer, drier climate, conducive to the growth of C4 vegetation.

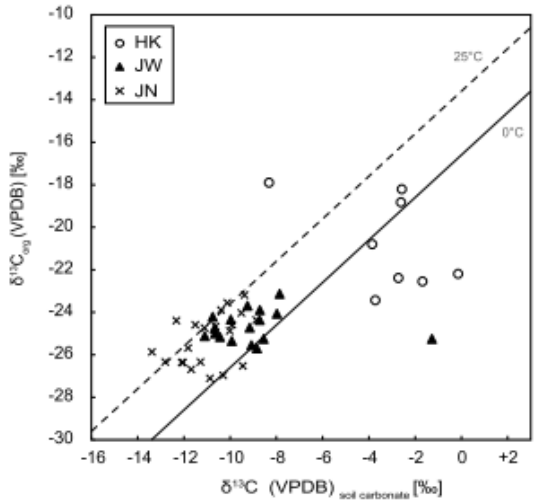

Fig. 4.6. δ13Csoil carb. of soil carbonate nodules vs. δ13Corg of co-existing organic matter of the western Dharamsala and Siwalik Group sections. Solid and dashed lines rep- resent isotopic values of pedogenic carbonate in isotopic equilibrium with the soil CO_2-derived from irreversible oxidation of organic matter in a diffusion controlled soil system at different temperatures (Cerling et al., 1989).

5.3. What caused the change of vegetation at ~7 Ma?

C3 and C4 plants grow in different environments and the $\delta^{13}C$ signal can therefore be used as an indirect climate indicator. Our data show that a change in vegetation occurred at ~7 Ma in the western Himalaya, but not in the east, where C3 plants have been dominant since the middle Miocene. As we have argued above, differences in floodplain setting (Galy et al., 2008a, 2011), while influencing the signal, cannot explain the observed lateral difference and neither can input of fossil organic carbon (Galy et al., 2008b). For this reason, there must be a remarkable lateral variation in the evolution of climate in the Himalayan region. The change at 7 Ma in the west and central Himalaya has been interpreted as resulting from a "stronger monsoon", characterized by greater seasonality (Quade et al., 1989, 1995a; Quade and Cerling, 1995). However, increased seasonality does not necessarily reflect higher amounts of monsoon precipitation; it could also indicate relatively less winter precipitation and thus a more arid (annual-average) climate (Molnar, 2005). C3 plants in the east indicate lower seasonality and higher annually averaged precipitation, consistent with modern precipitation patterns (Bookhagen and Burbank, 2010). The expansion of C4 plants in the west could therefore be a consequence of decreased winter precipitation, hence more seasonality associated with less (annually averaged) humidity, leading to a more arid climate. Overall, this difference in the $\delta^{13}C$ composition post-7 Ma is proposed to reflect water availability, with lower water availability in the west initiating a decline in C3 plants and a rise in C4 species (cf. Freeman and Colarusso, 2001). Dettman et al. (2001) likewise suggest a change in Indian summer monsoon characteristics and drying of the climate at 7.5 Ma. This scenario is supported by a change in $\delta^{18}O_{soil\ carb}$ towards more positive values.
Higher humidity in the east could be explained by the proximity to the Bay of Bengal, which is the major moisture source of precipitation in this area (Bookhagen et al., 2005). The western Himalaya is influenced by the Westerlies (Kotlia et al., 2015), which bring in winter precipitation. A decrease in the intensity of the Westerlies at 7 Ma would lead to more seasonality in

the western floodplain, with drier periods in winter. An alternative explanation for a generally more arid climate in the western Himalaya could be a decrease of moisture transport from the Bay of Bengal and the Arabian Sea, possibly linked to a decrease in the intensity of the ISM. However, this would result in less seasonality, hence a less favorable climate for C4 plants. The spatially variable record of $\delta^{13}C_{org}$ values strongly suggests that the change in vegetation at 7 Ma did not occur simultaneously along the Himalayan foreland, indicating that the change is at least partly driven by regional factors rather than being linked only to a global change in atmospheric pCO_2. This supports the findings of Pagani et al. (2005) and Beerling and Royer (2011), who noted that atmospheric pCO_2 levels favoring C4 plants were already reached during the Oligocene. Other dry regions such as the Mediterranean have been dominated by C3 plants since the Miocene (Quade et al., 1994, 1995b), also indicating that the late-Miocene expansion of C4 plants was not a global phenomenon. Regionally dependent factors, such as differences in seasonality or humidity, have clearly played a role in determining Himalayan vegetation patterns through time. Lateral variations in vegetation suggest that there is a threshold somewhere along the Himalayan front, where the amount of (either annual or winter) precipitation becomes too large for C4 plants to spread.

6. Conclusions

Stable carbon and oxygen isotopes were analyzed in carbonate nodules of the Joginder Nagar, Jawalamukhi and Haripur Kolar sections in the western Himalaya. $\delta^{13}C_{soilcarb.}$ values show a clear shift towards more positive values at 7 Ma, similar to the results of earlier studies in the western and central Himalaya. The lack of carbonate nodules in Siwalik sediments of the Kameng section, eastern Himalaya, is a first indicator that the lateral environmental and climatic differences in the modern Himalaya are representative of long-term climatic patterns. In order to directly compare the western and eastern sections, stable carbon isotopes on organic matter were analyzed and show a clear spatial difference. In the west, $\delta^{13}C_{org}$ values shift towards more

positive values at 7 Ma, consistent with the results on carbonate nodules, whereas they remain constant over the last 13 Ma in the east. The $\delta^{13}C$ of organic matter reflects the evolution of vegetation, with the development of C4 plants in the west and an environment that remains favorable for C3 plants in the east. Such variations in vegetation imply differences in climate, which became more seasonal and overall drier in the west at 7 Ma. The eastern Himalaya is more proximal to the main moisture source for precipitation (the Bay of Bengal); therefore, even though climate may have varied, it remained less seasonal and more humid, inhibiting the evolution of C4 plants. Therefore, the change in climate in the west and the onset of lateral variation is most likely caused by a change in strength of atmospheric circulation, such as a weakening of the influence of the Westerlies. These findings suggest that the late-Miocene expansion of C4 vegetation does not depend solely on atmospheric pCO_2 but also on regional changes in aridity and seasonality. Newly developed methods, such as clumped isotopes or stable isotopes on compound-specific organic carbon, even though unsuccessful in this study, could provide further insight into the climatic evolution and the development of C4 vegetation, both globally and regionally in the Himalayan region. This study has provided the first paleo-climate and -vegetation data from the eastern Himalaya; however, more such studies are needed to refine our understanding of the evolution of climate and vegetation in this area.

Acknowledgements

Montserrat Auladell-Mestre and David Hughes are thanked for the help preparing and measuring the samples. We acknowledge financial support from Initial Training Network (ITN) iTECC funded by the EU REA under the FP7 implementation of the Marie Curie Action, under grant agreement # 316966. ISTerre is part of the Labex OSUG@2020 (ANR10 LABX56). Reviews of earlier versions of this manuscript by Greg Retallack, Seema Sing and 3 anonymous reviewers have helped to significantly improve its clarity and focus.

5. Thesis synthesis and outlook

The main goal of this thesis was to create a better understanding in the (environmental) factors that influence surface water isotopes and organic proxies that are used for the reconstruction of precipitation, paleo-elevation and paleo-climate. By studying these secondary factors, we can get a more robust understanding of the development of climate in the past that have shaped the current conditions and landscape. Specifically we aimed to improve the understanding of which main processes drive the isotopic signature (δ^2H, $\delta^{18}O$ and *d*-excess) in both surface waters and biomarkers in soils along altitudinal transects in the NW Himalaya. In order to answer the research questions that were listed in chapter 2, we first investigated what the stable isotopes in the surface water signature from river waters reflect, regarding the hydrological conditions in the catchments. Second, we investigated how these stable isotopes are incorporated in the isotopic signature of biomarkers in chapter 3, by investigating the potential of δ^2H_{wax} in soils as a recorder of elevation. In addition to δ^2H_{wax} in soils, the distribution of brGDGTs and their potential to record elevation was assessed, in order to study the potential of recording elevation in biomarkers, using a multi-proxy approach. Ultimately, stable isotopes in soil organic matter and carbonates along the Himalayan arc analyzed in order to study monsoon intensity and seasonality over the last 20 Myr in chapter 4.

In the next chapter the answers to the research questions from chapter 1.6. will be summarized, after which an overall conclusion and future outlook is presented.

5.1. Different hydrological components contributing to the temporal en spatial isotopic signature of surface waters in the Himalaya

The first research question was focused on unraveling the complex mixture of the numerous different hydrological components of Himalayan surface waters by using of stable isotopes. By obtaining an extensive stable isotope (δ^2H and $\delta^{18}O$) surface water dataset covering an altitudinal range of 457 to 4,417 m asl, we found that lower elevation (<4,000 m asl) catchments in the Sutlej and Alaknanda are dominated by Rayleigh distillation processes. Therefore, these surface waters show an isotopic signature that agrees with monsoon-derived precipitation that originates from the Bay of Bengal.

At higher elevations (>4,000 m asl) there is a higher input from westerly-derived precipitation, as well as snow and glacial meltwater input affected by post-depositional processes such as sublimation. This signature is also found in the two one-yearlong timeseries, showing higher *d*-excess in the peak snowmelt season (coinciding with an areal decrease in remote-sensing derived snow-cover data), enabling the use of *d*-excess as a tracer for snow/ice melt in these surface waters.

5.2. Main processes influencing lipid biomarker δ^2H and brGDGT compositions and implications for paleoelevation studies

The second research question was aimed to find the processes that influence lipid biomarker lipid biomarker δ^2H values, as well as brGDGT compositions and the implications for paleoelevation studies. By comparing the surface water stable isotope dataset (as an annually integrated precipitation signal) to the soil δ^2H_{wax} values we found that these do generally record the surface water signature. However, the processes that influence this relationship are aridity and non-linear rainout processes. The brGDGT derived temperature (BayMBT MAAT) a highly significant correlation (r >0,8) in all catchments.

The combination of these proxies as a recorder of elevation resulted in the parameter $\Delta_{Elevation}$, which can reflect the hydrological conditions of the soil's depositional environment. Based on this finding, we suggest that paleosols showing large negative values for $\Delta_{Elevation}$ to be interpreted with caution. These soils could have been deposited during arid conditions, resulting in large offsets between reconstructed elevation and real sample site elevation.

5.3. Lateral variation in vegetation in the eastern and western Himalaya recorded in stable isotope compositions since the Miocene

The last research question was focused around stable isotopes in pedogenic carbonates and organic matter, and how these record the evolution of the monsoon, precipitation and the increase of C_4 plants. The spatially variable record (eastern and western Himalaya) of $\delta^{13}C$ values strongly suggests that the change in vegetation at 7 Ma did not occur simultaneously along the Himalayan foreland. The western section is located close to the moisture source, while the eastern section received less moisture, also supported by the lack of carbonate modules present in this section. The findings of this study show that the change in vegetation in the Himalayas was therefore not only driven by a global change in atmospheric pCO_2, but also partly by regional changes such as aridity and monsoon intensity, shown by the more positive $\delta^{18}O$ values in the soil carbonates. Extending the results from this study into a broader scientific view, it emphasizes the importance of close interplay between tectonic evolution of the Himalaya and climate.

5.4. Conclusion

In this thesis we unraveled the dominant environmental influences on elevation-recording proxies (i.e. surface water δ^2H, δ^2H_{wax}, and brGDGTs) in soils and surface waters. During our study we contributed to the creation of a more robust method (in the form of multiproxy analysis) for paleo-elevation

studies. The importance of precipitation on climate reconstruction tools was outlined in all three chapters:

- The analysis of stable isotopes in surface waters in Himalayan rivers provides important information regarding the Himalayan hydrological budget. Given the scope of the increasing temperatures due to climate change, surface water studies focusing on timing of snowmelt, melting processes and contribution of different components are indispensable.
- The multiproxy study (δ^2H_{wax}, and brGDGTs) of soils along elevational transects in the Himalaya implies that studies focusing on the tectonic uplift history of mountain ranges should employ a multiproxy approach, in order to attempt to create a more robust method for paleo-elevation/paleoclimate studies.
- Ultimately, the influence of aridity was observed in $\delta^{13}C$ and $\delta^{18}O$ in soil carbonates and bulk organic matter on the eastern and western parts of the Himalaya. The results showed that the monsoon influenced the evolution of vegetation (development of C4 plants in the west and an environment that remains favorable for C3 plants in the east) during the Miocene.

Beyond these findings, we have demonstrated the value in combining geochemical field-data with remote sensing data in chapter 2 and 3 of this thesis. Especially in large and remote areas such as the Himalayas, meteorological data is extremely scarce. With the use of remote sensing climate products as TRMM-derived precipitation, MODIS-derived MAT and a Digital Elevation Model (DEM), we were able to compare field data to timeseries of climate products. In order to collect this data in the field, a very challenging and time-consuming field trip would have to have been organized.

5.5. Future outlook

Overall, the key findings of this dissertation have extended the current knowledge of climatic influences on stable isotopes in surface waters, soil *n*-alkanes, soil carbonates and bulk organic matter that are used to reconstruct paleo-climate/elevation. In the section below I present my views on possible future experiments, in order to extend certain ideas or results that I encountered during my research.

5.5.1. Towards a Himalayan hydrological budget

My findings in the obtained high elevation surface water timeseries and the elevational transects of chapter 1 provide a basis for using d-excess to quantify hydrological budgets. However, in order to have a more extensive analysis of the seasonal influences in the surface waters along the altitudinal transects, it could help to unravel uncertainties of climatic influences. For the surface water study (chapter 2) we obtained two yearlong (weekly interval) datasets with surface water stable isotopes. However, these were both collected at relatively high elevation (Tabo: 3,280 m asl and Manali: 2,050 m asl.) The relative contribution of snowmelt along an altitudinal transect could be assessed with more certainty using more sampling stations at different elevations. In addition to an increase in the number of sampling locations, the collection of data at these stations should ideally be expanded. Currently, there is not much data on the weather conditions on these locations, due to the remoteness of the areas (and hence, a lack of meteorological stations). The recording of temperature and precipitation/weather circumstances can be valuable input in order to interpret trends in the isotopic signature of the samples with more certainty.

In support of this, creating a more extensive inventory of end-members could also allow us to interpret the isotope data with more certainty. Surface waters are a mixture of precipitation, surface runoff, snow- and glacial melt and groundwater. In the current surface water study we have collected existing data on the isotopic signature of precipitation and snow/glaciers in the area. However, a coupled field excursion sampling all

the end-members at the same time as the surface water samples are taken could provide us with more reliable data. Analyzing the isotopic signature of all the end members will make it easier to unravel the complex mixture of what surface water consists of. If there is a better handle on the snowmelt, in both quantity and timing this could result in valuable information for the people who rely on these rivers as their main water source.

5.5.2. Multiproxy analysis for a better handle on aridity

The Himalayan transects that were analysed in this thesis are situated along a very wide lateral transect (1,250 km long), covering different climatic conditions. This setting was very useful during the analysis of the δ^2H and brGDGT proxies. However, for the further development of the $\Delta_{Elevation}$ proxy it could be useful to test this in a different setting, where this can be tested under more stable climate conditions. This could involve a study area with a more linear temperature and precipitation decrease with elevation, to get a better answer on the major factors controlling $\Delta_{Elevation.}$

Second, in the experimental design of the soil study (chapter 3) all soils were assumed to be modern. However, this may not be the case in all areas. Even though only the top 5 cm of soils were sampled along the altitudinal transect, there could still be variation in age. Determining the age of soils by measuring the ^{14}C content in soil organic matter could be a great contribution to brGDGT and δ^2H_{wax} studies. In the example of Menges et al (2019) it was found that the modern top soils had a young ^{14}C bulk age of 42 years, while the deeper soil horizons had ^{14}C ages from 599 to 2,231 cal. BP. Combining the age data with the δ^2H_{wax} data showed that the upper valley was wetter during soil formation, after which drier conditions prevailed. Regarding the influence of environmental conditions on organic proxies, it is very valuable to collect information on the depositional environment.

5.5.3. Tracking monsoon intensity using stable isotopes

In the last chapter, stable isotopes of carbon and oxygen were employed to get a better handle on the late-Miocene expansion of C4 vegetation, finding

that this is not only influenced by $pCO_{2\text{-atm}}$, but also by the regional variation of seasonality and aridity. To explore the climatic evolution and expansion of C4 vegetation in these areas, methods such as clumped isotopes or isotopes on compound specific organic carbon (even though proven unsuccessful on these samples during our research due to the low organic matter content of the samples) could provide more insight. The leaf wax δ^2H, and brGDGT-derived MAT_{mr} could support our findings and interpretation on the $\delta^{13}C$ and $\delta^{18}O$ trend reflecting water availability.

Ultimately, this study has provided the first paleo- climate and -vegetation data from the eastern Himalaya. Despite the fact that there are numerous studies published on what caused the shift towards C4 plants in the Late Miocene, climate or tectonics, there is still no consensus on if this was a global or regional phenomenon. More paleoclimate records from this timeframe along the Himalayan Front could provide more information on the climate versus tectonics debate.

5.6. Our research in the bigger picture

As has been stated at the beginning of this dissertation: It is important to study past and current climate in the scope of global climate change. A key to the understanding of the future changes can be an assessment of the climate change that has taken place in de past. In its turn, in order to get a reliable image of the past climate, a good calibration of the aforementioned proxies is indispensable.

The contribution of our surface water stable isotope study to the larger climate change study has been the use of stable isotopes to assess the spatial and temporal changes in the current Himalayan water budget. Using stable isotopes of surface waters can pinpoint the timing of snowmelt from higher elevations, which large downstream populations depend on. The projected higher temperatures in the future could result in an earlier and stronger snow and glacial melt flux in the rivers, which can not only be a hazard to the population living downstream of these rivers, but could also lead to a depletion of the freshwater source for this population in time. Therefore, surface water monitoring using stable isotopes (δ^2H, $\delta^{18}O$ and *d*-

excess) is indispensible in these high mountainous areas. By setting up surface water sampling stations at several locations in trans-Himalayan rivers, the magnitude and duration of the snowmelt period can be monitored and developed into a snowmelt warning system. Moreover, this can system could be used to get a better handle on the total Himalayan water budget.

Second, the contribution of our study for stable isotopes (δ^2H_{wax}) and brGDGTs in soils for the paleoclimate studies has been the valuable information that is stored in these biomarkers. In the second chapter we demonstrated the strength of a multiproxy study to study the change of climate conditions along an orogen, supported by remote sensing climate products. Combining the two proxies into the $\Delta_{Elevation}$ proxy provided us with a tool to get information about hydrological conditions in the soil depositional environment. Our study has been carried out in modern soils, but our $\Delta_{Elevation}$ proxy can add important information when applied to paleosols studies attempting to unravel paleoelevation. The $\Delta_{Elevation}$ proxy does not only pinpoint which samples are showing a paleoelevation influenced by aridity, but also show the general hydrological conditions during soil formation. Applying this to paleoelevation studies could strengthen the current paleoelevation database and add valuable information on the depositional environment of (paleo)soils.

Third, the observed shift from C_3 to C_4 vegetation in the Himalayan foreland at 7 Ma tells us that the cause was not only the global increase of pCO_2, but could also be partly influenced by regional changes (aridity/monsoon intensity). Extending the results from this study into a broader scientific view, it emphasizes the importance of close interplay between tectonic evolution of the Himalaya and climate. The methodology from this study can also be applied in paleoclimate studies in other mountain ranges, to test if a similar trend is observed, and to get a better handle on the importance of regional changes in past C_3 to C_4 vegetation shifts.

Ultimately, the large diversity in analyses that were performed for this thesis provided us with the knowledge that a multiproxy analysis can provide a steady scientific framework on the past and current climate conditions. By

combining as many methods as possible, a clearer image will be unraveled about the timing of mountain uplift, the evolution of vegetation and the development of the current climate. Continuous development in the field of paleoclimate results in new methods and the discovery of new biomarkers. As a combined effort of the science community we will get closer to a more refined understanding of the interplay between tectonics and climate, and what shaped our current landscape.

7. References

Andermann C, Longuevergne L, Bonnet S, Crave A, Davy P, Gloaguen R. 2012. Impact of transient groundwater storage on the discharge of Himalayan rivers. *Nature Geoscience* **5** (2): 127–132 DOI: 10.1038/ngeo1356

Bai, Y., Fang, X. and Tian, Q. (2012) 'Spatial patterns of soil n -alkane δ D values on the Tibetan Plateau: Implications for monsoon boundaries and paleoelevation reconstructions', *Journal of Geophysical Research: Atmospheres*, 117(D20), p. n/a-n/a. doi: 10.1029/2012JD017803.

Bai, Y. Fang, X., Jia, G., Sun, J., Wen, R., Ye, Y. (2015) Different altitude effect of leaf wax n-alkane δD values in surface soils along two vapor transport pathways, southeastern Tibetan Plateau. *Geochimica et Cosmochimica Acta*, **170,** 94–107.

Bartaya SK, Bhattacharya SK, Ramesh R, Somayajulu BLK. 1995. δ18O and δD systematics in the surficial waters of the Gaula river catchment area, Kumaun Himalaya, India. *Journal of Hydrology* **167**: 11 DOI: 10.1016/0022-1694(94)02634-N

Beerling, D. J., and Royer, D. L., 2011, Convergent Cenozoic CO_2 history: Nature Geoscience, v. 4, no. 7, p. 418-420.

Benn, D. I., and Owen, L. A., 1998, The role of the Indian summer monsoon and the mid-latitude westerlies in Himalayan glaciation: review and speculative discussion: Journal of the Geological Society, London, v. 155, p. 353-363.

Bera, M.K., Sarkar, A., Tandon, S.K:, Samanta, A. and Sanyal, P., 2010, Does burial diagenesis reset pristine isotopic compositions in paleosol carbonates?: Earth and Planetary Science Letters, v. 300, p. 85-100.

Bershaw J, Penny S.M, Garzione C.N. (2012). Stable isotopes of modern water across the Himalaya and eastern Tibetan Plateau: Implications for estimates of paleoelevation and paleoclimate. *Journal of Geophysical Research: Atmospheres* **117**: 1–18 DOI: 10.1029/2011JD016132

Blasco F., Bellan M.F. and Aizpuru M., (1996) A vegetation map of tropical continental Asia at scale 1.5 million: Journal of Vegetation Science, v. 7, p.623–634.

Biggs TW, Lai C-T, Chandan P, Lee RM, Messina A, Lesher RS, Khatoon N. 2015. Evaporative fractions and elevation effects on stable isotopes of high elevation lakes and streams in arid western Himalaya. *Journal of Hydrology* **522**: 239–249 DOI: 10.1016/j.jhydrol.2014.12.023

Bookhagen B, Burbank DW. 2010. Toward a complete Himalayan hydrological budget: Spatiotemporal distribution of snowmelt and rainfall and their impact on river discharge. *Journal of Geophysical Research: Earth Surface* **115** (3): F03019 DOI: 10.1029/2009JF001426

Bookhagen B, Thiede RC, Strecker MR. 2005. Abnormal monsoon years and their control on erosion and sediment flux in the high, arid northwest Himalaya. *Earth and Planetary Science Letters* **231** (1–2): 131–146 DOI: 10.1016/j.epsl.2004.11.014

Bookhagen, B., Thiede, R. C., and Strecker, M. R., 2005, Late Quaternary intensified monsoon phases control landscape evolution in the northwest Himalaya: Geology, v. 33, no. 2, p. 149-152.

Bookhagen, B. *et al.* (2006) 'Holocene monsoonal dynamics and fluvial terrace formation in the northwest Himalaya, India', *Geology*, 34(7), p. 601. doi: 10.1130/G22698.1.

Bookhagen, B. and Burbank, D. W. (2006) 'Topography, relief, and TRMM-derived rainfall variations along the Himalaya', *Geophysical Research Letters*, 33(8), p. L08405. doi: 10.1029/2006GL026037.

Boos, W. R., and Kuang, Z., 2010, Dominant control of the South Asian monsoon by orographic insulation versus plateau heating: Nature, v. 463, no. 7278, p. 218-222.

Bowen GJ, Revenaugh J. 2003. Interpolating the isotopic composition of modern meteoric precipitation. *Water Resources Research* **39** (10): 1–13 DOI: 10.1029/2003WR002086

Burbank, D.W., Beck, R.A. and Mulder, T., 1996, The Himalayan foreland basin. In The Tectonic Evolution of Asia, Yin, A and Harrison, TM (eds) Cambridge University press, p. 149-188.

Bush, R.T., McInerney, F.A. (2013) Leaf wax n-alkane distributions in and across modern plants: Implications for paleoecology and chemotaxonomy. *Geochimica et Cosmochimica Acta*, **117**, 161–179.

Cannon, F. *et al.* (2016) 'Winter westerly disturbance dynamics and precipitation in the western Himalaya and Karakoram : a wave-tracking approach', *Theoretical and Applied Climatology*, pp. 27–44. doi: 10.1007/s00704-015-1489-8.

Cannon, F. , Carvalho, L.M.V., Jones, C., Bookhagen, B. (2014) Multi-annual variations in winter westerly disturbance activity affecting the Himalaya. *Climate Dynamics*, **44**, 441–455.

Caves, J. K., Winnick, M. J., Graham, S. A., Sjostrom, D. J., Mulch, A., and Chamberlain, C. P., 2015, Role of the westerlies in Central Asia climate over the Cenozoic: Earth and Planetary Science Letters, v. 428, p. 33-43.

Cerling, T. E., 1984, The stable isotopic composition of modern soil carbonate and its relationship to climate: Earth and Planetary Science Letters, v. 71, no. 2, p. 229-240.

Cerling, T. E., Harris, J. M., MacFadden, B. J., Leakey, M. G., Quade, J., Eisenmann, V., and Ehleringer, J. R., 1997, Global vegetation change through the Miocene/Pliocene boundary: Nature, v. 389, no. 6647, p. 153-158.

Cerling, T. E., Quade, J., Wang, Y., and Bowman, J. R., 1989, Carbon isotopes in soils and palaeosols as ecology and palaeoecology indicators: Nature, v. 341, no. 6238, p. 138-139.

Chen J, Gupta AK. 2012. Parametric Statistical Change Point Analysis. *Birkhäuser Boston: Boston*. DOI: 10.1007/978-0-8176-4801-5

Chikaraishi, Y. and Naraoka, H. (2003) 'Compound-specific δD-δ13C analyses of n-alkanes extracted from terrestrial and aquatic plants', *Phytochemistry*, 63(3), pp. 361–371. doi: 10.1016/S0031-9422(02)00749-5.

Chirouze, F., Dupont-Nivet, G., Huyghe, P., van der Beek, P., Chakraborti, T., Bernet, M., and Erens, V., 2012, Magnetostratigraphy of the Neogene Siwalik Group in the far eastern Himalaya: Kameng section, Arunachal Pradesh, India: Journal of Asian Earth Sciences, v. 44, p. 117-135.

Clark I, Fritz P. 1997. Environmental Isotopes in Hydrogeology. *Lewis Publishers, Boca Raton*. ISBN 1-56670-249-6

Clift, P. D. *et al.* (2008) 'Correlation of Himalayan exhumation rates and Asian monsoon intensity', *Nature Geoscience*, 1(12), pp. 875–880. doi: 10.1038/ngeo351.

Coffinet, S., Huguet, A., Pedentchouk, N., Bergonzini, L., Omuombo, C., Williamson, D., Anquetil, C., Jones, M., Majule, A., Wagner, T., Derenne, S. (2017) Evaluation of branched GDGTs and leaf wax n-alkane δ2H as (paleo) environmental proxies in East Africa. *Geochimica et Cosmochimica Acta*, **198**, 182–193.

Coffinet, S., Huguet, A., Williamson, D., Fosse, C., Derenne, S. (2014) Potential of GDGTs as a temperature proxy along an altitudinal transect at Mount Rungwe (Tanzania). Org. Geochem. **68**, 82–89.

Cotton, J.M., Cerling, T.E., Hoppe, K.A., Mosier, T.M., Still, C.J., 2016. Climate, CO_2, and the history of North American grasses since the Last Glacial Maximum. Science Advances 2, e1501346.

Dalai, T. K., Bhattacharya, S. K. and Krishnaswami, S. (2002) 'Stable isotopes in the source waters of the Yamuna and its tributaries: seasonal and altitudinal variations and relation to major cations', *Hydrological Processes*, **16**(17), pp. 3345–3364. doi: 10.1002/hyp.1104.

Dang, X., Yang, H., Naafs, B.D.A., Pancost, R.D., Xie, S. (2016) Evidence of moisture control on the methylation of branched glycerol dialkyl glycerol tetraethers in semi-arid and arid soils. *Geochimica et Cosmochimica Acta*, **189**, 24–36.

Dansgaard W. 1964. Stable isotopes in precipitation. *Tellus* **16** (4): 436–468 DOI: 10.3402/tellusa.v16i4.8993

Dansgaard, W., 1961, The isotopic composition of natural waters: Medd. om Gronland, v. 165, no. 2, p. 1-120.

Dash, S.K.,Kulkarni, M. Mohanty, U.C., Prasad, K.. (2009) Changes in the characteristics of rain events in India. *Journal of Geophysical Research*, 114, p.D10109

Davtian, N., Ménot, G., Bard, E., Poulenard, J. Podwojewski, P. (2016) Consideration of soil types for the calibration of molecular proxies for soil pH and temperature using global soil datasets and Vietnamese soil profiles. *Organic Geochemistry*, **101**, 140–153.

DeCelles, P. G., Gehrels, G. E., Quade, J., Ojha, T. P., Kapp, P. A., and Upreti, B. N., 1998, Neogene foreland basin deposits, erosional unroofing, and the kinematic history of the Himalayan fold-thrust belt, western Nepal: Geological Society of America Bulletin, v. 110, no. 1, p. 2-21.

De Jonge, C., Stadnitskaia, A., Hopmans, E. C., Cherkashov, G., Fedotov, A., Sinninghe Damsté, J.S., (2014a) In situ produced branched glycerol dialkyl glycerol tetraethers in suspended particulate matter from the Yenisei River, Eastern Siberia. *Geochimica et Cosmochimica Acta*, **125**, 476–491.

De Jonge, C. *et al.* (2014b) 'Occurrence and abundance of 6-methyl branched glycerol dialkyl glycerol tetraethers in soils: Implications for palaeoclimate reconstruction', *Geochimica et Cosmochimica Acta*, 141, pp. 97–112. doi: 10.1016/j.gca.2014.06.013.

De Jonge C., Radujkovic´ D., Sigurdsson B. D., Weedon J. T., Janssens I. and Peterse F. (2019) Lipid biomarker temperature proxy responds to abrupt shift in the bacterial community composition in geothermally heated soils. Org. Geochem. 137, 103897.

Dearing Crampton -Flood, E., Tierney, J.E., Peterse, F., Kirkels, F.M.S.A., Sinninghe Damsté, K.S. (2020) BayMBT: A Bayesian calibration model for branched glycerol

dialkyl glycerol tetraethers in soils and peats. *Geochimica et Cosmochimica Acta*, **268**, 142 - 159

Dettman, D.L., Fang, X., Garzione, C. N., Li, J. (2003) Uplift-driven climate change at 12 Ma: A long δ18O record from the NE margin of the Tibetan plateau. *Earth and Planetary Science Letters*, **214**, 267–277.

Dettman, D. L., Kohn, M. J., Quade, J., Ryerson, F. J., Ojha, T. P., and Hamidullah, S., 2001, Seasonal stable isotope evidence for a strong Asian monsoon throughout the past 10.7 m.y: Geology, v. 29, no. 1, p. 31-34.

Didan, K., 2015. MOD13C2 MODIS/Terra Vegetation Indices Monthly L3 Global 0.05Deg CMG V006. NASA EOSDIS Land Processes DAAC.

Diefendorf, A. F. and Freimuth, E. J. (2017) 'Extracting the most from terrestrial plant-derived n-alkyl lipids and their carbon isotopes from the sedimentary record: A review', *Organic Geochemistry*, 103, pp. 1–21. doi: 10.1016/j.orggeochem.2016.10.016.

Diefendorf, A.F., Freeman, K.H., Wing, S.L., Graham, H.V., (2011) Production of n-alkyl lipids in living plants and implications for the geologic past. *Geochimica et Cosmochimica Acta*, **75**, 7472–7485.

Dirghangi, S.S., Pagani, M., Hren, M.T., Tipple, B.J. (2013) Distribution of glycerol dialkyl glycerol tetraethers in soils from two environmental transects in the USA. *Organic Geochemistry*, **59,** 49–60.

Dobremez, J. F. et al., 1978, Carte écologique du Népal 1/250000. University of Grenoble, Grenoble.

Eglinton, G. and Hamilton, R. J. (1967) 'Leaf Epicuticular Waxes', *Science*, 156(3780), pp. 1322–1335. doi: 10.1126/science.156.3780.1322.

Eglinton, G. and Logan, G. A. (1991) 'Molecular Preservation [and Discussion]', p. 15. doi: https://doi.org/10.1098/rstb.1991.0081.

Ehleringer, J. R., 1988, Carbon isotope ratios and physiological processes in aridland plants. In Ehleringer, J.R., Nagy, K.A. (Eds.), Stable Isotopes in Ecological Research.: Springer, New York, p. 41-54.

Ernst, N. Peterse, F., Breitenbach, S. F. M., Syiemlieh, H.J., Eglinton, T. (2013) Biomarkers record environmental changes along an altitudinal transect in the wettest place on Earth. *Organic Geochemistry*, **60**, 93–99.

Farquhar, G. D., Ehleringer, J. R. and Hubick, K. T. (1989) 'Carbon Isotope Discrimination and Photosynthesis', *Annual Reviews in Plant Physiology and Plant Molecular Biology*, 40(1), pp. 503–537. doi: 10.1146/annurev.arplant.40.1.503.

Feakins, S.J. & Sessions, A.L. (2010). Controls on the D/H ratios of plant leaf waxes in an arid ecosystem. *Geochimica et Cosmochimica Acta*, **74**, 2128–2141.

France-Lanord, C., and Derry, L. A., 1994, $\delta^{13}C$ of organic carbon in the Bengal Fan: Source evolution and transport of C3 and C4 plant carbon to marine sediments: Geochimica et Cosmochimica Acta, v. 58, no. 21, p. 4809-4814.

Freeman, K. H., and Colarusso, L. A., 2001, Molecular and isotopic records of C4 grassland expansion in the late Miocene: Geochimica et Cosmochimica Acta, v. 65, no. 9, p. 1439-1454.

Fröhlich K. Gibson JJ, Aggarwal PK. (2001). Deuterium excess in precipitation and its climatological significance. *In: Study of environmental change using isotope techniques. Vienna, International Atomic Energy Agency*, pp 54–65 ISBN 92–0–116402–5

Galewsky, J. (2009) 'Orographic precipitation isotopic ratios in stratified atmospheric flows: Implications for paleoelevation studies', *Geology*, 37(9), pp. 791–794. doi: 10.1130/G30008A.1.

Galy, V., France-Lanord, C., and Lartiges, B., 2008a, Loading and fate of particulate organic carbon from the Himalaya to the Ganga–Brahmaputra delta: Geochimica et Cosmochimica Acta, v. 72, no. 7, p. 1767-1787.

Galy, V., Beyssac, O., France-Lanord, C., and Eglinton, T., 2008b, Recycling of graphite during Himalayan erosion: A geological stabilization of carbon in the crust: Science, v. 322, p. 943-945.

Galy, V., Eglinton, T., France-Lanord, C., and Sylva, S., 2011, The provenance of vegetation and environmental signatures encoded in vascular plant biomarkers carried by the Ganges–Brahmaputra rivers: Earth and Planetary Science Letters, v. 304, no. 1–2, p. 1-12.

Gansser, A. (1964) 'The Geology of the Himalayas', 10(10).

Garcin, Y. *et al.* (2012) 'Hydrogen isotope ratios of lacustrine sedimentary n-alkanes as proxies of tropical African hydrology: Insights from a calibration transect across Cameroon', *Geochimica et Cosmochimica Acta*, 79, pp. 106–126. doi: 10.1016/j.gca.2011.11.039.

Garzione, C. N., Dettman, D. L., *et al.* (2000) 'High times on the Tibetan Plateau: Paleoelevation of the Thakkhola graben, Nepal', *Geology*, 28(4), pp. 339–342. doi: 10.1130/0091-7613(2000)

Garzione CN, Quade J, Decelles PG, English NB. 2000. Predicting paleoelevation of Tibet and the Himalaya from N 18 O vs . altitude gradients in meteoric water across the Nepal Himalaya. *Earth Planet. Sci. Lett.* **183,** 215–229.

Gat JR. 1996. Oxygen and Hydrogen Isotopes in the Hydrologic Cycle. *Annual Review of Earth and Planetary Sciences* **24** (1): 225–262 DOI: 10.1146/annurev.earth.24.1.225

Gat, J., and I. Carmi (1970), Evolution of the isotopic composition of atmospheric waters in the Mediterranean Sea area, *J. Geophys. Res.*, **75**, 3039–3048, doi:10.1029/JC075i015p03039.

Gat JR, Confiantini R. 1981. Stable Isotope Hydrology: Deuterium and Oxygen-18 in the Water Cycle. *IAEA Technical Reports Series No. 210*: 339 DOI: 10.1029/EO063i045p00861

Hall DK, Riggs GA. 2016. MODIS/Aqua Snow Cover Monthly L3 Global 0.05Deg CMG, Version 6. Boulder, Colorado USA. NASA National Snow and Ice Data Center Distributed Active Archive Center DOI: http://dx.doi.org/10.5067/MODIS/MYD10CM.006

Hayes, J. M. (1993) 'Factors controlling 13C contents of sedimentary organic compounds: Principles and evidence', *Marine geology*, p. 15.

Herbert, T.D., Lawrence, K.T., Tzanova, A., Peterson, L.C., Caballero-Gill, R., Kelly, C.S., 2016. Late Miocene global cooling and the rise of modern ecosystems. Nature Geosci. 9, 843–847.

Herrmann, N. *et al.* (2017) 'Hydrogen isotope fractionation of leaf wax n -alkanes in southern African soils', *Organic Geochemistry*. doi: 10.1016/j.orggeochem.2017.03.008.

Hobbie, E. and Werner, R. A. (2004) 'Intramolecular, compound-specific, and bulk carbon isotope patterns in C_3 and C_4 plants: a review and synthesis', *New Phytologist*, 161(2), pp. 371–385. doi: 10.1111/j.1469-8137.2004.00970.x.

Hoffmann B, Feakins SJ, Bookhagen B, Olen SM, Adhikari DP, Mainali J, Sachse D. 2016. Climatic and geomorphic drivers of plant organic matter transport in the Arun River, E Nepal. *Earth and Planetary Science Letters* **452**: 104–114 DOI: 10.1016/j.epsl.2016.07.008

Hoorn, C., Ohja T., Quade J., 2000. Palynological evidence for vegetation development and climate change in the Sub-Himalayan Zone (Neogene, Central Nepal).Palaeogeogr.Palaeoclimatol. Palaeoecol. 163, 133–161.

Hopmans, E., Schouten, S., Sinninghe Damsté, J.S. (2016) The effect of improved chromatography chromatography on GDGT-based palaeoproxies. Org. Geochem. **93**, 1–6.

Hou, J. *et al.* (2007) 'Hydrogen isotopic variability in leaf waxes among terrestrial and aquatic plants around Blood Pond, Massachusetts (USA)', *Organic Geochemistry*, 38(6), pp. 977–984. doi: 10.1016/j.orggeochem.2006.12.009.

Hou, J., D'Andrea, W. J. and Huang, Y. (2008) 'Can sedimentary leaf waxes record D/H ratios of continental precipitation? Field, model, and experimental assessments', *Geochimica et Cosmochimica Acta*, 72(14), pp. 3503–3517. doi: 10.1016/j.gca.2008.04.030.

Hren MT, Bookhagen B, Blisniuk PM, Booth AL, Chamberlain CP. 2009. δ18O and δD of streamwaters across the Himalaya and Tibetan Plateau: Implications for moisture sources and paleoelevation reconstructions. *Earth and Planetary Science Letters* **288** (1–2): 20–32 DOI: 10.1016/j.epsl.2009.08.041

Hren, M.T., Pagani, M., Erwin, D.M., Brandon, M., (2010) Biomarker reconstruction of the early Eocene paleotopography and paleoclimate of the northern Sierra Nevada. *Geology*, **38**, 7–10.

Huang, Y., Shuman, B., Wang, Y. and Webb, T. (2004) 'Hydrogen isotope ratios of individual lipids in lake sediments as novel tracers of climatic and environmental change: a surface sediment test', *Journal of Paleolimnology*, 31(3), pp. 363–375. doi: 10.1023/B:JOPL.0000021855.80535.13.

Huffman, G. J. *et al.* (2014) 'TRMM3B42 3-Hour Realtime TRMM Multi-satellite Precipitation Analysis', *NASA/GSFC, Greenbelt, MD, USA, ftp://arthurhou.pps.eosdis.nasa.gov/trmmdata/*, p. 2014.

Hughes, M., Hall, A. & Fovell, R.G. (2009) Blocking in Areas of Complex Topography, and Its Influence on Rainfall Distribution. *Journal of the Atmospheric Sciences*, 66, 508–518.

Immerzeel WW, Droogers P, de Jong SM, Bierkens MFP. 2009. Large-scale monitoring of snow cover and runoff simulation in Himalayan river basins using remote sensing. *Remote Sensing of Environment* **113** (1): 40–49 DOI: 10.1016/j.rse.2008.08.010

IPCC. 2014. *Climate Change 2014 - Synthesis Report. Contribution of Working Groups I, II and III to the Fifth Assessment Report of the Intergovernmental Panel on Climate Change [Core Writing Team, R.K. Pachauri and L.A. Meyer (eds.)]. IPCC, Geneva, Switzerland, 151 p*. DOI: 10.1017/CBO9781107415324

Ives JD, Messerli B. 1990. The Himalayan dilemma: Reconciling development and conservation. *United Nations University* **7** (1): 93–94 DOI: 10.1016/0264-8377(90)90063-5

Jaeschke, A., Rethemeyer, J., Lappé, M., Schouten, S., Boeckx, P., Schefuß, E. (2018) "Influence of Land Use on Distribution of Soil n-Alkane ΔD and BrGDGTs along an Altitudinal Transect in Ethiopia : Implications for (Paleo)Environmental Studies." *Organic Geochemistry*, **124,** 77–87.

Jarvis A, Reuter HI, Nelson E, Guevara. 2008. Hole-filled seamless SRTM data V4, International Centre for Tropical Agriculture (CIAT), available from http://srtm.csi.cgiar.org.

Jay, Q., Cerling, T. E. and Bowman, J. R. (1989) 'Development of Asian Monsoon revealed by marked ecological shift during the latest Miocene in northern Pakistan', *Nature*, 342(September), pp. 189–92. doi: 10.1038/340301a0.

Jeelani Gh, Bhat N a., Shivanna K. 2010. Use of δ18O tracer to identify stream and spring origins of a mountainous catchment: A case study from Liddar watershed, Western Himalaya, India. *Journal of Hydrology* **393** (3–4): 257–264 DOI: 10.1016/j.jhydrol.2010.08.021

Jia, G. *et al.* (2008) 'Soil n-alkane δD vs. altitude gradients along Mount Gongga, China', *Geochimica et Cosmochimica Acta*, 72(21), pp. 5165–5174. doi: 10.1016/j.gca.2008.08.004.

Jouzel, J., and L. Merlivat (1984), Deuterium and oxygen-18 in precipitation: Modeling of the isotope effects during snow formation, *J. Geophys. Res.,* **89**, 11,749–11,757. doi:10.1029/JD089iD07p11749.

Kahmen, A., Schefuß, E., Sachse, D. (2013a) Leaf water deuterium enrichment shapes leaf wax n-alkane δD values of angiosperm plants I: Experimental evidence

and mechanistic insights. *Geochimica et Cosmochimica Acta*, **111**, 39–49.

Kahmen, A., Hoffmann, B., Schefuß, E., Arndt, S.K., Cernusak, L.A., West, J.B., Sachse, D.(2013b) Leaf water deuterium enrichment shapes leaf wax n-alkane δD values of angiosperm plants II: Observational evidence and global implications. *Geochimica et Cosmochimica Acta*, **111**, 50–63.

Karim A, Veizer J. 2002. Water balance of the Indus River Basin and moisture source in the Karakoram and western Himalayas: Implications from hydrogen and oxygen isotopes in river water. *Journal of Geophysical Research: Atmospheres* **107**: 1–12 DOI: 10.1029/2000JD000253

Kendall, C., Coplen, T.B. (2001) Distribution of oxygen-18 and deuteriun in river waters across the United States. *Hydrological Processes*, **15**, 363–1393.

Kotlia, B.S., Singh, A.K., Joshi, L.M., Dhaila, B.S., 2015. Precipitation variability in the Indian Central Himalaya during last ca. 4,000 years inferred from a speleothem record: Impact of Indian Summer Monsoon (ISM) and Westerlies. Quat. Int. 371, 244–253.

Kumar B, Rai SP, Kumar US, Verma SK, Garg P, Kumar SVV, Jaiswal R, Purendra BK, Kumar SR, Pande NG. 2010. Isotopic characteristics of Indian precipitation. *Water Resources Research* **46** (August 2009): 1–15 DOI: 10.1029/2009WR008532

Kumar V, Singh P, Singh V. 2007. Snow and glacier melt contribution in the Beas River at Pandoh Dam, Himachal Pradesh, India. *Hydrological Sciences Journal* **52** (2): 376–388 DOI: 10.1623/hysj.52.2.376

Lai, C.-T., Ehleringer, J.R., Bond, B.J., Paw, K., T., (2006) Contributions of evaporation, isotopic non-steady state transpiration and atmospheric mixing on the delta18O of water vapour in Pacific Northwest coniferous forests. *Plant, cell & environment*, **29**, 77–94.

Lang, T. J. and Barros, A. P. (2004) 'Winter Storms in the Central Himalayas', *Journal of the Meteorological Society of Japan*, 82Das(3), pp. 829–844. doi: 10.2151/jmsj.2004.829.

Lechler AR, Niemi NA. 2012. The influence of snow sublimation on the isotopic composition of spring and surface waters in the southwestern United States : Implications for stable isotope – based paleoaltimetry and hydrologic studies. *GSA Bulletin* (3): 318–334 DOI: 10.1130/B30467.1

Licht, A., van Cappelle, M., Abels, H. A., Ladant, J. B., Trabucho-Alexandre, J., France-Lanord, C., Donnadieu, Y., Vandenberghe, J., Rigaudier, T., Lecuyer, C., Terry Jr, D., Adriaens, R., Boura, A., Guo, Z., Soe, A. N., Quade, J., Dupont-Nivet, G., and Jaeger, J. J., 2014, Asian monsoons in a late Eocene greenhouse world: Nature, v. 513, no. 7519, p. 501-506.

Liu, W., Yang, H. (2008) Multiple controls for the variability of hydrogen isotopic compositions in higher plant n-alkanes from modern ecosystems. *Global Change Biology*, **14**, 2166–2177.

Luo, P., Peng, P., Gleixner, G., Zheng, Z., Pang, Z., Ding, Z., (2011) Empirical relationship between leaf wax n-alkane δD and altitude in the Wuyi, Shennongjia and Tianshan Mountains, China: Implications for paleoaltimetry. *Earth and Planetary Science Letters*, **301**, 285–296.

Maurya, A.S., Shah, M., Deshpande, R.D., Bhardwal, R.M., Prasad, A., Gupta, S.K, (2011). Hydrograph separation and precipitation source identification using stable water isotopes and conductivity: River Ganga at Himalayan foothills. *Hydrological Processes*, **25**, 1521–1530.

Meese, B., Bookhagen, B., Olen, S.M., Barthold, F., Sachse, D.., (2018) The effect of Indian Summer Monsoon rainfall on surface water δD values in the central Himalaya. *Hydrological Processes*, **32**, 3662–3674.

Meigs, A. J., Burbank, D. W., and Beck, R. A., 1995, Middle-late Miocene (>10 Ma) formation of the Main Boundary thrust in the western Himalaya: Geology, v. 23, no. 5, p. 423-426.

Menges, J., Huguet, C., Alcañiz, J.M., Fietz, S., Sachse, D., Rosell-Melé, A., (2014) Influence of water availability in the distributions of branched glycerol dialkyl glycerol

tetraether in soils of the Iberian Peninsula. *Biogeosciences*, **11,** 2571–2581.

Molnar, P., England, P. (1990). Late Cenozoic uplift of mountain ranges and global climate change: chicken or egg? *Nature*, 3**46**, 29–34.

Molnar, P., 2005, Mio-Pliocene Growth of the Tibetan Plateau and Evolution of East Asian Climate: Palaeontologia Electronica, v. 8, no. 1, p. 1-23.

Molnar, P., Boos, W. R., and Battisti, D. S., 2010, Orographic Controls on Climate and Paleoclimate of Asia: Thermal and Mechanical Roles for the Tibetan Plateau: Annual Review of Earth & Planetary Sciences, v. 38, p. 77-102.

Moser, H., and W. Stichler, Deuterium and oxygen-18 contents as index of the properties of snow blankets, in Proceedings of the Grindelwald Symposium on Snow Mechanics, April 1974, *IAHS Publ.* **114**, pp. 122–135, 1975.

Mulch, A. *et al.* (2004) 'Reconstructing paleoelevation in eroded orogens', *Geology*, 32(6), p. 525. doi: 10.1130/G20394.1.

Naafs, B.D.A., Gallego-Sala, A.V., Inglis, G.N., Pancost, R.D. (2017) Refining the global branched glycerol dialkyl glycerol tetraether (brGDGT) soil temperature calibration. *Organic Geochemistry*, **106**, 48–56.

Newberry, S.L., Nelson, D.B., Kahmen, A. (2017) Cryogenic vacuum artifacts do not affect plant water-uptake studies using stable isotope analysis. *Ecohydrology*, **10**, 1892.

Nijampurkar VN, Rao DK. 1992. Ice dynamics and climatic studies on Himalayan glaciers based on stable and radioactive isotopes. *International Symposium on Snow and Glacier Hydrology* (218): 355–369. DOI: 10.3189/172756502781831511

Nieto-Moreno, V., Rohrmann, A., van der Meer, M. T. J., Sinninghe Damsté, J.S., Sachse, D., Tofelde, S., Niedermeyer, E.M., Strecker, M.R., Mulch, A., (2016) Elevation-dependent changes in n-alkane δD and soil GDGTs across the South Central Andes. *Earth and Planetary Science Letters*, **453**, 234–242.

Norris J, Carvalho LM V, Jones C, Cannon F, Bookhagen B, Palazzi E, Tahir AA. 2016. The spatiotemporal variability of precipitation over the Himalaya: evaluation of one-year WRF model simulation. *Climate Dynamics*: 1–26 DOI: 10.1007/s00382-016-3414-y

Pagani, M., Zachos, J. C., Freeman, K. H., Tipple, B., and Bohaty, S., 2005, Marked decline in atmospheric carbon dioxide concentrations during the Paleogene: Science, v. 309, p. 600.

Pande K, Padia JT, Ramesh R, Sharma KK. 2000. Stable isotope systematics of surface water bodies in the Himalayan and Trans-Himalayan (Kashmir) region. *Proceedings of the Indian Academy of Sciences, Earth and Planetary Sciences* **109** (1): 109–115 DOI: 10.1007/bf02719154

Pang H, Hou S, Kaspari S, Mayewski P, Introne D, Masson-Delmotte V, Jouzel J, Li Z, He Y, Hong S, et al. 2012. Atmospheric circulation change in the central Himalayas indicated by a high-resolution ice core deuterium excess record. *Climate Research* **53** (1): 1–12 DOI: 10.3354/cr01090

Pedentchouk, N., Sumner, W., Tipple, B., Pagaini, M. (2008) $\delta^{13}C$ and δD compositions of n-alkanes from modern angiosperms and conifers: An experimental set up in central Washington State, USA. *Organic Geochemistry*, **39**, 1066–1071.

Peters, K. E., Walters, C. C. and Moldowan, J. M. (2005) 'The Biomarker Guide', in *The Biomarker Guide*, pp. 198–251. doi: https://doi.org/10.1017/CBO9780511524868.

Peterse, F., van der Meer, M.T.J., Schouten, S., Jia, G., Ossebaar, J., Blokker, J., Sinninghe Damsté, J.S. (2009) Assessment of soil n-alkane δD and branched tetraether membrane lipid distributions as tools for paleoelevation reconstruction. *Biogeosciences Discussions*, **6,** 2799–2807.

Peterse, F., van der Meer, M.T.J., Schouten, S,, Weijers, J.H.W., Fierer, N., Jackson, R.B., Kim, J-H., Sinninghe Damsté, J.S. (2012) Revised calibration of the MBT-CBT paleotemperature proxy based on branched tetraether membrane lipids in surface soils. *Geochimica et Cosmochimica Acta*, **96**, 215–229.

Petit, J.R., Jouzel, J., Raynaud, D., Barkov, N.I., Barnola, J.-M., Basile, I., Bender, M., Chappellaz, J., Davis, M., Delaygue, G., Delmotte, M., Kotlyakov, V.M., Legrand, M., Lipenkov, V.Y., Lorius, C., Pepin, L., Ritz, C., Saltzman, E., Stievenard, M., 1999. Climate and atmospheric history of the past 420,000 years from the Vostok ice core, Antarctica. *Nature* **399**, 429–436. DOI: 10.1038/20859

Pfeffer WT, Arendt AA, Bliss A, Bolch T, Cogley JG, Gardner AS, Hagen J, Hock R, Kaser G, Kienholz C, et al. 2014. The Randolph Glacier Inventory : a globally complete inventory of glaciers. *Journal of Glaciology* **60** (221): 537–552 DOI: 10.3189/2014JoG13J176

Poage, M. A. (2001) 'Empirical relationships between elevation and the stable isotope composition of precipitation and surface waters: considerations for studies of paleoelevation change', *American Journal of Science*, 301(1), pp. 1–15. doi: 10.2475/ajs.301.1.1.

Polissar, P.J., Freeman, K.H., Rowley, D.B., McInerney, F.A., Currie, B.S. (2009) Paleoaltimetry of the Tibetan Plateau from D/H ratios of lipid biomarkers. *Earth and Planetary Science Letters*, **287**, 64–76.

Polissar, P.J., Freeman, K.H. (2010). Effects of aridity and vegetation on plant-wax δD in modern lake sediments. *Geochimica et Cosmochimica Acta*, **74,** 5785–5797.

Poulsen, C.J., Ehlers, T.A. & Insel, N. (2010).Onset of Convective Rainfall During Gradual Late Miocene Rise of the Central Andes. *Science*, **328**, 490–493.

Quade, J., Cerling, T. E. and Bowman, J. R. (1989) 'Development of Asian monsoon revealed by marked ecological shift during the latest Miocene in northern Pakistan', *Nature*, 342(6246), pp. 163–166. doi: 10.1038/342163a0.

Quade, J., Solounias, N., and Cerling, T. E., 1994, Stable isotopic evidence from paleosol carbonates and fossil teeth in Greece for forest or woodlands over the past 11 Ma: Palaeogeography, Palaeoclimatology, Palaeoecology, v. 108, no. 1, p. 41-53.

Quade, J. *et al.* (1995) 'Late Miocene environmental change in Nepal and the northern Indian subcontinent: Stable isotopic evidence from paleosols', *Geological Society of America Bulletin*, p. 17.

Quade, J. and Cerling, T. E. (1995) 'Expansion of C4 grasses in the late miocene of nortern pakistan: Evidence from stable isotopes in paleosols', *Pelaeogeography, paleoclimatology, paleoecology*, 115, pp. 91–116.

Quade, J., Cerling, T. E., Andrews, P., and Alpagut, B., 1995b, Paleodietary reconstruction of Miocene faunas from Paşalar, Turkey using stable carbon and oxygen isotopes of fossil tooth enamel: Journal of Human Evolution, v. 28, no. 4, p. 373-384.

Quade, J., Garzione, C. and Eiler, J. (2007) 'Paleoelevation Reconstruction using Pedogenic Carbonates', *Reviews in Mineralogy and Geochemistry*, **66**, pp. 53–87. doi: 10.2138/rmg.2007.66.3.

Racoviteanu AE, Armstrong R, Williams MW. 2013. Evaluation of an ice ablation model to estimate the contribution of melting glacier ice to annual discharge in the Nepal Himalaya. *Water Resources Research* **49** (9): 5117–5133 DOI: 10.1002/wrcr.20370

Radke J., Bechtel A., Gaupp R., Puttmann W., Schwark L., Sachse D. and Gleixner G. (2005) Correlation between hydrogen isotope ratios of lipid biomarkers and sediment maturity. Geochim. Cosmochim. Acta **69**, 5517–5530.

Rai SP, Thayyen RJ, Purushothaman P, Kumar B. 2016. Isotopic characteristics of cryospheric waters in parts of Western Himalayas , India. *Environmental Earth Sciences* **75** (7): 1–9 DOI: 10.1007/s12665-016-5417-8

Ramesh R, Sarin. 1992. Stable isotope study of the Ganga (Ganges) river system. *Journal of Hydrology* **139**: 49–62. DOI:10.1016/0022-1694(92)90194-Z

Rees, H. G. and Collins, D. N. (2006) 'Regional differences in response of flow in glacier-fed Himalayan rivers to climatic warming', 2169, pp. 2157–2169. doi: 10.1002/hyp.

Reichle, R. De Lannoy, G., Koster, R.D., Crow, W.T., Kimball, J.S. (2016) SMAP L4 9 km EASE-Grid Surface and Root Zone Soil Moisture Geophysical Data, Version 2. [SPL4SMAU]. *Boulder, Colorado USA. NASA National Snow and Ice Data Center Distributed Active Archive Center*.

Risi C, Landais a., Winkler R, Vimeux F. (2013). Can we determine what controls the spatio-temporal distribution of d-excess and ^{17}O-excess in precipitation using the LMDZ general circulation model? *Climate of the Past* **9** (5): 2173–2193 DOI: 10.5194/cp-9-2173-2013

Rohrmann A, Strecker MR, Bookhagen B, Mulch A, Sachse D, Pingel H, Alonso RN, Schildgen TF, Montero C. 2014. Can stable isotopes ride out the storms ? The role of convection for water isotopes in models , records , and paleoaltimetry studies in the central Andes. *Earth and Planetary Science Letters* **407**: 187–195 DOI: 10.1016/j.epsl.2014.09.021

Rohrmann, A., Sachse, D., Mulch, A., Pingel, H., Tofelde, S., Alonso, R., Strecker, M. (2016). Miocene orographic uplift forces rapid hydrological change in the southern central Andes, *Scientific Reports*, **6**, 35678.

Rowley, D. B. and Currie, B. S. (2006) 'Palaeo-altimetry of the late Eocene to Miocene Lunpola basin, central Tibet', *Nature*, 439(7077), pp. 677–681. doi: 10.1038/nature04506.

Rowley DB, Pierrehumbert RT, Currie BS. 2001. A new approach to stable isotope-based paleoaltimetry: Implications for paleoaltimetry and paleohypsometry of the High Himalaya since the late Miocene. *Earth and Planetary Science Letters* **188** (1–2): 253–268 DOI: 10.1016/S0012-821X(01)00324-7

Rowley D. B. (2007) Stable Isotope-Based Paleoaltimetry: Theory and Validation. *Rev. Mineral. Geochemistry* **66**, 23–52.

Rozanski K, Araguás-Araguás L, Gonfiantini R. 1993. Isotopic patterns in modern global precipitation: *Journal of geophysical research*, **103** 1–36 DOI: 10.1029/GM078p0001

Ruddiman, W.F., and Kutzbach, J.E., 1989, Forcing of late Cenozoic Northern Hemisphere climate by plateau uplift in southern Asia and the American West: Journal of Geophysical Re- search, v. 94, p. 18,409–18,427.

Ruddiman, W. F. (2007) *Earth ' s Climate, Past and future*, *Earth's Climate-Past and Future*.

Sachse, D., Billault, I., Bowen, G.J., Chikaraishi, Y., Dawson, T. E., Feakins, S.J., Freeman, K.H., Magill, C. R., McInerney, F.A., van der Meer, M.T.J., Polissar, P., Robins, R. J., Sachs, J., P. Schmidt, H. J., Sessions, A. L., White, J.W.C., West, J.B., Kahmen, A., (2012). Molecular Paleohydrology: Interpreting the Hydrogen-Isotopic Composition of Lipid Biomarkers from Photosynthesizing Organisms. *Annual Review of Earth and Planetary Sciences*, **40**, 221–249.

Sachse, D., Radke, J., Gleixner, G. (2004). Hydrogen isotope ratios of recent lacustrine sedimentary n-alkanes record modern climate variability. *Geochimica et Cosmochimica Acta*, **68,** 4877–4889.

Sachse, D., Radke, J., Gleixner, G., 2006. δD values of individual n-alkanes from terrestrial plants along a climatic gradient – Implications for the sedimentary biomarker record. *Organic Geochemistry*, **37**, 469–483.

Sangode, S. J., Kumar, R., and Ghosh, S. K., 1996, Magnetic Polarity Stratigraphy of the Siwalik Sequence of Haripur area (H.P.), NW Himalaya: Journal Geological Society India, v. 47, no. June 1996, p. 683-704.

Sanyal, P., Bhattacharya, S.K., Kumar, R., Ghosh, S.K., Sangode, S.J., 2004. Mio-Pliocene monsoonal record from Himalayan foreland basin (Indian Siwalik) and its relation to vegetational change. Palaeogeogr. Palaeoclimatol. Palaeoecol. 205, 23–41.

Sanyal, P., Sarkar, A., Bhattacharya, S. K., Kumar, R., Ghosh, S. K., and Agrawal, S., 2010, Intensification of monsoon, microclimate and asynchronous C4 appearance: Isotopic evidence from the Indian Siwalik sediments: Palaeogeography, Palaeoclimatology, Palaeoecology, v. 296, no. 1–2, p. 165-173.

Sarkar S, Prasad S, Wilkes H, Riedel N, Stebich M, Basavaiah N, Sachse D. 2015. Monsoon source shifts during the drying mid-Holocene: Biomarker isotope based evidence from the core 'monsoon zone' (CMZ) of India. *Quaternary Science Reviews* **123** (December): 144–157 DOI: 10.1016/j.quascirev.2015.06.020

Sauer, P. E. *et al.* (2001) 'Compound-specific D/H ratios of lipid biomarkers from sediments as a proxy for environmental and climatic conditions', *Geochimica et Cosmochimica Acta*, 65(2), pp. 213–222. doi: 10.1016/S0016-7037(00)00520-2.

Schouten, S., Hopmans, E. C. and Sinninghe Damsté, J. S. (2013) 'The organic geochemistry of glycerol dialkyl glycerol tetraether lipids: A review', *Organic Geochemistry*, 54, pp. 19–61. doi: 10.1016/j.orggeochem.2012.09.006.

Schwab, V.F., Garcin, Y., Sachse, D., Todou, G., Séné, O., Onana, J-M., Achoundong, G., Gleixner, G. (2015) Effect of aridity on $\delta^{13}C$ and δD values of C3 plant- and C4 graminoid-derived leaf wax lipids from soils along an environmental gradient in Cameroon (Western Central Africa). *Organic Geochemistry*, **78**, 99–109.

Schwanghart W, Scherler D. 2014. Short Communication: TopoToolbox 2 – MATLAB-based software for topographic analysis and modeling in Earth surface sciences. *Earth Surface Dynamics* **2** (1): 1–7 DOI: 10.5194/esurf-2-1-2014

Sengupta S, Sarkar A. 2006. Stable isotope evidence of dual (Arabian Sea and Bay of Bengal) vapour sources in monsoonal precipitation over north India. *Earth and Planetary Science Letters* **250** (3–4): 511–521 DOI: 10.1016/j.epsl.2006.08.011

Sessions, A.L. Burgoyne, T.W., Schimmelman, A., Hayes, J.M. (1999). Fractionation of hydrogen isotopes in lipid biosynthesis. *Organic Geochemistry*, **30,** 1193–1200

Singh, J. S. and Singh, S. P. (1987) 'Forest Vegetation of the Himalaya', *Botanical Review, Vol. 53, No. 1 (Jan. - Mar., 1987), pp. 80-192*, 01(1), pp. 80–192.

Singh P, Jain SK. 2007. Snow and glacier melt in the Satluj River at Bhakra Dam in the western Himalayan region Snow and glacier melt in the Satluj River at. *Hydrological Sciences Journal* **6667** (November) DOI: 10.1080/02626660209492910

Singh, B. P., Lee, Y. I., Pawar, J. S., and Charak, R. S., 2007. Biogenic features in calcretes developed on mudstone: Examples from Paleogene sequences of the Himalaya, India: Sedimentary Geology, v. 201, no. 1–2, p. 149-156.

Singh, S. *et al.* (2013) 'Tectonics or climate: What drove the Miocene global expansion of C4 grasslands?', *International Journal of Earth Sciences*, 102(7), pp. 2019–2031. doi: 10.1007/s00531-013-0893-5.

Sinninghe Damsté, J. S. *et al.* (2008) 'Altitudinal shifts in the branched tetraether lipid distribution in soil from Mt. Kilimanjaro (Tanzania): Implications for the MBT/CBT continental palaeothermometer', *Organic Geochemistry*, 39(8), pp. 1072–1076. doi: 10.1016/j.orggeochem.2007.11.011.

Smith, F. A. and Freeman, K. H. (2006) 'Influence of physiology and climate on δD of leaf wax n-alkanes from C3 and C4 grasses', *Geochimica et Cosmochimica Acta*, 70(5), pp. 1172–1187. doi: 10.1016/j.gca.2005.11.006.

Smith, T. and Bookhagen, B. (2018) 'Changes in seasonal snow water equivalent distribution in High Mountain Asia (1987 to 2009)', *Science Advances*, 4(1), p. e1701550. doi: 10.1126/sciadv.1701550.

Smith T, Bookhagen B. 2016. Assessing uncertainty and sensor biases in passive microwave data across High Mountain Asia. *Remote Sensing of Environment* **181**: 174–185 DOI: 10.1016/j.rse.2016.03.037

Steinke, S., Groeneveld, J., Johnstone, H., and Rendle-Bühring, R., 2010, East Asian summer monsoon weakening after 7.5 Ma: Evidence from combined planktonic foraminifera Mg/Ca and δ18O (ODP Site 1146; northern South China Sea): Palaeogeography, Palaeoclimatology, Palaeoecology, v. 289, no. 1–4, p. 33-43.

Stichler W, Schotterer U, Fröhlich K, Ginot P, Kull C, Gäggeler H, Pouyaud B. 2001. Influence of sublimation on stable isotope records recovered from high-altitude glaciers in the tropical Andes. *Journal of Geophysical Research* **106** (D19): 22613 DOI: 10.1029/2001JD900179

Tian L, Yao T, MacClune K, White JWC, Schilla a., Vaughn B, Vachon R, Ichiyanagi K. 2007. Stable isotopic variations in west China: A consideration of moisture sources. *Journal of Geophysical Research* **112** (D10): D10112 DOI: 10.1029/2006JD007718

Tipple, B.J., Berke, M. A., Doman, C. E., Khachaturyan, S., Ehleringer, J.R. (2013) Leaf-wax n-alkanes record the plant-water environment at leaf flush. *Proceedings of the National Academy of Sciences of the United States of America*, **110**, 2659–64.

Trabucco, A. & Zomer, R.J. (2009) Global Aridity Index (Global- Aridity) and Global Potential Evapo-Transpiration (Global-PET) Geospatial Database, CGIAR Consortium for Spatial Information. *Www.Cgiar-Csi.Org*

USGS, (2006) Shuttle Radar Topography Mission, 3Arc Second Scene. Global Land Cover Facility. University of Maryland, College Park, MD.

van der Veen, I. *et al.* (2020) 'Validation and calibration of soil δ2H and brGDGTs along (E-W) and strike (N-S) of the Himalayan climatic gradient', *Geochimica et Cosmochimica Acta*, 290, pp. 408–423. doi: 10.1016/j.gca.2020.09.014.

Varay LS, Rai SP, Singh SK, Jain V. 2017. Estimation of snow and glacial melt contribution through stable isotopes and assessment of its impact on river morphology through stream power approach in two Himalayan river basins. *Environmental Earth Sciences* **76** (23): 809 DOI: 10.1007/s12665-017-7142-3

Vögeli, N. *et al.* (2017) 'Lateral variations in vegetation in the Himalaya since the Miocene and implications for climate evolution', *Earth and Planetary Science Letters*, 471, pp. 1–9. doi: 10.1016/j.epsl.2017.04.037.

von Fischer, J.C. and Tieszen L.L., 1995, Carbon isotope characterization of vegetation and soil organic matter in subtropical forests in Luquillo, Puerto Rico: Biotropica, v. 27, p. 138-148.

Voss, K. A., Bookhagen, B., Sachse, D., and Chadwick, O. A.: Variation of deuterium excess in surface-waters across a 5000-m elevation gradient in the east-central Himalaya, *Journal of Hydrology*. **586** DOI: 10.1016/j.jhydrol.2020.124802

Wan, Z. and Hulley, G. (2015) *MOD11C3 MODIS/Terra Land Surface Temperature/Emissivity Monthly L3 Global 0.05Deg CMG V006. NASA EOSDIS Land Processes DAAC*. Available at: https://doi.org/10.5067/MODIS/MOD11C3.006.

Wan, Z., Li, Z.-L. (2011). MODIS Land Surface Temperature and Emissivity. In *Land Remote Sensing and Global Environmental Change*. 894.

Wang, C. *et al.* (2017) 'Soil n-alkane δD and glycerol dialkyl glycerol tetraether (GDGT) distributions along an altitudinal transect from southwest China: Evaluating organic molecular proxies for paleoclimate and paleoelevation', *Organic Geochemistry*, 107, pp. 21–32. doi: 10.1016/j.orggeochem.2017.01.006.

Wang, H., Liu, W. and Zhang, C. L. (2014) 'Dependence of the cyclization of branched tetraethers on soil moisture in alkaline soils from arid-subhumid China: Implications for palaeorainfall reconstructions on the Chinese Loess Plateau', *Biogeosciences*, 11(23), pp. 6755–6768. doi: 10.5194/bg-11-6755-2014.

Wang, Y. *et al.* (2008) 'Stable isotopic variations in modern herbivore tooth enamel, plants and water on the Tibetan Plateau: Implications for paleoclimate and paleoelevation reconstructions', *Palaeogeography, Palaeoclimatology, Palaeoecology*, 260(3–4), pp. 359–374. doi: 10.1016/j.palaeo.2007.11.012.

Weijers, J. W. H. *et al.* (2006) 'Occurrence and distribution of tetraether membrane lipids in soils: Implications for the use of the TEX86 proxy and the BIT index', *Organic Geochemistry*, 37(12), pp. 1680–1693. doi: 10.1016/j.orggeochem.2006.07.018.

Weijers, J. W. H. *et al.* (2007) 'Environmental controls on bacterial tetraether membrane lipid distribution in soils', *Geochimica et Cosmochimica Acta*, 71(3), pp. 703–713. doi: 10.1016/j.gca.2006.10.003.

Wentz FJ, Meissner T, Gentemann C, Hillburn KA, Scott J. 2014. Remote Sensing Systems GCOM-W1 AMSR2 [Monthly] Environmental Suite on 0.25 deg grid, Version 7.2, [SWE]. Remote Sensing Systems, Santa Rosa, CA. Available online at www.remss.com/missions/amsre

Whillans IM, Grootes PM. 1985. Isotopic diffusion in cold snow and firn. *Journal of Geophysical Research* **90** (4): 3910–3918. DOI: 10.1029/JD090iD02p03910
Winiger M, Gumpert M, Yamout H. 2005. Karakorum-Hindukush-western Himalaya: Assessing high-altitude water resources. *Hydrological Processes* **19** (12): 2329–2338 DOI: 10.1002/hyp.5887

Whipple, K. X. (2009) 'The influence of climate on the tectonic evolution of mountain belts', *Nature Geoscience*, 2(2), pp. 97–104. doi: 10.1038/ngeo413.
Winiger, M., Gumpert, M. and Yamout, H. (2005) 'Karakorum-Hindukush-western Himalaya: Assessing high-altitude water resources', *Hydrological Processes*, 19(12), pp. 2329–2338. doi: 10.1002/hyp.5887.

White, N. M., Parrish, R. R., Bickle, M. J., Najman, Y. M. R., Burbank, D., and Maithani, A., 2001, Metamorphism and exhumation of the NW Himalaya constrained by U–Th–Pb analyses of detrital monazite grains from early foreland basin sediments: Journal of the Geological Society, v. 158, no. 4, p. 625-635.

Wobus, C. W., Hodges, K. V., and Whipple, K. X., 2003, Has focused denudation sustained active thrusting at the Himalayan topographic front?: Geology, v. 31, no. 10, p. 861-864.

Wulf H, Bookhagen B, Scherler D. 2010. Seasonal precipitation gradients and their impact on fluvial sediment flux in the Northwest Himalaya. *Geomorphology* **118** (1–2): 13–21 DOI: 10.1016/j.geomorph.2009.12.003

Wulf H, Bookhagen B, Scherler D. 2016. Differentiating between rain, snow, and glacier contributions to river discharge in the western Himalaya using remote-sensing data and distributed hydrological modeling. *Advances in Water Resources* **88**: 1–81 DOI: 10.1016/j.advwatres.2015.12.004

Xu, Q. *et al.* (2010) 'Stable isotopes of modern herbivore tooth enamel in the Tibetan Plateau: Implications for paleoelevation reconstructions', *Chinese Science Bulletin*, 55(1), pp. 45–54. doi: 10.1007/s11434-009-0543-2.

Yin, A. and Harrison, T. Mark (2000) 'Geologic Evolution of the Himalayan-Tibetan Orogen', *Annual Review of Earth and Planetary Sciences*, 28(1), pp. 211–280. doi: 10.1146/annurev.earth.28.1.211.

Zech M., Zech R., Rozanski K., Gleixner G., Zech W. (2015). Do n-alkane biomarkers in soils/sediments reflect the δ2H isotopic composition of precipitation? A case study from Mt. Kilimanjaro and implications for paleoaltimetry and paleoclimate research. *Isoopes in Environmental and Health Studies*, 51, 508–524.

Zhisheng, A. *et al.* (2001) 'Evolution of Asian monsoons and phased uplift of the Himalaya–Tibetan plateau since Late Miocene times', *Nature*, 411(6833), pp. 62–66. doi: 10.1038/35075035.

Zhuang, G., Brandon, M. T., Pagani, M., Krishnan, S. (2014) Leaf wax stable isotopes from Northern Tibetan Plateau: Implications for uplift and climate since 15 Ma. *Earth and Planetary Science Letters*, **390**, 186–198.

8. Supplemental material

Chapter 2

Van der Veen, Iris (2021) Research data to: “Identifying seasonal snowmelt in the western Himalaya using stable isotopes of modern surface waters and remote sensing”, Mendeley data, V1, doi (*reserved*) http://dx.doi.org/10.17632/7fmgz7pshs.1

https://data.mendeley.com/datasets/7fmgz7pshs/draft?a=7fc0ccaa-db82-4bbe-94c2-308eeff625a6

Chapter 3

van der Veen, Iris (2020), “Research data to: " Validation and calibration of soil δ2H and brGDGTs along (E-W) and strike (N-S) of the Himalayan climatic gradient" ”, Mendeley Data, V1, doi: 10.17632/cvdnf723k5.1

http://dx.doi.org/10.17632/cvdnf723k5.1

Chapter 4

Vögeli, N. *et al.* (2017) ‘Lateral variations in vegetation in the Himalaya since the Miocene and implications for climate evolution’, *Earth and Planetary Science Letters*, 471, pp. 1–9. doi: 10.1016/j.epsl.2017.04.037.

https://doi.org/10.1016/j.epsl.2017.04.037